132 p
$t \sim 4.00$
$mf \sim 1.00$

PHILCO.

A SUBSIDIARY OF *Ford Motor Company,*

RESEARCH LABORATORIES

RPL-TDR-64-79

FIRST QUARTERLY TECHNICAL REPORT

AN INVESTIGATION AND DEVELOPMENT OF FILM PROTECTED-CONVECTIVELY COOLED NOZZLES

Prepared for: Air Force Rocket Propulsion Laboratory
Research and Technology Division
Edwards Air Force Base, California

Under Contract: AF 04(611)-9705

Prepared by: W. H. Armour
R. L. Mitchell
H. L. Moody
A. M. Saul
W. L. Smallwood
R. H. Williams
F. W. Marble (Consultant)
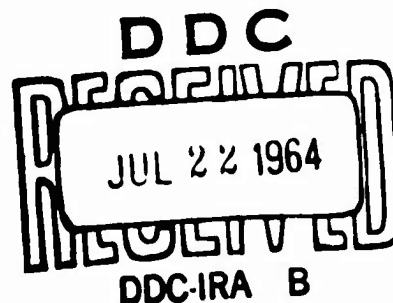
22 May 1964

ABSTRACT

This report summarizes the work conducted at the Philco Research Laboratories on Contract AF 04(611)-9705, "An Investigation and Demonstration Of Film Protected-Convectively Cooled Nozzles". Detail analytical and experimental studies were conducted during this reporting period on internal convection and conduction heat transfer, coolant selection, thermochemistry, and the fluid mechanic aspects of injection through discrete holes in a reacting turbulent boundary layer. Laboratory experiments were conducted to provide insight, data, and direction to the analysis.

CONTENTS

ILLUSTRATIONS

ILLUSTRATIONS (Continued)

SECTION 1

INTRODUCTION

The emphasis in present and future propellants for solid rocket motors has been toward higher impulse. This can be accomplished with either reducing the molecular weight of the exhaust products, increasing the flame temperature, or both. Presently, flame temperatures of the order of $6500^{\circ}F$ to $6800^{\circ}F$ are being considered, and indeed many tests have been conducted with propellants in this category. However, this increase in temperature has produced problems in nozzle design and integrity, especially for long duration firings.

The investigations and results of contract AF 04(611)-8387, "Applied Research for Advanced Cooled Nozzles" showed that several thermal protection concepts are capable of containing these high energy corrosive propellants. One of these concepts, film protected-convectively cooled nozzles, looked extremely promising, however, further analytical definition was required as well as experimental verification.

This report summarizes the work conducted during the first quarter at the Philco Research Laboratories on the "Investigation and Development of Film Protected-Convectively Cooled Nozzles". This effort includes an analytical and experimental investigation of the fluid mechanic aspects of injection into turbulent boundary layers associated with reacting nozzle flows; a thermochemical analysis of the reactions encountered in the boundary layer between the injection fluid and free stream; a thermochemical analysis and experimental study of the reactions between the injectant fluid and the nozzle wall material, as a function of wall temperature. Heat transfer analysis for both the internal convection and conduction were conducted for various coolants, heat sink thicknesses, coolant flow rates and coolant hole size and spacing. A very versatile heat transfer program, existing at the Philco Research Laboratories, was used for the internal convection and conduction studies. The effects of dissociation and particle flow with radiation were also studied analytically for the coolant flow. The flame side forced convection heat transfer to the nozzle wall without film protective was also investigated. Future investigations will include the effects

of boundary layer injection.

Also during this quarter, laboratory experiments were conducted in order to provide insight into the thermochemical aspects of fluid injection and convection. Cold flow experiments for fluid injection into turbulent boundary layers were also performed in order to gain a fundamental insight into the phenomena occurring, and to provide some limited data on flow separation parameters, mixing region length, hole size and spacing variables, as well as hole angles and flow rates.

The culmination of the various aspects of this investigation is to provide a sufficient analytical and experimental background to allow one to reliably design an optimized film protected-convectively cooled nozzle. However, as shown in this report, a great deal of effort is still required in several of the above mentioned areas. These will be more fully explored during the course of this program.

SECTION 2

STUDY AND ANALYSIS

2.1 THERMOCHEMISTRY

During the first quarter, a considerable effort has been devoted to the thermochemical evaluation of potential injection fluids. A preliminary cooling system design and weight analysis was performed to determine the relative advantages of working fluids which, in their storage state, would be gases, liquids or solids. (This analysis will be refined and presented in a later report.) It was concluded that the gas storage system would be the most practical for the present purposes and that it is competitive with liquid and solid storage systems on a weight basis. Several liquids, particularly NH_3 and CCl_4, apparently have significant potential but no attractive solids were found. In general, the gases and liquids of interest have been examined according to the following thermochemical criteria:

1. Thermal stability of gases under the predicted pressures and temperatures within the convection cooling passages

2. Chemical stability of gases and their dissociation products relative to the pyrolytic ;raphite walls of the convection cooling passages

3. Chemical stability of the pure injection gases relative to the pyrolytic graphite throat surface at the prevailing nozzle pressures and over the graphite surface temperatures of interest

4. Chemical stability of the injection gases relative to the propellant combustion products as a function of pressure, temperature and mixture ratio

5. Chemical stability of the injection gas-combustion product mixture relative to the pyrolytic graphite throat contour.

In addition, the following specific considerations are regarded as desirable and have provided basis for selection or rejection of some cooling fluids:

1. Only endothermic dissociation and no reactions with the graphite in the cooling passages are allowed.

2. The injection gas must be less corrosive than the propellant combustion products at the graphite design surface temperatures.

3. It is desirable to add unstable carbon based molecules to the boundary layer.

4. The injection gas should have high potential as a convection coolant and a high total enthalpy change from ambient to flame temperatures.

5. Readjustment of the combustion product boundary layer, due to dilution and consequent chemical reaction, should not be exothermic.

Potential injection fluid classes were examined and the following compounds were chosen for detailed study: He, Ar, N_2, CO, H_2, CH_4, BF_3, CCl_4, CF_4 and CS_2. The helium/argon will have the same influence on nozzle corrosion, with their potential (1) as a convection coolant, (2) influence on chemical diffusion, and (3) storage weight depend on their molecular weights. The nitrogen and carbon monoxide represent inert constiutents of the combustion products which will behave like the He and A except for their influence on the boundary layer equilibrium composition. Nitrogen has been examined in detail and will be discussed separately. The net thermal effect expected from any of the inerts, when the they dilute the combustion product boundary layer gases, is slightly endothermic due to an increase in the dissociation of hydrogen. The inerts achieve corrosion control primarily through diffusion boundary layer thickness and conductance changes. The corrosion control and internal convection requirements apparently conflict for the inerts. However, helium is favored among these because of lower storage weight and high impulse, at least for propellants which yield the smallest amounts of CO_2 and H_2O.

Carbon-sulfur compounds, such as carb n disulfide, CS_2, were considered but were rejected on the basis of the relatively high decomposition pressures of carbon monosulfide and gaseous sulfur, that is, $2CS_2(g)=2CS(g)+S_2(g)$. At the temperatures of interest the product gaseous sulfur should react extensively with the graphite walls of the injection capillaries to form additional gaseous carbon sulfides. The same conclusion was extended to cover all sulfur compounds and this class has been eliminated from further consideration.

Carbon tetrafluoride was considered but was also rejected on the basis of relatively high decomposition pressures from the reaction $CF_4(g) = CF_3(g) + F(g)$. The monatomic fluorine should react extensively with the capillary walls to form gaseous C_2F_2. Because the CF_4 is the most stable carbon-fluorine compound, the freons can also be eliminated. However, BF_3 because of its high thermal stability, was investigated further. It was subsequently concluded that the addition of fluorine compounds invariably leads to exothermic reaction in the combustion product boundary layer. Furthermore, these reactions produce species, such as BOF, which will, in turn, react with the graphite walls. HF is the least reactive of the class and would be expected to behave like an inert gas of intermediate molecular weight.

Carbon tetrachloride was also considered since it decomposed completely to carbon and chlorine. The resultant chlorine is relatively unreactive with the walls of the injection capillaries. Carbon tetrachloride, however, is a liquid under ambient conditions; and its use involves the problems of flow regulation and boiling. Because of this, interest in the use of CCl_4 as an injection fluid has been deferred until the study of other promising fluids, which are and can be stored as gases, is completed. Compounds such as chloroform ($CHCl_3$) are also of interest. These will be investigated further during the second quarter and their potential advantages will be pointed out in the discussion of methane. It should be noted that the saturated carbon-chlorine, carbon-hydrogen-chlorine and carbon-hydrogen compounds all undergo endothermic dissociation, producing condensed carbon. The saturated compounds tend to be exothermic. The more complex saturated liquid C-H-Cl and C-H compounds are of interest but their behavior can be inferred from that of CCl_4 and CH_4.

The results of the detailed calculations for methane and nitrogen are presented in the subsequent paragraphs. The behavior of hydrogen can be inferred from that of the dissociated methane. Hydrogen has been rejected because of its high reactivity with graphite at temperatures above about $4000^{\circ}F$. On the other hand, methane appears to be the most attractive injection gas discovered to date. This is basically due to the addition of excess carbon to the boundary layer. Both the combustion product oxidizers and the hydrogen (which forms C_2H_2 at temperatures above $4000^{\circ}F$) react with this carbon instead of the wall material. Endothermic reaction enhances thermal control and it becomes possible to virtually eliminate contour corrosion.

a.   Methane

Figure 1 shows the computed equilibrium composition of methane at an assumed injection pressure of 700 psia. Above $1600^{\circ}K$ ($2880^{\circ}R$) the methane is essentially all decomposed. Condensed carbon, which is not included in the graph, is the major product of decomposition. As discussed in Section 3.1, Laboratory Experiments, the particle size of the condensed carbon has been found to be on the order of 0.1 micron and should not significantly lag the gas flow. To a large extent, then, the product hydrogen in the methane stream remains saturated with respect to these carbon particles, preventing reaction with the capillary walls.

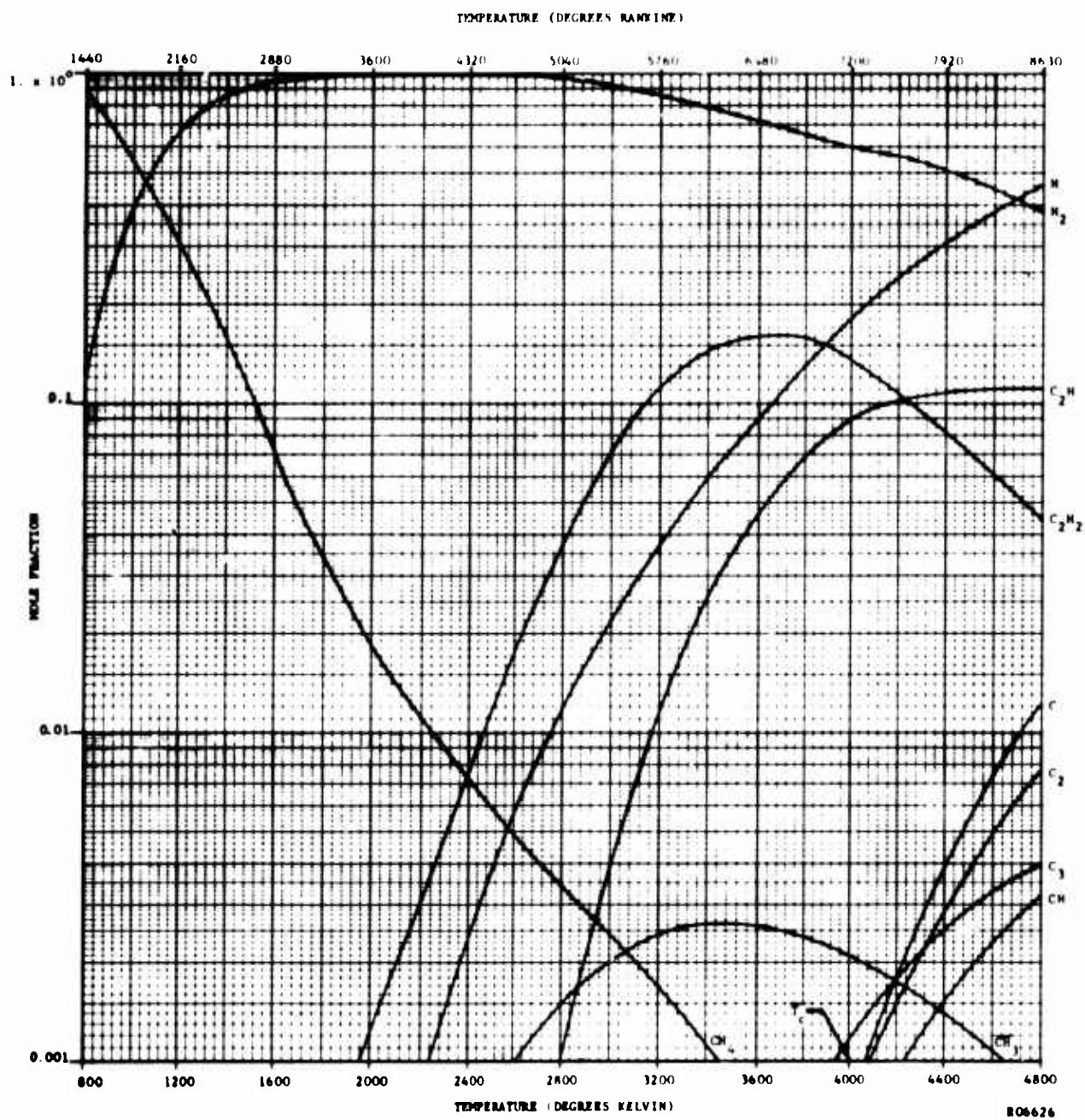The point of injection is assumed to be upstream of the throat at a

FIGURE 1. EQUILIBRIUM COMPOSITION OF CH_4 AT 700 PSIA (GASEOUS SPECIES)

pressure approximating 400 psia. Because the injected gas film has a chemical composition which differs from that of the combustion free stream, it will act as a sink for chemical species. As the two streams flow away from the point of injection they will tend to diffuse into each other because of the gradients in the concentration of the various gaseous species. The depth of penetration of the reactant gases into the injected film will be an exponential function of time, mass diffusivity, and any initial difference in concentration. To simulate this variable condition three ratios of injection gas to combustion gas mass flows have been considered, $1 \cdot 9$, $1 \cdot 1$, and $9 \cdot 1$. The combustion product spectrum chosen is that from the $6720^\circ F$ aluminized propellant system simulated in composition by the so-called "Hot-Solid" composition given in Table I. Table I also lists the important products to be found in the free stream at the throat.

As evidenced in Figures 2 through 8, the equilibration of methane with the free stream substantially reduces the concentration of the principal species which can react with the nozzle wall CO_2, H_2O, O, OH, and condensed Al_2O_3, with consequent increases in the CO H_2 H, and condensed AN species. Figure 9 shows the disproportionate increase in the number of gaseous moles per 100 grams of the mixture which is the result of hydrogen addition and chemical reaction. This suggests that there will be a substantial amount of gaseous blowing in the boundary layer. In Figure 10, the amount of wall material required to theoretically saturate one gram of the gas mixture (injection gas plus combustion products) is designated "B". A negative "B" value implies that there is more than sufficient carbon from the decomposition of the injectant methane gas to saturate the mixture. Thus, below $3600^\circ K$ ($6450^\circ R$) all methane mixtures should substantially reduce the extent of chemical reaction of the nozzle wall with the combustion product gases. The rise in "B" values above about $2500^\circ K$ ($4500^\circ R$) which occurs with the addition of methane can be attributed to the increasing stability with temperature of gaseous C_2H_2. Until the "B" values become positive, at higher temperatures, the hydrogen resulting from the CH decomposition will consume the excess carbon in the boundary layer endothermically but otherwise to no advantage. The carbon-chlorine injection gases should lead to negative "B" values to significantly higher graphite temperatures. Evidently a 30% CH_4 mixture will still be inert to the graphite wall at $5000^\circ F$.

"B" values have also been computed for the case of the methane within the injection capillaries, a d are shown in Figure 11. Negative "B" values are encountered up to $3500^\circ K$ ($6270^\circ R$). Above this temperature, the stability of C_2H_2 gives rise to positive "B" values.

The enthalpy, in BTU/lb, of the free stream and the free stream plus various weight percentages of methane have also been computed as a function of temperature and are shown in Figure 12. The enthalpy values shown represent the summation of the heat of formation at $536^\circ R$ plus the change in enthalpy above that temperature of all of the combustion products and of the products of the reaction of the combustion products with methane. These data, then, include the heats of any reactions which occur when methane is mixed with the free stream. Figure 12 also gives the enthalpy values if no chemical reactions between the methane and the combustion product species are allowed to occur.
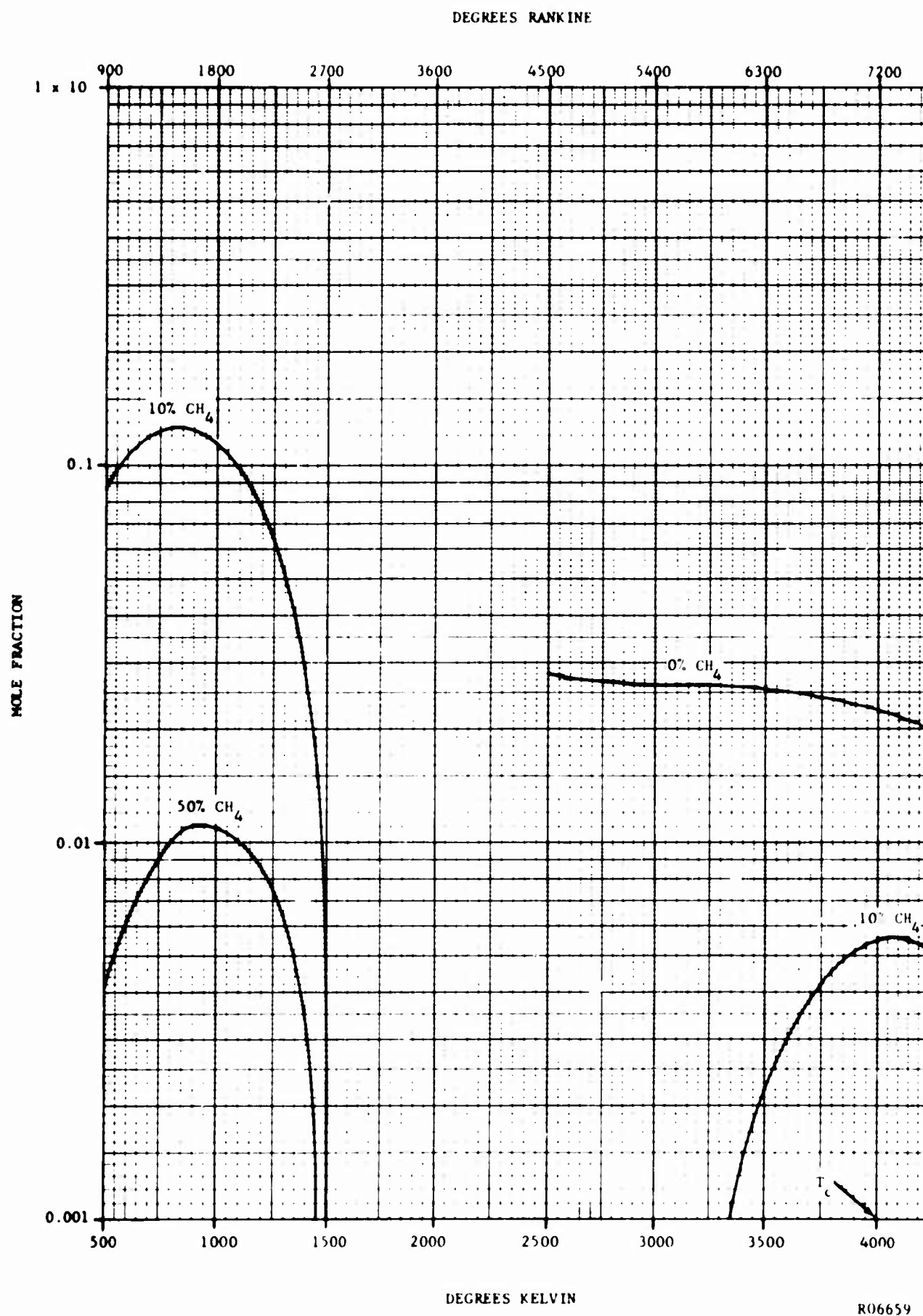
FIGURE 2. EQUILIBRIUM CO_2 CONCENTRATION FOR "HOT SOLID" – CH_4 MIXTURES
AT 400 PSIA

DEGREES RANKINE
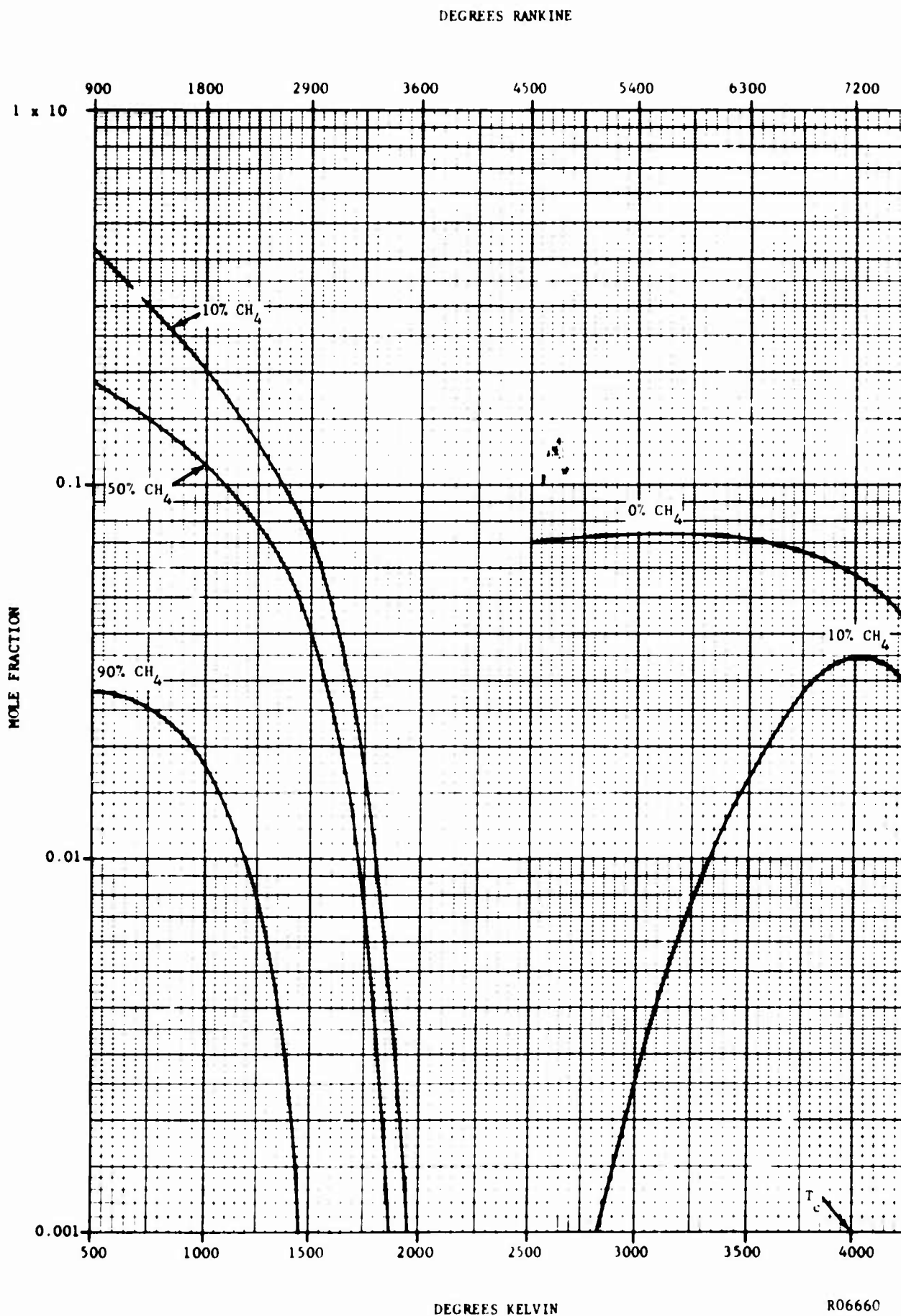
FIGURE 3.   EQUILIBRIUM H₂O CONCENTRATION FOR "HOT SOLID" - CH₄ MIXTURES
AT 400 PSIA
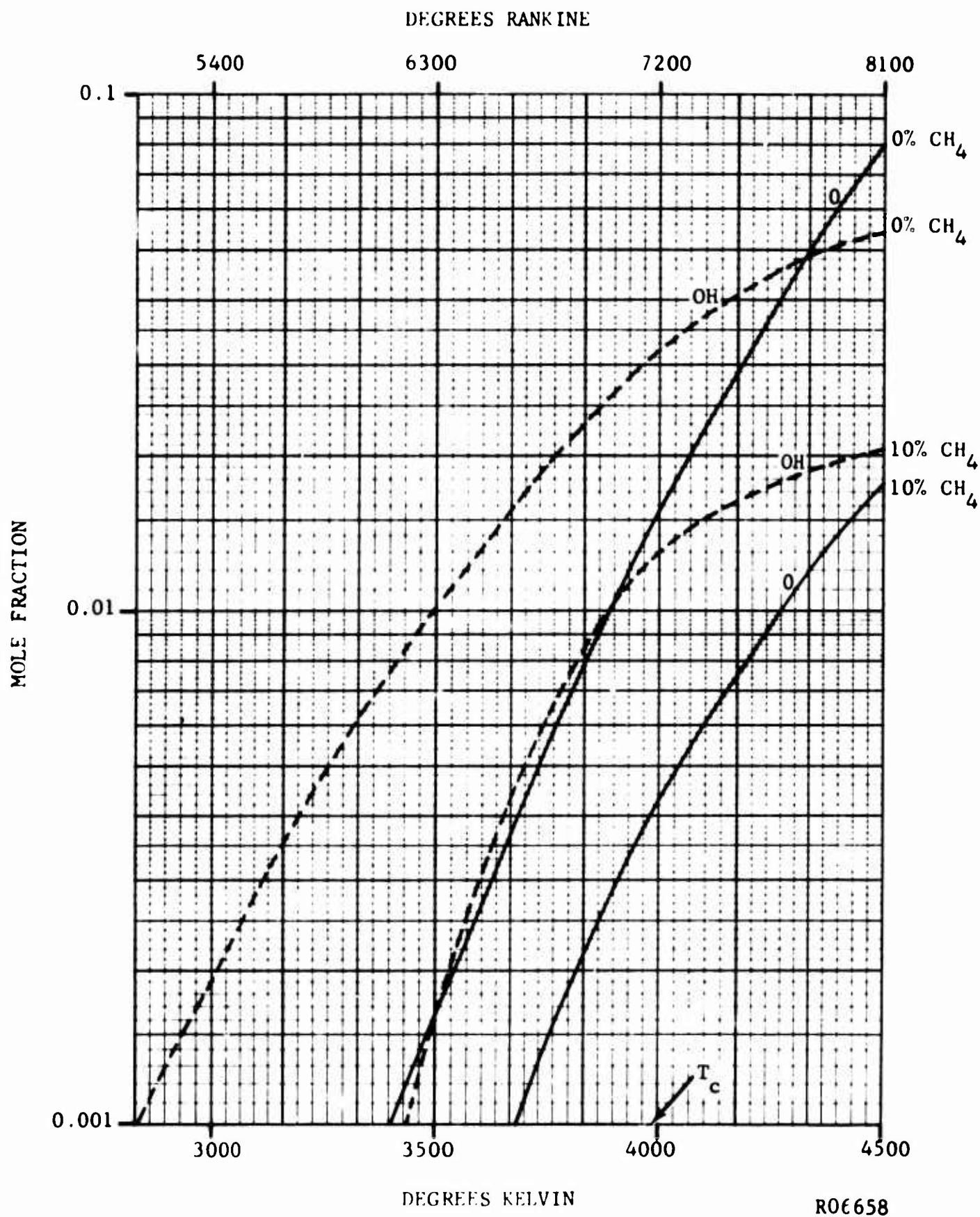
FIGURE 4.   EQUILIBRIUM OH AND O CONCENTRATIONS FOR "HOT SOLID" -
CH$_4$ MIXTURES AT 400 PSIA
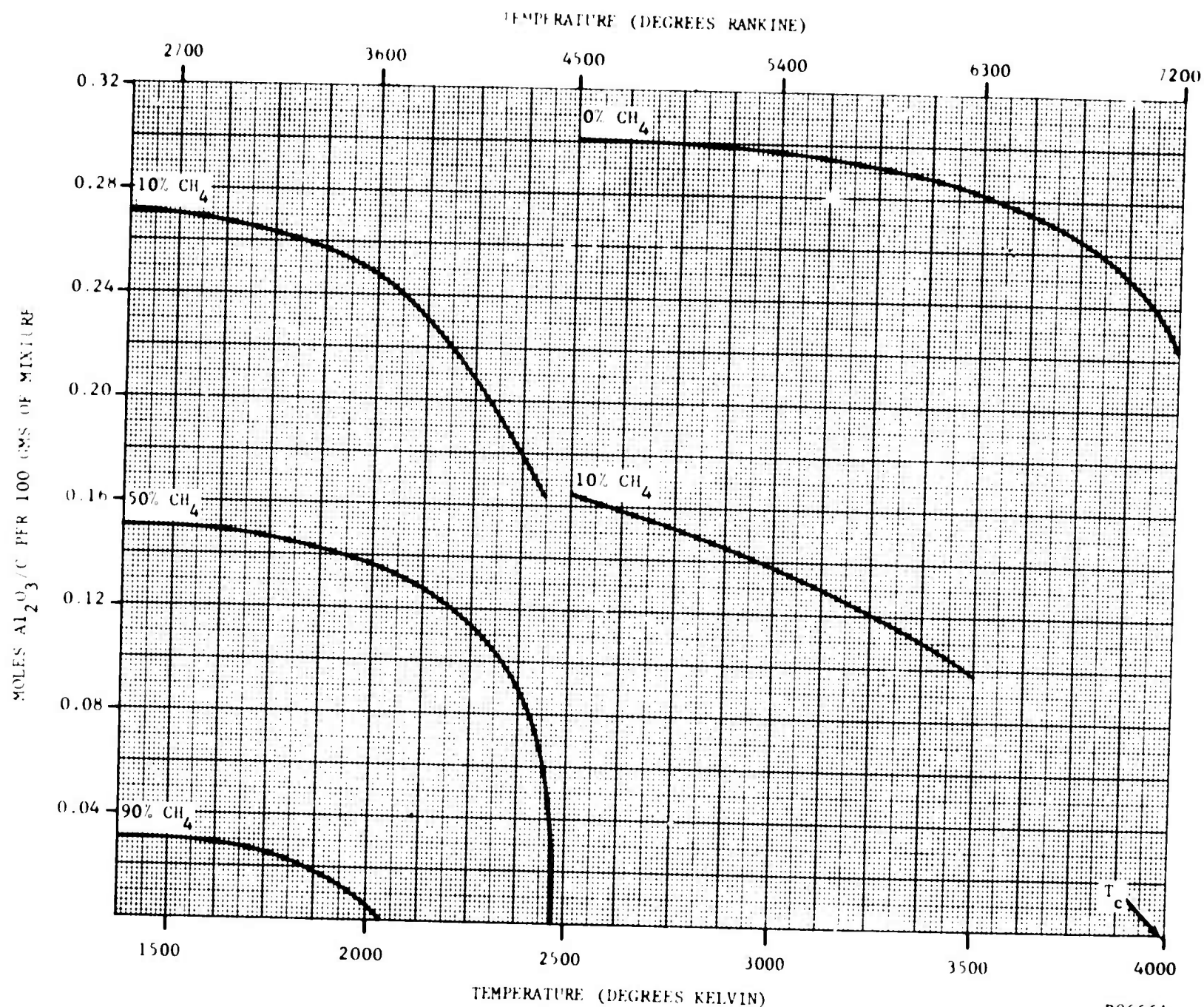
BLANK PAGE

FIGURE 5. EQUILIBRIUM Al₂O₃/CONDENSED CONCENTRATION FOR "HOT SOLID" CH₄ MIXTURES AT 400 PSIA
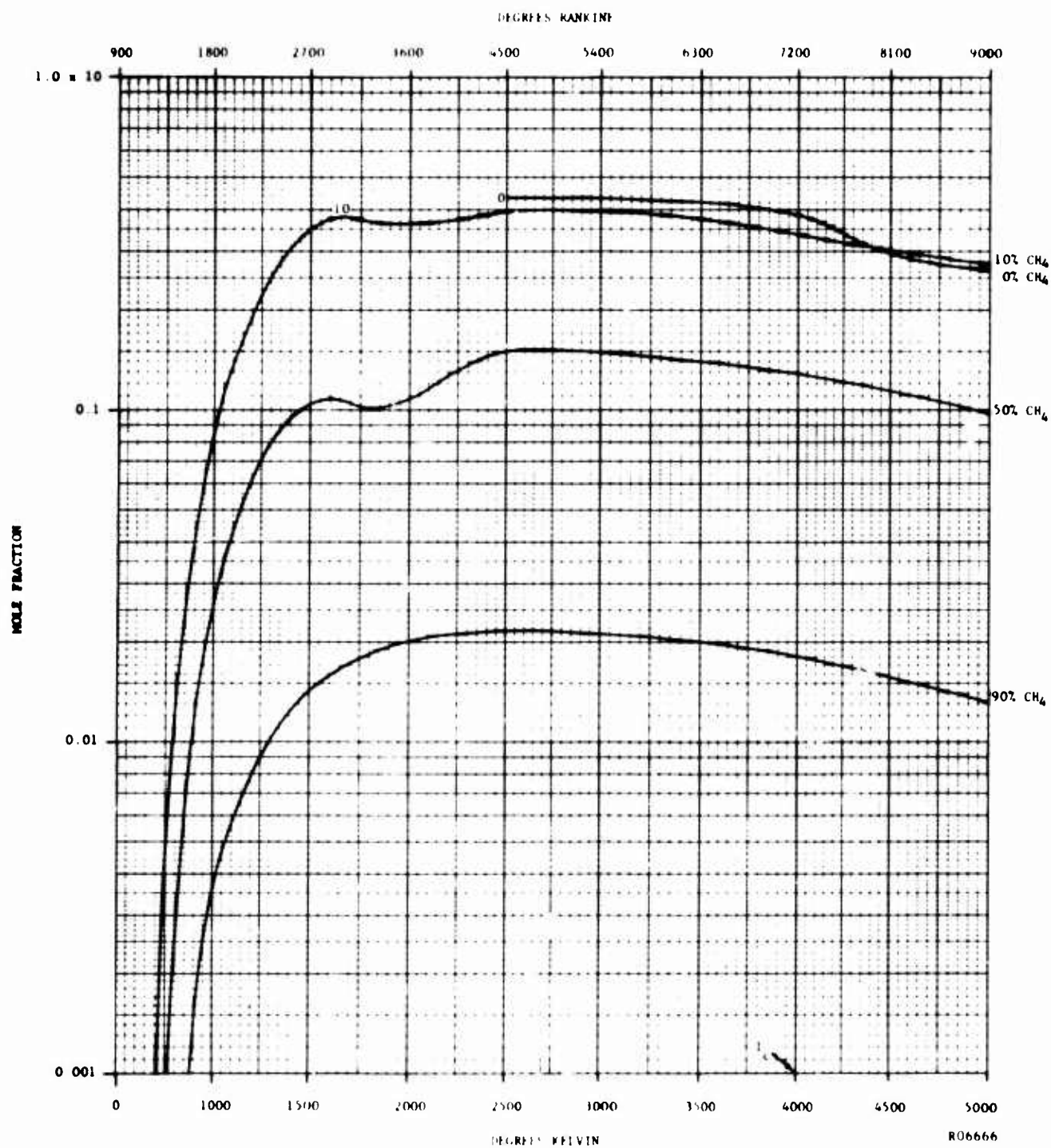
FIGURE 6.   EQUILIBRIUM CO CONCENTRATION FOR "HOT SOLID" - CH_4 MIXTURES AT 400 PSIA

-12-
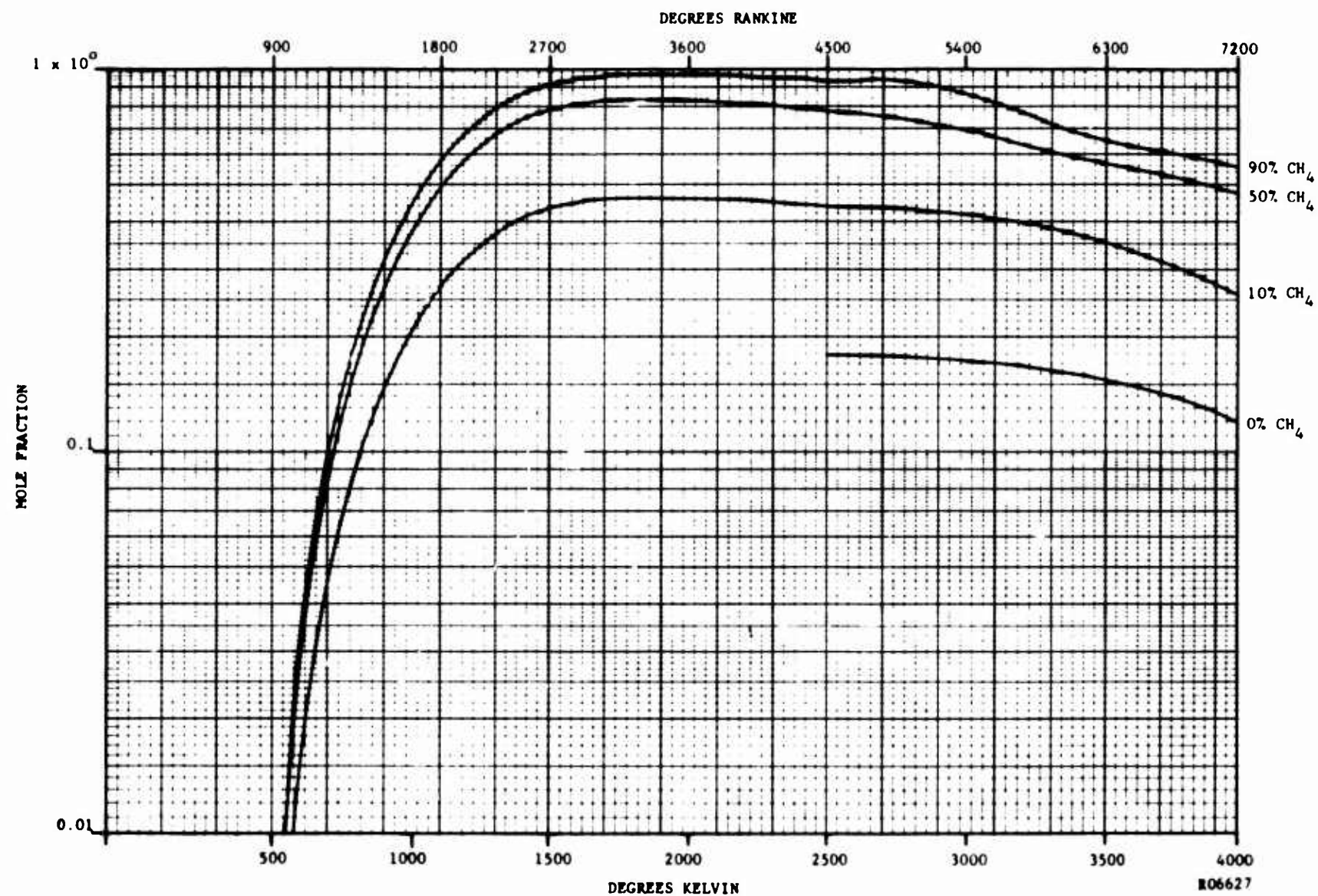
BLANK PAGE

FIGURE 7. EQUILIBRIUM H_2 CONCENTRATION FOR "HOT SOLID" - CH_4 MIXTURES AT 400 PSIA
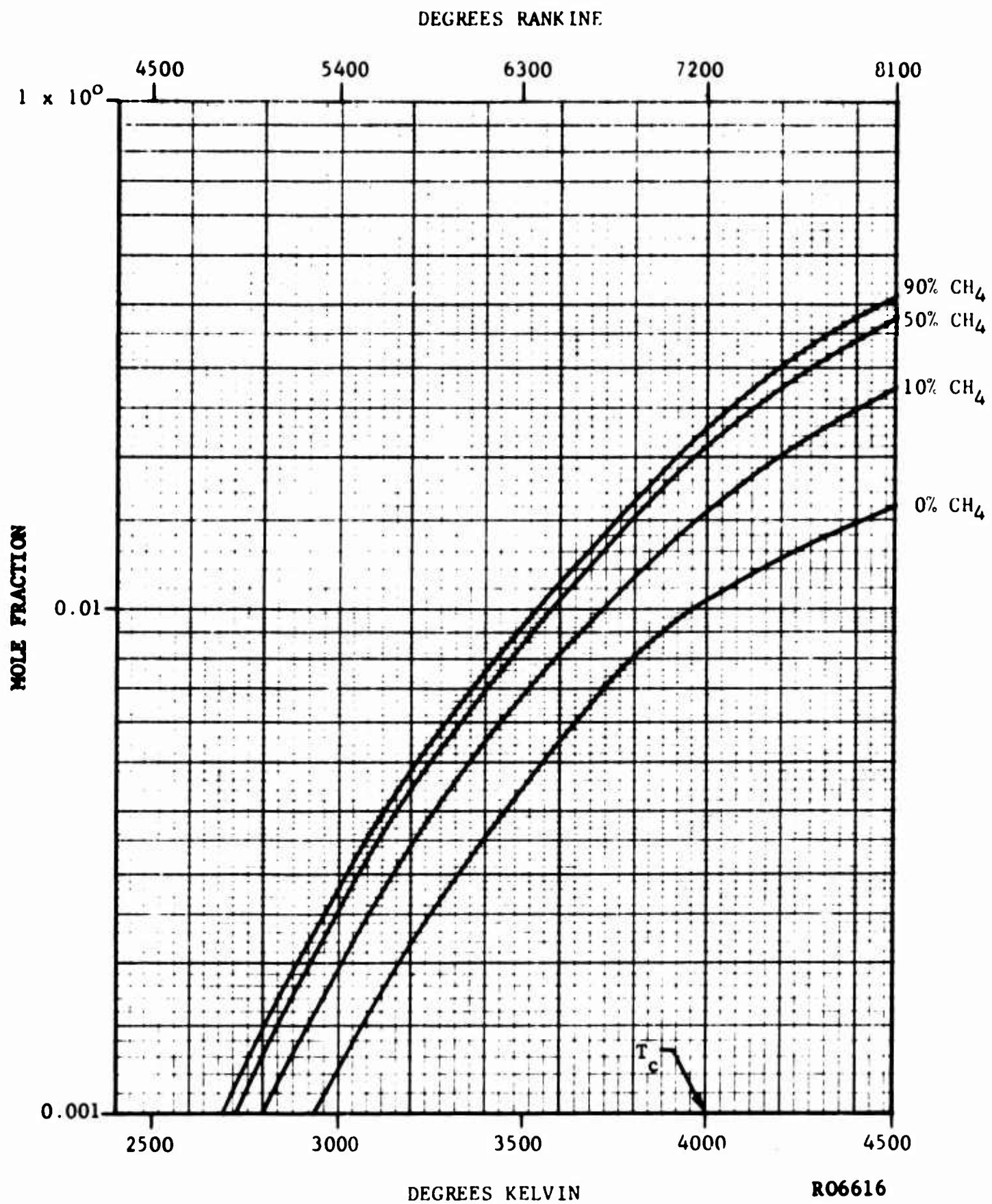
FIGURE 8. EQUILIBRIUM H CONCENTRATION FOR "HOT SOLID" - CH_4 MIXTURES AT 400 PSIA

BLANK PAGE
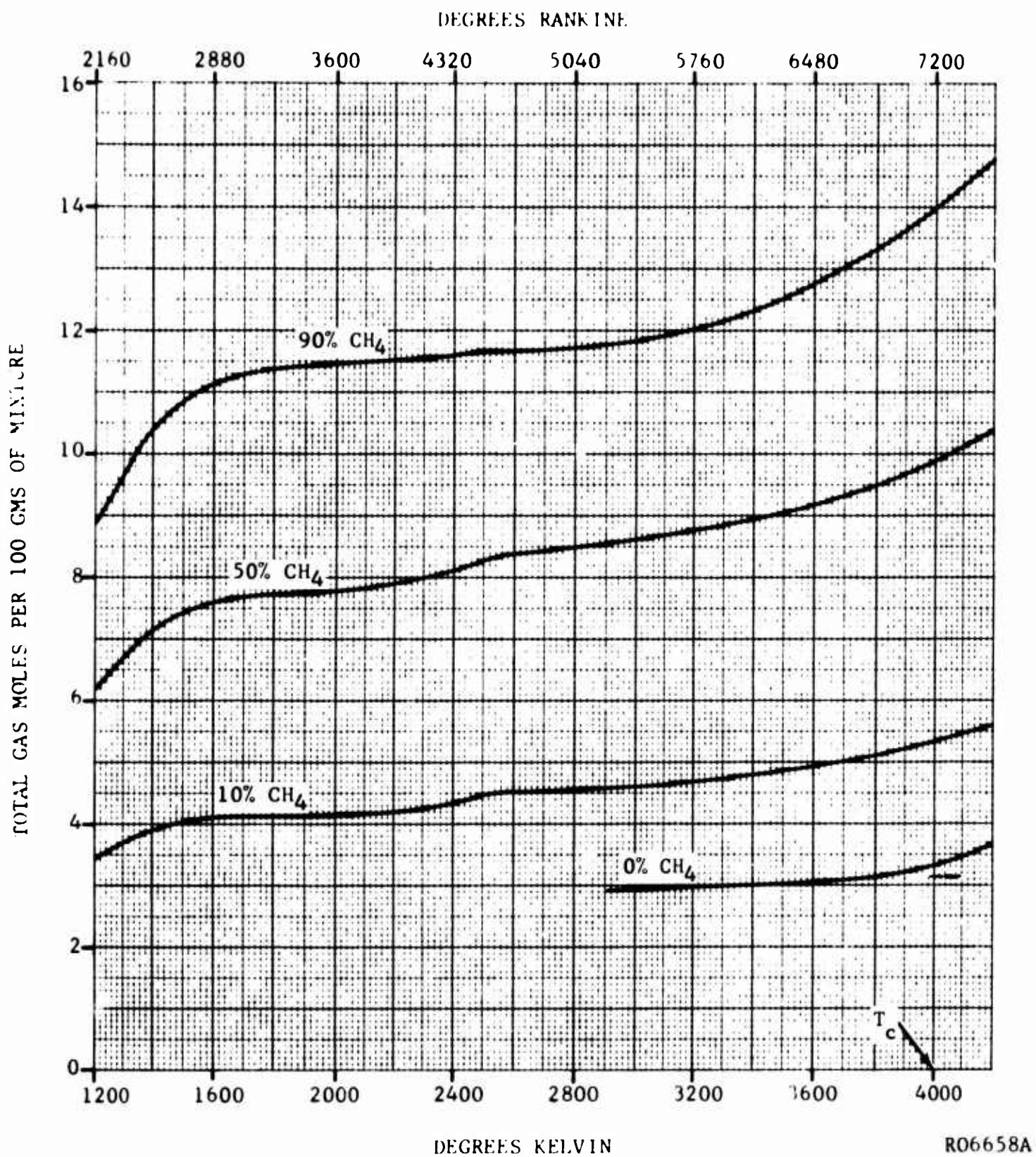
FIGURE 9.   TOTAL GAS MOLES OF EQUILIBRIUM "HOT SOLID" - CH₄ MIXTURES
AT 400 PSIA

-15-
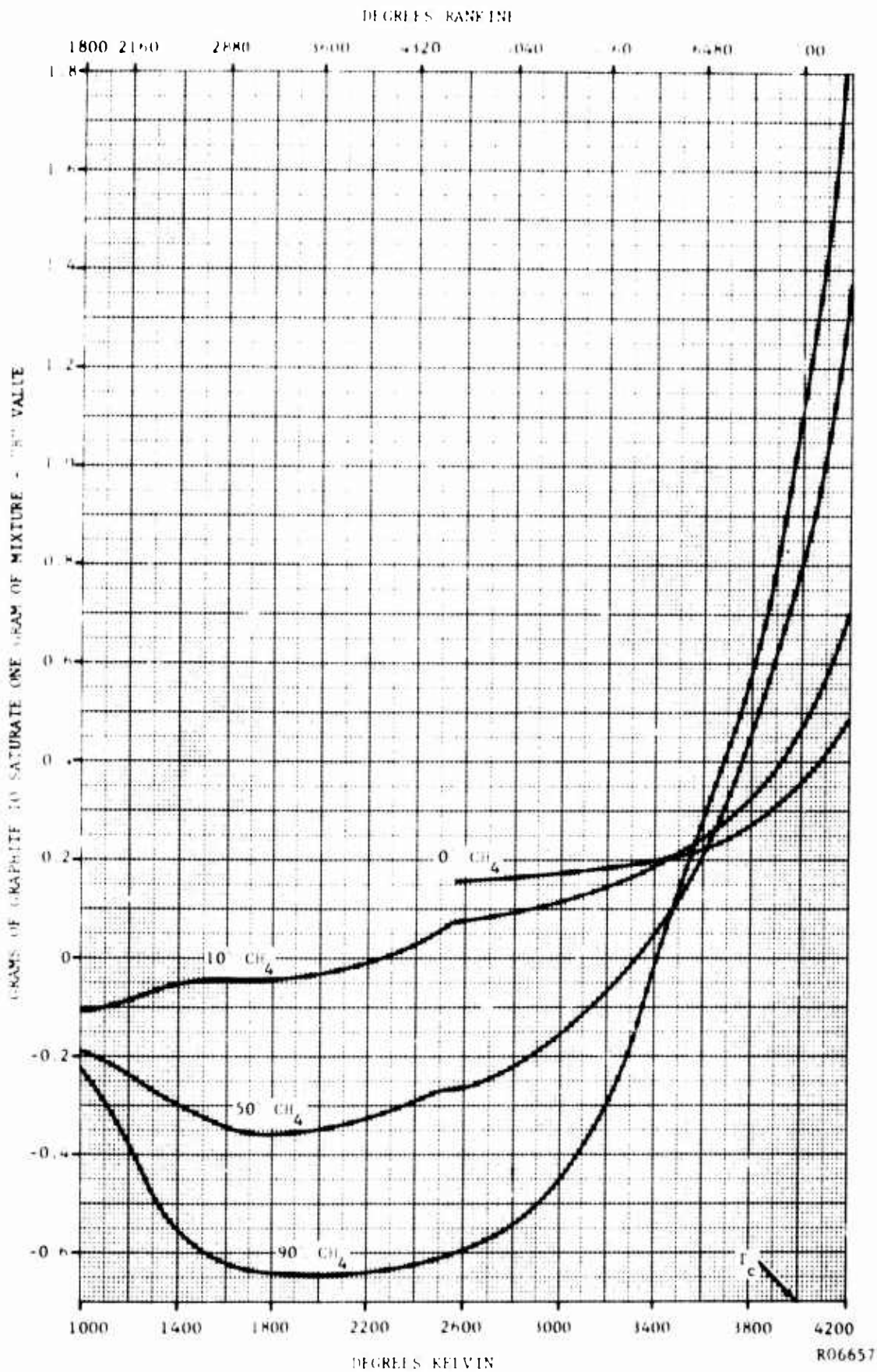
FIGURE 10. "B" VALUES FOR GRAPHITE IN EQUILIBRIUM WITH "HOT SOLID" - CH_4 MIXTURES AT 400 PSIA

DEGREES RANKINE
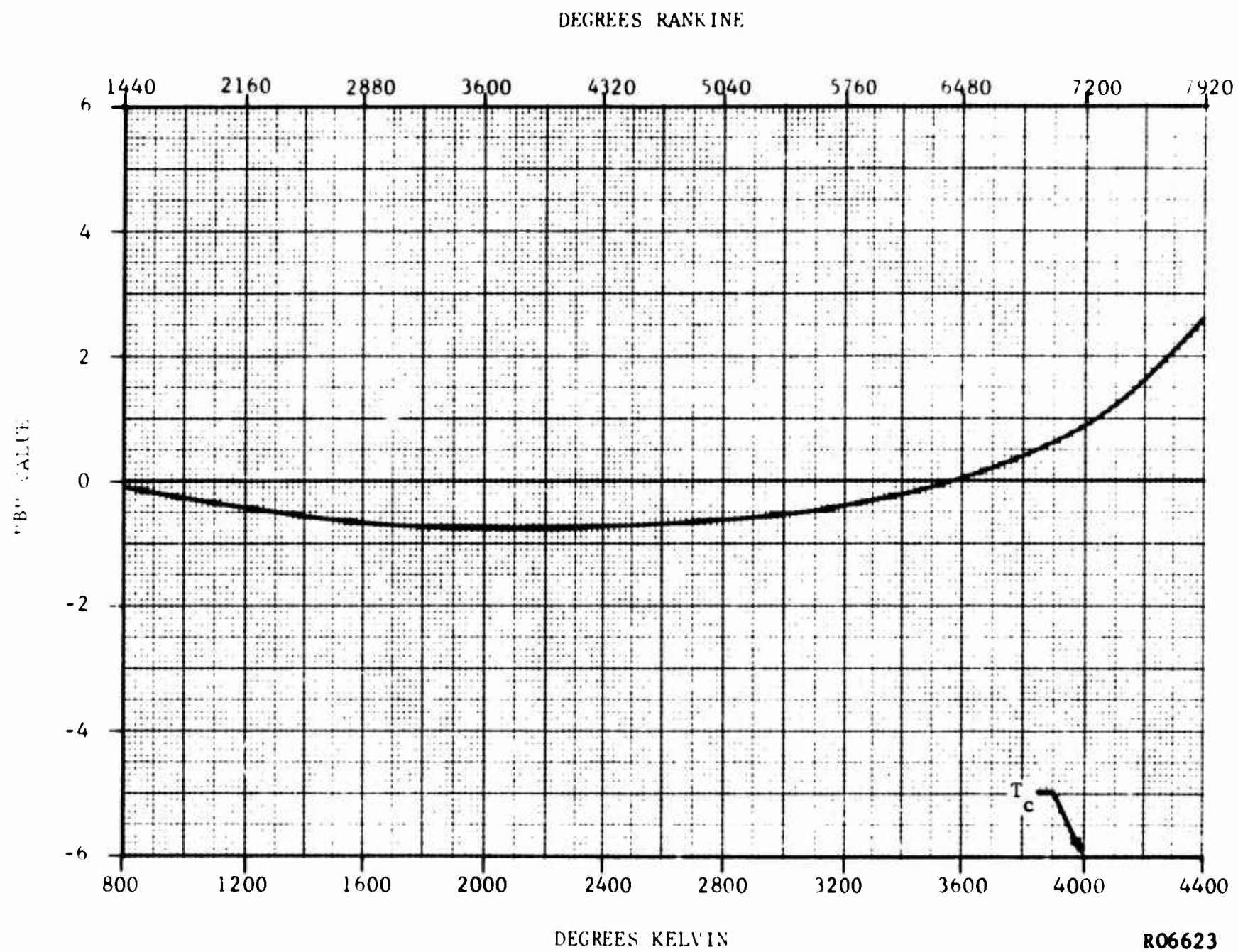
FIGURE 11. AMOUNT OF GRAPHITE TO SATURATE ONE GRAM OF CH_4 AT 700 PSIA

R06623

-17-
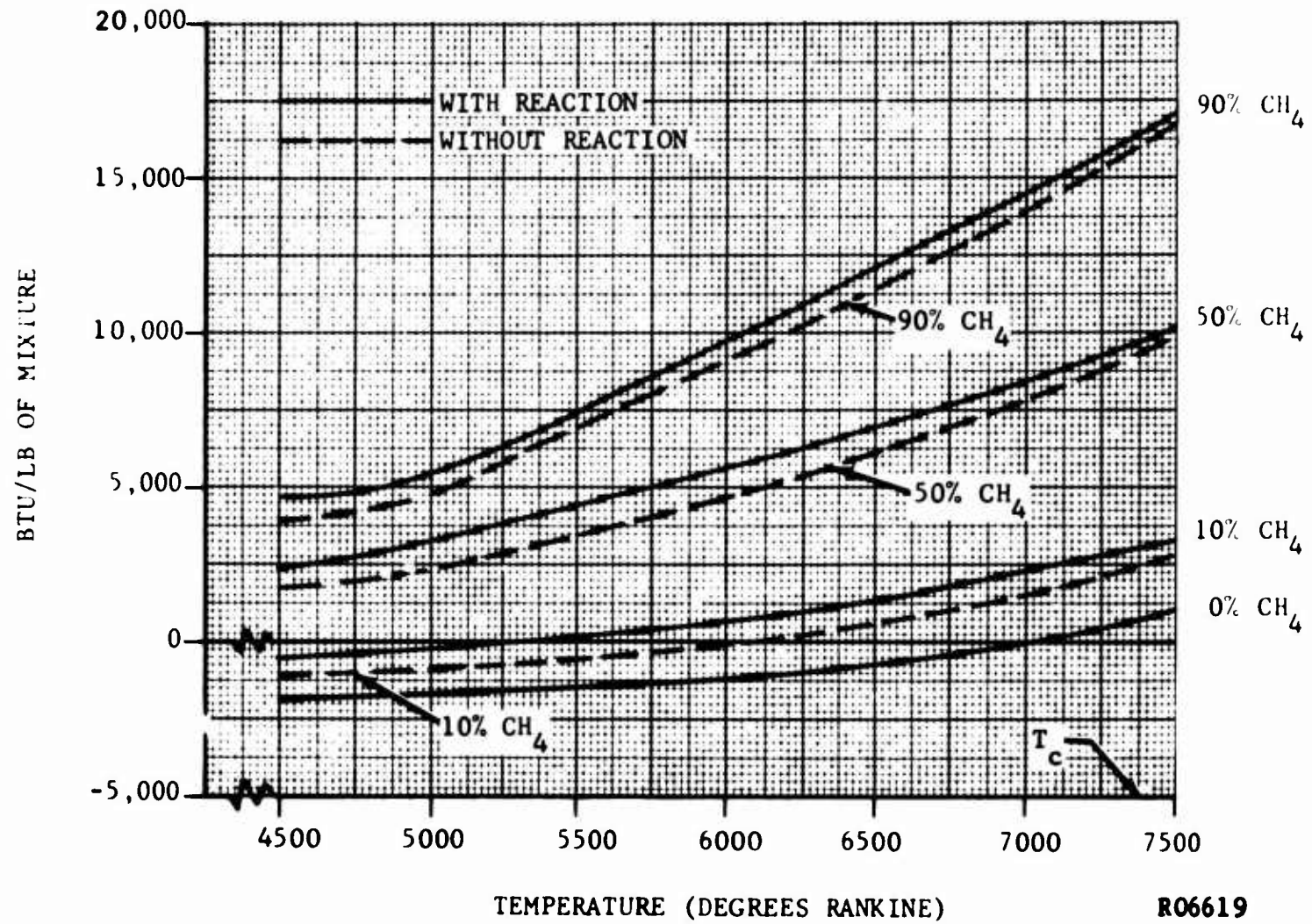
FIGURE 12. ENTHALPY VERSUS TEMPERATURE FOR "HOT SOLID" - CH4 MIXTURES
AT 400 PSIA

-18-

R06619

TABLE I

"HOT-SOLID" PROPELLANT
CALCULATED COMPOSITION OF CHAMBER AND
EXHAUST PRODUCTS
(mols/100 grams propellant)
(PARTIAL LIST)

Species	Chamber	Throat
$AlCl$	0.0536	0.0445
CHO	0.0008	0.0006
CO	1.2623	1.2632
CO_2	0.0757	0.0751
Cl	0.0568	0.0568
HCl	0.1357	0.1487
ClO	0.0001	0.0000
H	0.2586	0.2412
HN	0.0002	0.0001
OH	0.0811	0.0674
H_2	0.4094	0.4209
H_2O	0.2090	0.2086
N	0.0003	0.0002
NO	0.0163	0.0123
N_2	0.5340	0.5362
O	0.0282	0.0215
O_2	0.0056	0.0042
Al_2O_3/c		

Chamber Pressure: 700 psia

Throat Pressure: 405 psia
   (equilibrium)

T chamber: $3991^{\circ}K$ $(7180^{\circ}R)$

T throat: $3800^{\circ}K$ $(6830^{\circ}R)$
   (equilibrium)

Assuming the enthlpy of mixing is zero, the difference in the enthalpy values at any given temperature with and without reaction represents the net heat of reaction at that temperature. The reactions are highly endothermic and are a function of the degree of mixing, pressure and temperature. As an example, 3 pounds of methane mixed in equal proportions with the combustion products at 5000^OF requires the addition of about 6000 BTU to maintain the temperature. For the 10% methane mixture, 24,000 BTU are absorbed. This effect will significantly reduce the nozzle wall heat transfer and is vastly superior to the ordinary film cooling effects because of the dependency on the degree of mixing.

b. Boron Trifluoride

Boron trifluoride appears to be quite stable with respect to dissociation at temperatures up to about 2800^OK (5040^OR) and as such would not be expected to react with the graphite capillary walls. This is confirmed by the "B" value calculations (not shown). As in the case of methane, three ratios of injection gas to "Hot-Solid" combustion gas mixture ratios have been considered, 1:9, 1:1, and 9:1. The results are not presented in detail since fluorides have been rejected as injection fluids.

The equilibration of BF_3 with the free stream principally effects the H_2) and the aluminum oxide species, both gaseous and condensed. A reduction in the concentration of these species is observed with consequent increase in concentration of g seous HBO. BHO_2, BOH (large), $AlOF$, AlF, AlF_2, AlF_3, and monatomic fluorine.

The amount of graphite nozzle wall material required to theoretically saturate one gram of three stream (injection gas plus combustion products) is shown in Figure 13. Interestingly, above 3200^OK the "B" values for BF_3 + combustion products are significantly lower then the "B" values for CH_4 + combustion products, indicating, from a thermochemical stantpoint, correspondingly lower amounts of reaction with the nozzle walls. However, the "B" values can never be negative so corrosion can only be reduced, provided that the mass transfer rates of the reactive fluoride species are not significantly greater than for the combustion products without injection. Close examination of Figure 14 shows that the reactions are exothermic for the temperature range of interest.

c. Nitrogen

Nitrogen, of course, represents an inert gas and would not be expected to react with the graphite walls of the injection capillaries. The increasing stability of gaseous CN above 2600^OK (4680^OR), however, indicates some minor reaction will occur above this temperature

As in the case of methane and BF_3, three ratios of nitrogen injection gas to "Hot-Solid" combustion gas mass flows have been considered, 1:9, 1:1, 9:1. In general, the equilibration of nitrogen with the free stream does not have major effects (other than dilution) on the concentration of the combustion product species. Exceptions are gaseous N_2, N, NO, H, and O. The dilution

FIGURE 13. "B" VALUES FOR GRAPHITE IN EQUILIBRIUM WITH "HOT SOLID" - BF_3 MIXTURES AT 400 PSIA
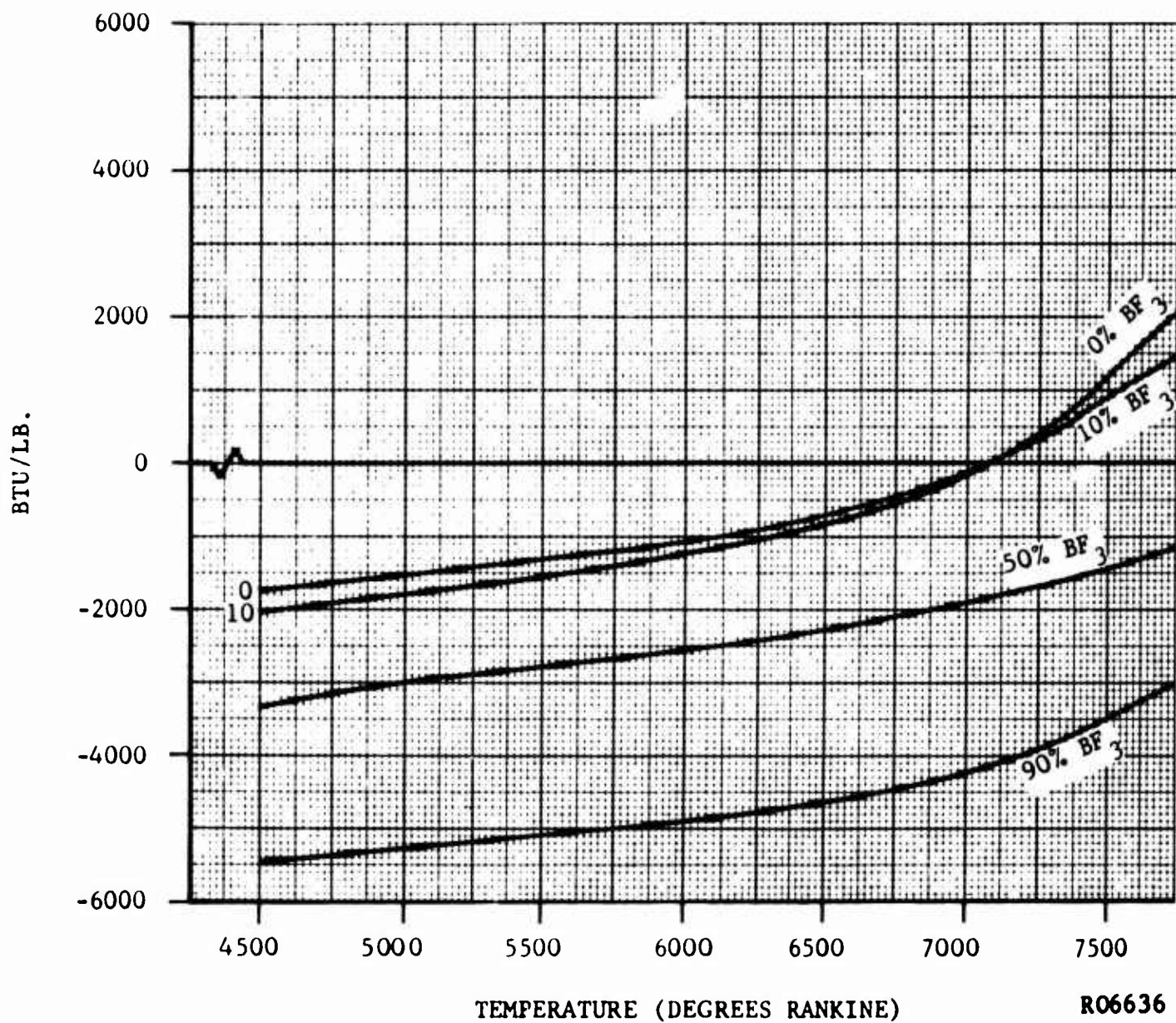
FIGURE 14. ENTHALPY VERSUS TEMPERATURE FOR EQUILIBRIUM MIXTURES OF "HOT SOLID" - BF_3 AT 400 PSIA

-22-

tends to increase the dissociation of H_2, H_2O, O_2, and CO_2, but the heat absorbed is apparently much less than for the case of methane addition.

Figure 15 shows the amount of wall material required to theoretically saturate one gram of free stream (injection gas plus free stream). The difference in "B" values in going from 0 w/o N_2 to 90 w/o N_2 at any temperature reflects principally a dilution effect rather than changes in the reactivity of the gaseous mixture with the graphite

Figure 16 gives the enthalpy, in BTU/lb, of the combustion product free stream and the free stream plus various ... t percentages of N_2. Apparently, the outer portions of the boundary layer will be effected by the endothermic reactions, but a wall at 5000° F would not be equally affected due to the exothermic recombination reactions which would occur

d. Conclusions

It is clear that the equilibrium thermochemical analysis does not provide a completely valid description of the boundary layer chemistry in the rocket nozzle. The assumption of equilibrium is apparently unavoidable but there are at least two reasons why it can be doubted. Thus, it is difficult to imagine that the Al_2O_3 particles could be in equilibrium in the injection boundary layer, either relative to the condensed carbon for methane injection or to the combustion product-injection gas mixture. In fact, the concentration of Al_2O_3 in the boundary layer may be significantly different than in the main combustion product flow, whereas uniform distribution has been assumed. Consequently, calculations were performed for methane injection with the condensed Al_2O_3 removed. The results are not completely reduced for presentation in this report. Apparently the removal of the Al_2O_3 has little influence on effectiveness of the methane. The H_2O, CO_2, O_2, O, and OH concentrations are reduced even farther and the zero "B" values are shifted to slightly higher temperatures at comparable mixture ratios.

It is also rather doubtful that the carbon particles which result from the methane dissociation in the cooling passages will achieve equilibrium with the gas phase. Due to flow turning, flow acceleration, and boundary layer turbulence the carbon particles may not be distributed uniformly across the boundary layer. It would be preferable to force the condensed carbon to form after injection into the boundary layer to achieve the smallest particle size. In general, this would require lower injection temperatures or higher injection rates, neither of which is desirable. Evidently, the efficiency of the injected carbon as a chemical reaction filter can only be determined by actual motor firings. However, it has been estimated that the injection design flow rate of one half percent of the subscale combustion product flow yields carbon equivalent to the corrosion rate of about 5 mils per second over 40 in^2 of nozzle surface at temperatures below about 5000^oF. Since the no injection corrosion rate should not be more than about one mil per second, it is concluded that the methane injection provides excess carbon which will improve the apparent effectiveness of the injection.
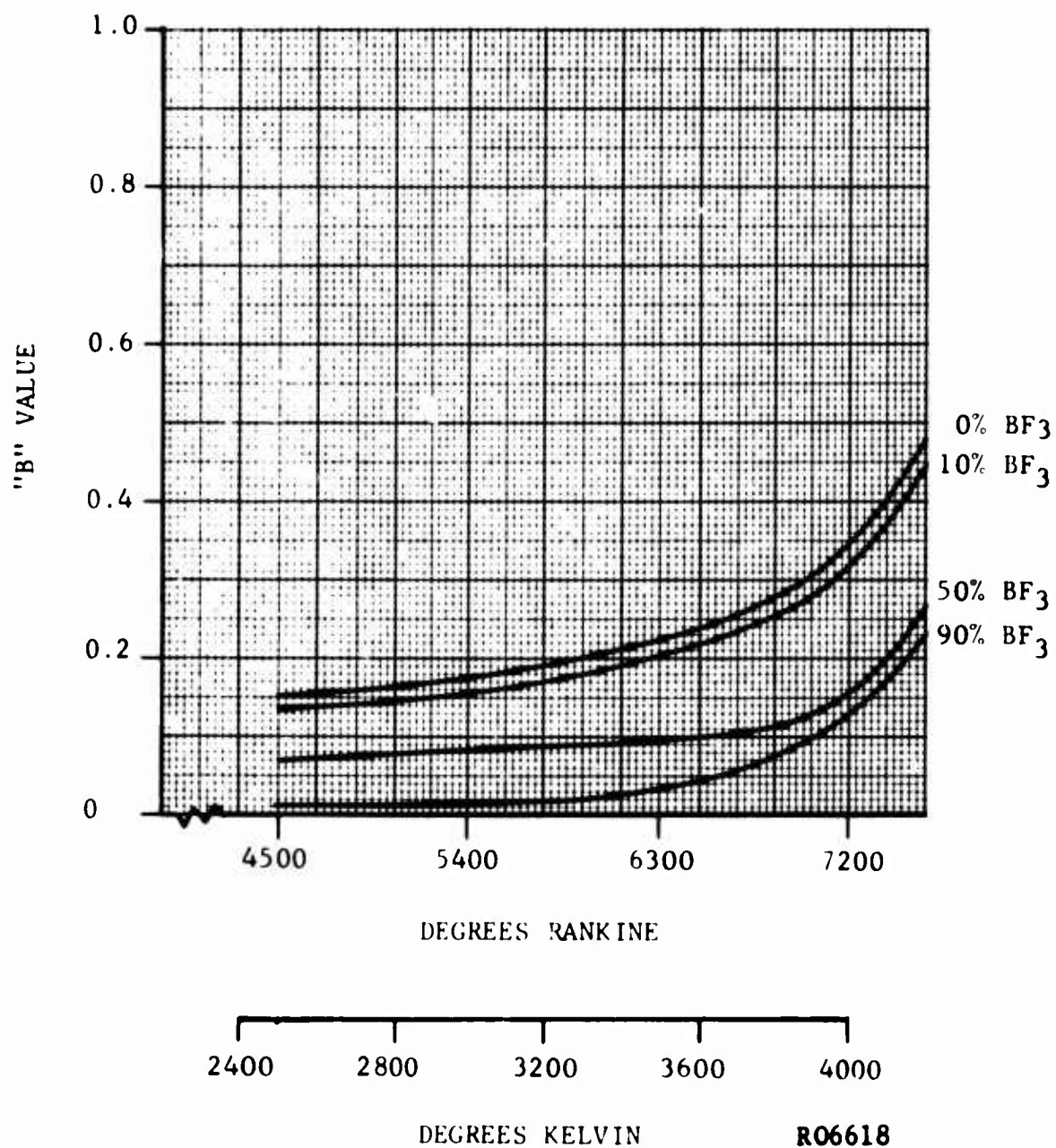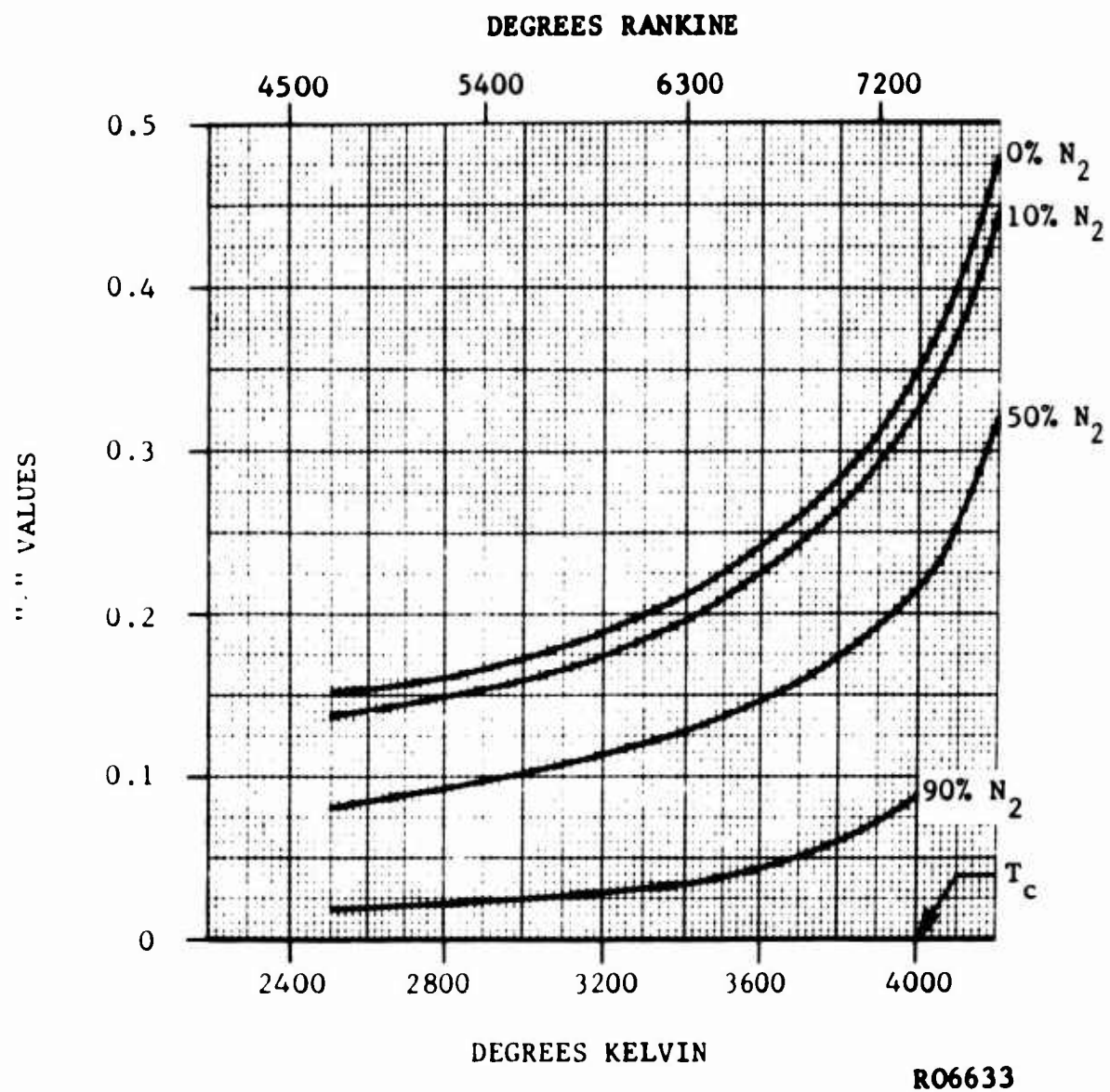
FIGURE 15. "B" VALUES FOR GRAPHITE IN EQUILIBRIUM WITH "HOT SOLID" - N_2
MIXTURES AT 400 PSIA
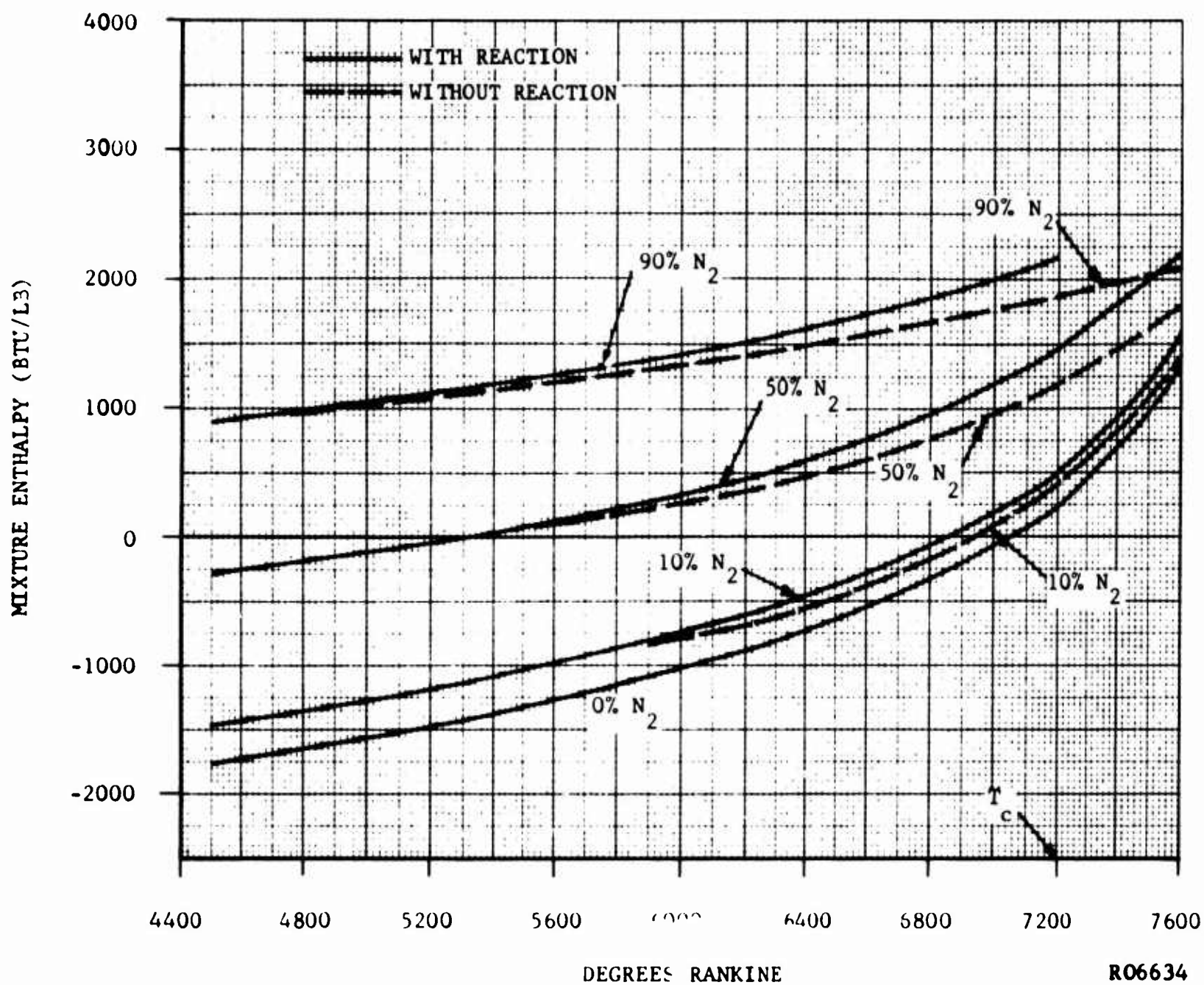
FIGURE 16. ENTHALPY VERSUS TEMPERATURE FOR EQUILIBRIUM MIXTURES OF "HOT-SOLID" - N_2 AT 400 PSIA

-25-

Another point which should be considered involves the assumed composition of the combustion products which are displaced by the injection. Since solid propellant motors and the Philco simulator use ablative chamber liners, there will be a significant amount of boundary layer mass addition up stream of the nozzle inlet. It is expected that, for the present propellant simulation, there may be significant H_2, N_2, and possibly H_2O enrichment of the nozzle boundary layer. There may also be some carbon enrichment resulting from the injection of the phenolic pyrolysis products through the porous chamber liner. It is interesting to speculate that the corrosion rates with no injection in solid propellant motors may be significantly effected by the choice of ablative liner material, engine size, the time dependence of the pyrolysis rate and the use of porous graphite liners. These factors should all be considered. It is currently felt that the pyrolysis mass addition generally increases the requirements for nozzle surface temperature control to minimize the influence of the hydrogen enrichment. At the same time, it is expected that temperature control will be potentially more effective in corrosion control.

In spite of these deviations from the ideal conditions assumed for analysis, it is felt that the control of corrosion by boundary layer injection will be extremely effective The major theoretical advantages of carbon injection provide the basis for preferentially choosing injection fluids from the C-H, C-Cl or C-H-Cl compounds. A number of inert gases can provide significant corrosion reduction through the chemical sink and dilution mechanisms.

During the second quarter, work will proceed in evaluating (1) the methane - no Al_2O_3 (2) the CCl_4 and (3) the C-H-Cl injection systems. It is anticipated that some additional calculations will be required to provide the temperature-pressure-enthalpy-composition relations for the injection fluid or fluids chosen for the subscale tests. This information will eventually be required for use with the boundary layer film analysis.

2.2 FLUID MECHANICS

A primary advantage of the nozzle concept under study is that fluid injection over the throat contour provides the designer with the opportunity to moderate the interaction of the combustion products with the nozzle wall. It is clear that materials, chemical, thermal and structural responses will be effected and can be controlled to the same degree that the injection fluid behavior can be predicted and controlled. The boundary layer fluid mechanics studies have essentially been split into two areas, namely, (1) fluid injection and (2) injection film analysis. These areas will be discussed briefly before proceeding with the presentation of the results of the work of the first quarter.

A great deal of study and analysis of slot and hole injection for film cooling has preceeded this investigation. Unfortunately, the results have lacked sophistication and/or feature mass injection rates which are greater than either those considered here or the displaced boundary layer mass flow. Because the present injection is essentially a boundary layer problem, very little of the previous work in film cooling is thought to apply. It is clear, however, that the most efficient film injection can be achieved by tangential slot injection. For the present design concept, very low mass injection rates lead to very narrow slots, the dimensional stability of which could not be maintained during a nozzle test. A transpiration injection, such as it described in Reference 1, could also efficiently generate a uniform film. This approach would be unsatisfactory for coolants which decompose to carbon. Other disadvantages of this injection method were considered during contract AF 04(611)-8387 and, consequently, it is not actively being considered. The last choice is to inject the fluid through a large number of discrete holes in the wall. The advantages of this type of injection are currently thought to outweigh the disadvantages. However, the three dimensional wall jet, with heat transfer, diffusion and chemical reaction, cannot be reasonably analyzed. Therefore, the study of hole type injection is primarily being approached experimentally. Areas of interest which have been or will be investigated include:

(1) the influence of the various jet and free stream flow parameters on the jet attachment to or detachment from the wall,

(2) the momentum mixing which occurs along the jet-free stream boundary,

(3) the influence of injection parameters on jet spreading and coalescence,

(4) the influence of the initial jet and free stream boundary layers on the injection interaction,

(5) the influence of jet density and nozzle acceleration on the injection and spreading.

From the results obtained to date, it is apparent that the injection jets will attach to the wall for the anticipated nozzle design and flow conditions

(including angular injection). It is also evident that the diffusive spreading of the injection fluid is slow so that jet coalescence in short distances can be achieved only through extensive turbulent mixing (not desired) or by increasing the work done on the jet by the free stream. In the latter case, the introduction of a small circumferential swirl component, to the injection velocity vector, may spread the jet without introducing excessive mixing or turbulence. The recognition of the overall complexity of the injection interaction problem has delayed (and possibly precludes) the formulation of definitive statements concerning the choice of parameters such as hole angles, hole spacing, hole size, axial position for injection, fluid density, etc. However, it has been tentatively concluded that; injection in the flow acceleration region is not desirable; minimum practical hole spacings are desired; injection angles near 15° are satisfactory, the fluid injection velocities should approach the local free stream velocity; and minimum hole size, approaching the displaced combustion product boundary layer thickness, is desirable. It should also be noted that, the generation of a continuous film is not an absolute requirement of the injection. Of course, a discontinuous film will not be as efficient, thermally or chemically, as a continuous one. Also, additional turbulence generated by the swirl type injection could significantly reduce the protection length of a continuous film generated in that manner.

It has been necessary to assume that the injection could produce a continuous film for the purposes of analyzing the subsequent behavior of the injection fluid in the nozzle. Immediately after injection, the two streams will tend to exchange mass, momentum and energy at rates which should decrease exponentially with time. Any turbulence, in addition to that characteristic of the two streams at injection, generated due to the momentum mixing at the free stream-jet interface will tend to accelerate the mass and energy mixing. That is, injection induced turbulent convective mixing will be more important than the mass diffusion and thermal conduction. Apparently, it is desirable that the net transfer of momentum between the streams be close to zero. The extent of the initial injection mixing, and consequently the subsequent thermal and chemical behavior of the modified film, cannot be accurately predicted because of poor understanding of the fundamentals of turbulence. Following the initial mixing, the momentum and energy discontinuities in the boundary layer will tend to disappear and the modified boundary layer will continue to develop in a relatively normal manner. In general; the new energy thicknesses will be larger; the momentum thicknesses are likely to be larger, but could be smaller for high injection mass flux; the two fluids will continue to mix chemically under the influence of convective and diffusional mass transport; and the detailed film boundary layer development will be dependent on the chemical reactions which occur during mixing. Under reasonable injection conditions, the composition of the fluid immediately adjacent to the wall will not change (from the injection fluid composition) for a distance downstream which may be as great as ten hole diameters. Subsequently, dilution by the most mobile of the free stream species will proceed. For the methane injection, the dilution by the reactive species (H_2O, CO_2, O_2, etc.) will be retarded or eliminated by chemical reactions in the chemical mixing region of the boundary layer. The compositional readjustments are expected to persist throughout the nozzle, partially due to the very short residence times. The heat transfer in the nozzle throat region will be reduced by several mechanisms, namely:

(1) the increases in boundary layer energy and momentum thicknesses
     due to the initial energy and momentum decrements of the injected
     fluid,

(2) similar increases in boundary layer parameters and heat blocking
     due to endothermic chemical reactions,

(3) repression of free stream recombination reactions near the wall,

(4) alteration of the boundary layer heat transfer properties due to
     composition changes.

It should be noted that the similarity between the heat and mass transfer
phenomenon suggests that corrosion rates will also be reduced in the same manner.
It may also be observed that the increases in boundary layer thicknesses will
induce proportional thrust losses unless the injection fluid has higher impulse
that the combustion products it replaces. This would be a strong argument for the
use of methane (which decomposes to hydrogen) or helium except that the boundary
layer losses are small to begin with and the preservation of the throat contour
precludes other thrust losses.

Investigation of the fluid mechanic properties of a three-dimensional
wall jet is currently in progress. This study is divided into three avenues of
approach, all directed toward the achievement of an efficient film injection
design. The avenues consist of (1) cold flow and chemical reaction experiments,
(2) mathematical solution of the pertinent boundary layer equations, and (3) a
literature survey. Since the cold flow and chemical reaction experiments are
discussed in Sections 3.2 and 3.1, respectively, this section discusses the
latter two methods of approach.

During the first quarter of the contract period there have been two
mathematical treatments devised to calculate fluid mechanic and heat transfer
phenomena in the nozzle with film injection. Each of these is regarded as
impractical for application to the present problem. The first assumes uniform
slot injection parallel to the free stream. The boundary layer, downstream from
injection was divided into two regions. In the region near the wall (laminar
layer) a constant shearing stress was assumed (linear velocity distribution) and
the momentum equation was solved by the integral method. This layer is assumed
to be defined by, and contain, the injection fluid. In the second region (turbulent
layer) a 1/7 power velocity distribution was assumed and the appropriate momentum
equation solved. To combine the two momentum equations, the shearing stresses
are equated at the interface of the two regions. The height of the laminar layer
is found from a mass balance on the injected fluid and, by similarity, the heat
transfer can be found. The assumptions of a linear velocity and injectant mass
balance in the laminar layer are invalid when the injected velocity or the height
of the injection slot is large relative to the velocity and thickness of the
laminar sublayer existing in the nozzle.

A second analysis was devised for predicting the temperature and velocity

distribution that exists in the mixing and developed regions of the injection film. The analysis was not actually carried out because of a requirement for the development of a very complicated computer program for performing the calculations. A brief description of the analysis follows.

Assuming a two-dimensional wall jet and tangential injection with respect to the surface, the conventional mass, momentum and energy equations for a compressible, turbulent boundary layer may be written. Assuming that the Lewis and turbulent Prandlt numbers are unity (diffusion and energy equation are independent and eddy viscosity equals eddy conductivity), the boundary layer is separated into two regions and the eddy viscosities of Diessler are used (Ref. 2).

Region 1 (near wall) $y^+ < 26$

$$\epsilon = 0.124 \, Uy \left[1 - \exp \left(-n^2 yU/\mu\rho \right) \right]$$

Region 2 $Y^+ > 26$

$$\epsilon = 0.36 \frac{(U/dy)^3}{(d^2U/dy)^2}$$

where $Y^+ = \dfrac{Y\sqrt{\tau_w/\rho}}{\nu}$

Introducing a stream function which satisfies the continuity equation (i.e. $\dfrac{\partial \rho U}{\partial x} + \dfrac{\partial \rho V}{\partial y} = 0$ and $\dfrac{\partial \psi}{\partial y} = \rho U$, $\partial \psi / \partial x = -\rho V$) one may solve the momentum and energy equation by a numerical method if the initial velocity and temperature profiles are given at the point of injection. It may be noted that no limitation is imposed on the velocity distribution in the jet mixing region; although a singularity point may arise at the point of injection, i.e., where the free stream transfers from the wall to a free shear region. This problem has been solved by Denison and Baum (Ref. 3) by use of a transformation which eliminates this singularity point.

At the present time a third mathematical approach to the injection film analysis is in progress. This method will eliminate the poor assumptions of the first method and the excessive cost of the second.

A literature search is in progress and certain conclusions have been obtained concerning various film parameters. Some of these conclusions appear to require experimental verification. A few of the important parameters are discussed below.

Seban and Back (Ref. 4) have found that the effect of an accelerating flow on the thermal protection aspects of film injection depends largely on the location of large acceleration with respect to the initial momentum mixing region. These investigators have shown, experimentally, that a remarkable decrease in

thermal protection occurs if large acceleration exists in the mixing region, whereas a negligible decrease results if acceleration is outside of the mixing region. Although the experiments were performed for cold flow and with a two-dimensional wall jet, these results will be applied to a test nozzle, in which the mixing region will exist upstream of an inlet area ratio of 1.3 (starting point of large acceleration).

The dependence of the initial free stream velocity boundary layer thickness on heat transfer has been reported in Reference 5. It was experimentally shown that relatively small changes in heat transfer resulted from large changes in upstream boundary layer thickness. This conclusion was applicable to a two-dimensional jet and may not be applied to a three-dimensional jet. That is, because of the difference in the hydrodynamic flow field, a three-dimensional wall jet has a relatively large contact area or region with the free stream (in comparison with a two-dimensional jet) and, thus, the shearing stress at the jet-free stream interface may significantly alter the flow field. Therefore, it is concluded that the study of the variation in velocity boundary layer thickness should be included in the cold flow tests.

The machining properties of the nozzle material (pyrolytic graphite) impose certain limitations upon selection of the injection hole geometry. These limitations result from the fact that it is almost impossible to accurately drill a hole less than 0.040 inch in diameter at angles greater than 45°. The angle limitation implies that the injection angle (with respect to free stream) may be at maximum 15° for a 30° nozzle inlet angle.

The effect of injection angle on heat transfer has been reported in References 6 and 7. It was found that injection angle significantly influences downstream heat transfer. This may be due to the rather strong turbulent transport near the injection point that is produced by angled injection. Apparently, for maximum thermal protection, a minimum injection angle is required. Currently the effect of injection angle on wall coverage is being studied in the cold flow experiments with no definite conclusions resulting as of yet.

From the machining limitations, a hole size of 0.040 inch was selected for the nozzle. The selection of a minimum hole size is indicated from the fact that for minimum turbulent mixing between jet and free stream, it is desired that the wall jet remain near the nozzle surface and expose a minimum amount of its surface area to the free stream. That is, minimum turbulent mixing results when the jet, essentially, replaces a portion of the free stream boundary layer. If the jet diameter is sufficiently greater than the boundary layer height, the intense turbulence of the free stream will rapidly initiate mixing and a large amount of "protective fluid" will be lost. This suggests that for ideal injection a two-dimensional slot with a height equal to approximately the laminar sublayer of the free stream is desired. Therefore, in order to approach slot injection and reduce turbulent mixing, a minimum hole size and spacing are desired. Choice of hole spacing is dependent on jet spreading and is discussed in Section 3.2.

For a given total injectant mass flow rate and hole spacing, the selection of a minimum injection diameter produces a maximum $(\rho U)_{inj} / (\rho U)_\infty$. It has been found (Ref. 5) that for a two-dimensional jet the amount of thermal protection increases with $(\rho U)_{inj} / (\rho U)_\infty$ and reaches a maximum at a ratio of 0.90. Ratios larger than 1.1 result in a decrease of thermal protection. Therefore, assuming that this applies to a three-dimensional jet, it is desired to obtain an injection ρU ratio near unity. Additional influences of the ρU ratio on jet fluid mechanics are discussed in Section 3.2. It may be of interest to note that the ρU ratio for a single hole in the actual nozzle will not exceed 0.80 for methane injection.

It was origionally suggested that a study of injecting the coolant through a passage which consisted of a recess in the wall would be of interest. This design has been rejected because of the fluid dynamic properties of a step. For low $(\rho U)_{inj} / (\rho U)_\infty$ the flow approaches simple step flow. That is, down stream of the step the heat transfer increases considerably due to the reattachment of the free stream to the wall. From Reference 5 it has been shown that this phenomenon exists for $(\rho U)_{inj} / (\rho U)_\infty$ as large as 0.20 under cold flow conditions.

2.3 HEAT TRANSFER

a. Thermal Analyzer Program

Because of the three-dimensional geometry and the effects of the cooling gas, analytical solutions are not adequate for predicting the temperature distributions within the nozzle heat sink. Calculations of temperature distributions were therefore performed with the aid of a digital computer program called the Thermal Analyzer.

The equations solved by the Thermal Analyzer can be obtained by differencing the general partial differential equation for conduction in solids (For Fourier equation). Conceptually, however, it is simpler to derive the equations by performing an energy balance on a small section of the heat sink material.

The first step is to imagine that the heat sink is divided into a number of more or less rectangular sections. These sections are commonly called nodes since, in the electric circuit analogous to a thermal conduction problem, there is a node corresponding to each section. To obtain maximum accuracy for a given computing time, relatively small nodes should be used in regions where high temperature gradients are expected. Each node is identified by a number.

The next step is to perform an energy balance on each node. The heat capacity of a node times the node temperature rise in a given time interval must equal the heat conducted into the node from all adjoining nodes during the interval, i.e.

$$C_n(T_n^1 - T_n) = \left[\sum_m \frac{T_m - T_n}{R_{m,n}} \right] \angle t \qquad (1)$$

where

C_n = heat capacity of node n, $BTU/°F$

T_n^1 = temperature of node n at the end of time interval $\angle t$, $°F$

T_n = temperature of node n at the start of time interval Δt, $°F$

T_m = temperature of an adjoining node (designation number m) at the start of time interval t, $°F$

$R_{m,n}$ = the thermal resistance between nodes m and n,

$\frac{°Fsec}{BTU}$

Δt = time interval, sec

-33-

This equation can be rearranged to give

$$T_n^1 = T_n + \frac{\Delta t}{C_n} \sum_m \frac{T_m - T_n}{R_{m,n}} \qquad (2)$$

Note that the quantity $\sum_m \dfrac{T_m - T_n}{R_{m,n}}$ is assumed to be constant over the time

interval. The error introduced by this assumption, called truncation error, may be reduced by using a small Δt.

Equation (1) actually represents a set of equations, one for each node. The equations are applied step by step starting with known initial temperatures. The temperatures computed for the end of one time step form the starting temperatures for the next step. Thus complete temperature histories for each node are obtained.

It can be shown that the numerical solution described above will be unstable if the time increment, Δt, is too large. The condition which must be met to insure stability is

$$\Delta t < \Delta t_{RC_n} = \frac{C_n}{\sum_m \frac{1}{R_{m,n}}} \quad sec$$

for each node. The Thermal Analyzer Program automatically computes the "RC time", Δt_{RC}, for each node and sets Δt to 1/4 of the minimum value. This not only insures numerical stability, but tends to keep the truncation error small.

The nodal division used for one nozzle configuration is shown in Figure 17. This configuration will be used to illustrate how the Thermal Analyzer Program is being applied. Note that, because of symmetry, the profile surfaces of the wedge section shown can be assumed insulated.

Equation (2) written for node 4 of Figure 17 would be

$$T_4^1 = T_4 + \frac{\Delta t}{C_4} \frac{T_{hg} - T_4}{R_{4,hg}} + \frac{T_3 - T_4}{R_{3,4}} + \frac{T_5 - T_4}{R_{4,5}} + \frac{T_{10} - T_4}{R_{4,10}}$$

(the subscript hg represents the he ᵤ .

The heat capacity of node 4 is given by

$$C_4 = V_4 \, \rho \, c$$

-34-
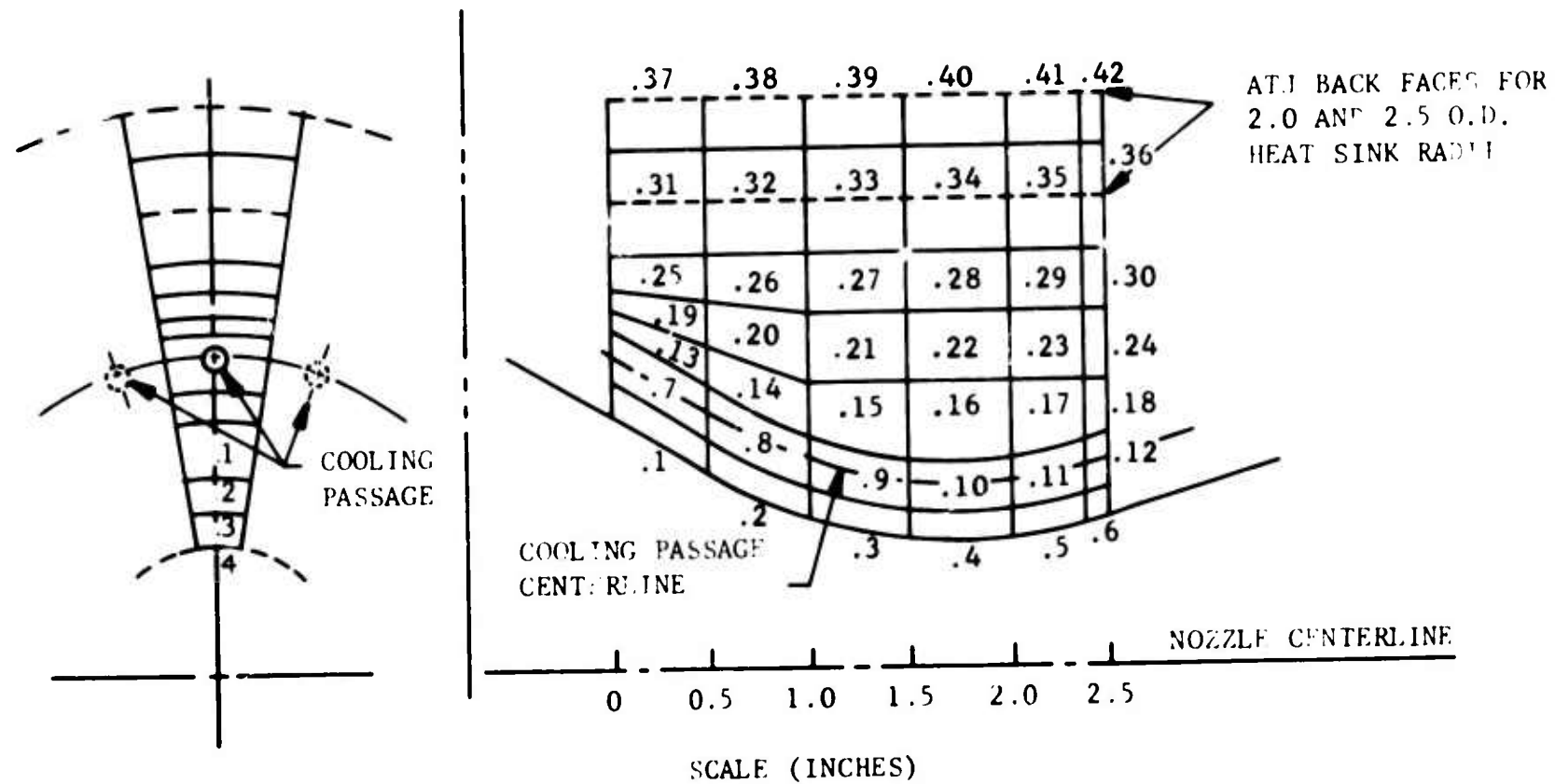
FIGURE 17. TYPICAL NODE BREAKDOWN - SUB-SCALE NOZZLE

-35-

R06665

where V_4 is the volume of node 4, ρ is the pyrolytic-graphite density, and c is the PG specific heat. Since specific heat is a function of temperature, it is evaluated at each time step as a function of T_4.

The thermal resistance between node 4 and the hot gas is taken

$$R_{4,hg} = \frac{1}{h_{hg} A_{4,hg}}$$

where h_{hg} is the local hot gas heat transfer coefficient at the center of node 4 and $A_{4,hg}$ is the area of the face of node 4 exposed to the hot gas.

The thermal resistance between nodes 4 and 10 was assumed to be

$$R_{4,10} = \frac{\ell_{4,10}}{A_{4,10} k_a}$$

where $\ell_{4,10}$ is the distance between the centers of nodes 4 and 10, $A_{4,10}$ is the area of the common interface between nodes 4 and 10, and k_a is the PG a-direction conductivity. Since k_a is a function of temperature, it was evaluated at each time step as a function of the <u>average</u> temperature between nodes 4 and 10.

The thermal resistance between nodes 3 and 4 was computed from

$$R_{3,4} = \frac{\ell_{3,4}}{A_{3,4} k_c}$$

where k_c is the PG c-direction thermal conductivity evaluated at the average temperature between nodes 3 and 4.

The formulas given for C_4, $R_{4,hg}$, $R_{4,10}$, and $R_{3,4}$ illustrate the methods used to compute all "circuit constants" except those required in the cooling gas calculations.

Because of the flow of the cooling gas, special equations are required for the cooling gas temperature evaluation. (While the hot gas also flows, no special equations are required for the hot gas temperature evaluation since the recovery temperature can be assumed constant with negligible error).

The cooling gas temperature is described by the following differential equation.

$$A \rho_g C_g \frac{\partial T}{\partial t} + \dot{w} C_g \frac{\partial T}{\partial x} = h_{cg} P(T_w - T) \tag{3}$$

where A is the local cross-sectional area of the cooling passage, ρ g is the local cooling gas density, c$_g$ is the cooling gas specific heat (function of temperature), $\dot{w}$ is the flow rate, h$_{cg}$ is the local heat transfer coefficient, P is the local cooling passage perimeter, Tw is the local PG wall temperature, t is time, and x is a coordinate measured along the cooling passage axis. An order of magnitude analysis shows that, for the conditions being investigated, the first term on the left hand side of this equation may be neglected. The remaining equation may be differenced to give*

$$\frac{T_{n+1} - T_n}{\ell} = \frac{h_{cg} P}{\dot{w} c_{cg}} \left(T_m - \frac{T_{n+1} + T_n}{2} \right) \tag{4}$$

where

T_n is the temperature of cooling gas fluid node n, ^oF

T_{n+1} is the temperature of the next fluid node downstream of n, ^oF

ℓ is the distance between nodes m and n (along axis of cooling passage)

T_m is the temperature of a PG node with a center half-way between nodes n and n + 1

In this equation, c$_g$ is evaluated at the average temperature of nodes n and n + 1.

With the set of equations represented by (4) the temperatures of all cooling gas nodes can be computed at the start of each time step. The known entrance temperature is used to compute the first downstream temperature which in turn is used to compute the next downstream temperature, etc. In cases where the gas specific heat is a function of temperature, it is necessary to evaluate c$_g$ with the temperature obtained from the previous time step in order to keep (4) an explicit equation for T_{n+1}.

---

* The cooling passage is assumed to be divided into "fluid nodes". In Figure there are fluid node centers coincident with the center of node 12; at the centers of the interfaces between nodes 7, 8, 9, 10, 11 and 12; and at the downstream end of node

b.   **Conduction - Internal Convection**

(1)   **Introduction**

This area of the analysis is concerned with the interrelation of a pyrolytic graphite heat sink with heat internally extracted by convection to a gaseous coolant. The purpose of the convection cooling is to lower the asymptotic value of the wall temperature so that corrosion will be decreased. This analysis will ultimately be combined with the injected film analysis to obtain an overall optimization. Presently, however, the study involves only the conduction - internal convection with given hot gas side convection coefficients to indicate the heat sink temperature response with variations in heat sink size, coolant flow rate, material and coolant thermal properties, and scaling.

Initially, the problem was attacked empirically utilizing data obtained in Contract AF 04(611)-8387. Then the thermal analyzer computer program, described in Section 2.3a, was applied for detailed solutions. The purpose of the empirical analysis was to estimate heat absorption required by the coolant as a function of wall temperature and duration. This analysis aided in selecting inputs for the computer program.

Since methane appears to be the best coolant for this application based on chemical and heat transfer studies (See Section 2.1), determination of its heat transfer coefficient in a tube with chemical reaction, two-phase flow and radiation effects is in progress. Preliminary results of this analysis indicate a significant improvement in the heat transfer coefficient over that predicted using the properties of undissociated methane. The computer calculations presented in this report are based on the latter, hence they are quite conservative.

(2)   **Empirical Analysis of Cooled Heat Sink**

A preliminary approach to study the percentages of the total heat transferred to the nozzle which are absorbed by the coolant and the solid heat sink was accomplished using the computer results and test results of the first demonstration nozzle tested under Contract AF 04(611)-8387. These results are reported in Ref. 8   and are reproduced here in Figure 18.   The nozzle produced 5000 lb. thrust with a 2.5 inch diameter throat and had a heat sink outside diameter of 7.0 inches. The combustion temperature was 6450°F and the convection heat transfer coefficient was 0.0053 BTU/sec in^2 °F. These values are somewhat lower than those being considered in this contract (T_g =6720°F and h_g =.006 BTU/sec in^2 °F); however, they are representative and are sufficient for the purposes of this preliminary analysis.

By plotting log T versus log r with time, t, as a parameter where T in temperature, °F, and r is radius, inches; an empirical equation can be written of the form

$$T = a(t) \ r^{-b(t)}$$

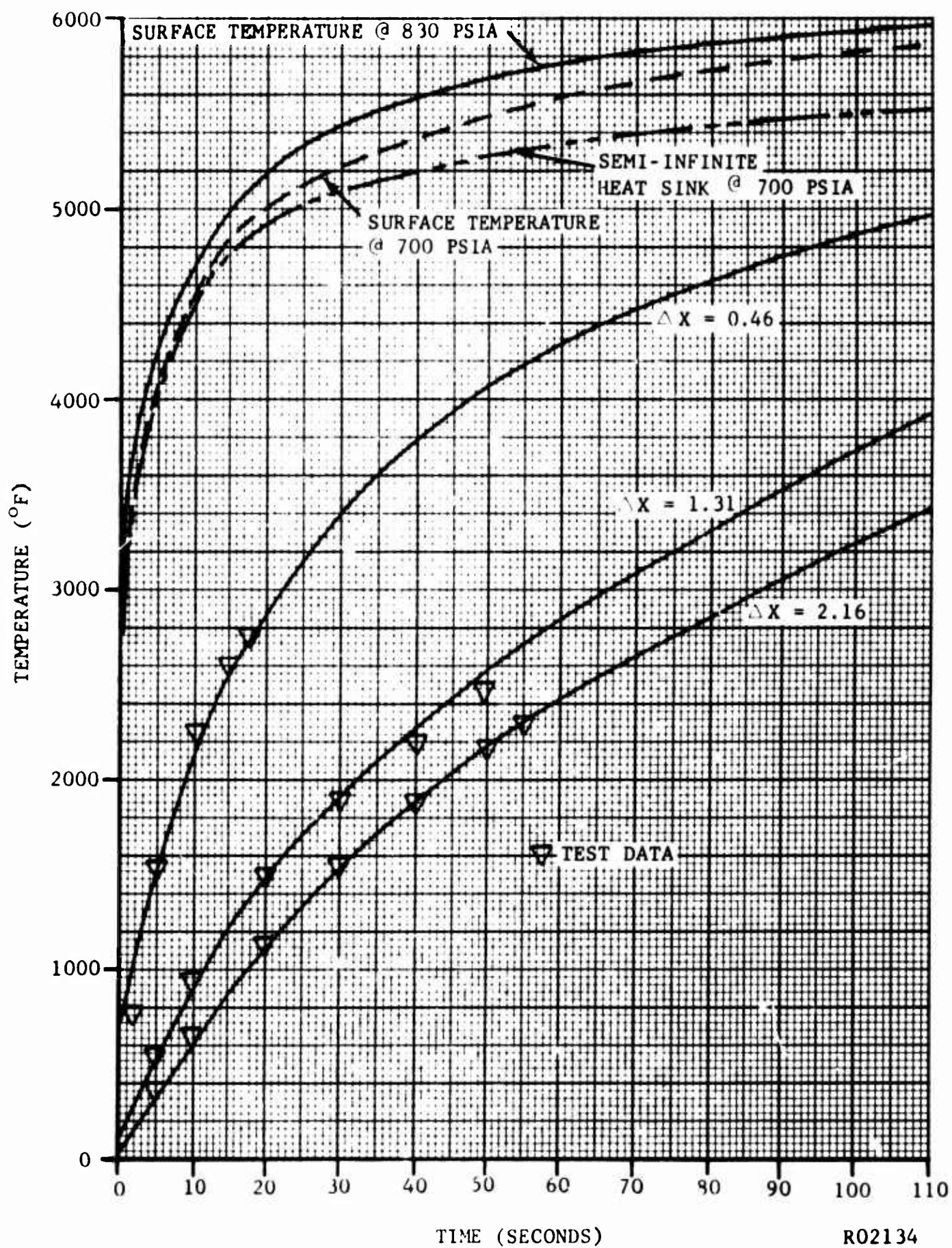where a linear log-log plot is obtained. The actual plot was very nearly linear

FIGURE 18. PYROLYTIC GRAPHITE HEAT SINK TEMPERATURE HISTORY
AT THROAT COMPARING CALCULATIONS AND TEST DATA

-39-

hence this method could be utilized. The equation obtained was

$$T = \frac{3550\ t^{0.11}}{\dfrac{r}{r_o}\ 12.4t^{-0.65}}$$

where the r_o is the inside radius of the nozzle. The numerator of the right hand side is, of course, the wall temperature. By holding the wall temperature at a desired value, the heat sink temperature distribution as a function of time can be obtained. This method gives a result approximately the same as can be obtained from the graphical Schmidt method. This method assumes the surface temperature control is obtained by extracting the surplus heat at $r=r_o$. Figure 19 shows the result obtained by allowing the wall temperature to increase to 4800^oF and then held constant, as compared with the normal heat sink response.

The heat stored in the heat sink at any time can easily be computed using appropriate temperature profile and the total heat versus temperature curve for pyrolytic graphite shown in Figure 20 (Ref. 9). Also knowing the wall temperature history, the total heat transferred to the wall up to any given time can be calculated. The results of this calculation for the nozzle described at the beginning of the section are shown in Figure 21 . The heat which must be removed to maintain a wall temperature of 4800^oF is the difference between the top curve (heat stored in heat sink with temperature control). The curve showing heat transferred to and absorbed by an uncooled heat sink is included for comparison. These calculations are based on a nozzle section one inch long located at the throat. Figure 22 depicts the rate at which heat must be removed as a function of time to maintain 4800^oF wall temperature. The dashed curve in the same figure indicates the profile achieved by varying the coolant flow rate linearly starting at a value one-half the final flow rate. Computer results with this type of flow rate variation are presented in Section 2.3b (3).

(3) Conduction - Convection Computer Study

The thermal response of a convectively-cooled heat sink was studied in more detail using the Lockheed Thermal Analyzer program described in Section 2.3a. The analyses to date have been, out of necessity, a study of trends established by varying heat sink thermal conductivity, heat sink size, coolant flow rate and composition, hot gas side convection coefficient and nozzle size (scaling). The exception to his general treatment was the fairly exact analysis of the sub-scale (1000 lbs. thrust) configuration with no injection.

Concurrent with this computer study, the determination of the convection heat transfer coefficient of methane including the effects of dissociation has been in progress (See the following paragraph 4). In the meantime, the values used for the computer input were calculated using the properties of undissociated methane. As will be discussed later, the actual value is considerably higher than that used in these calculations. This will mean that all calculation made
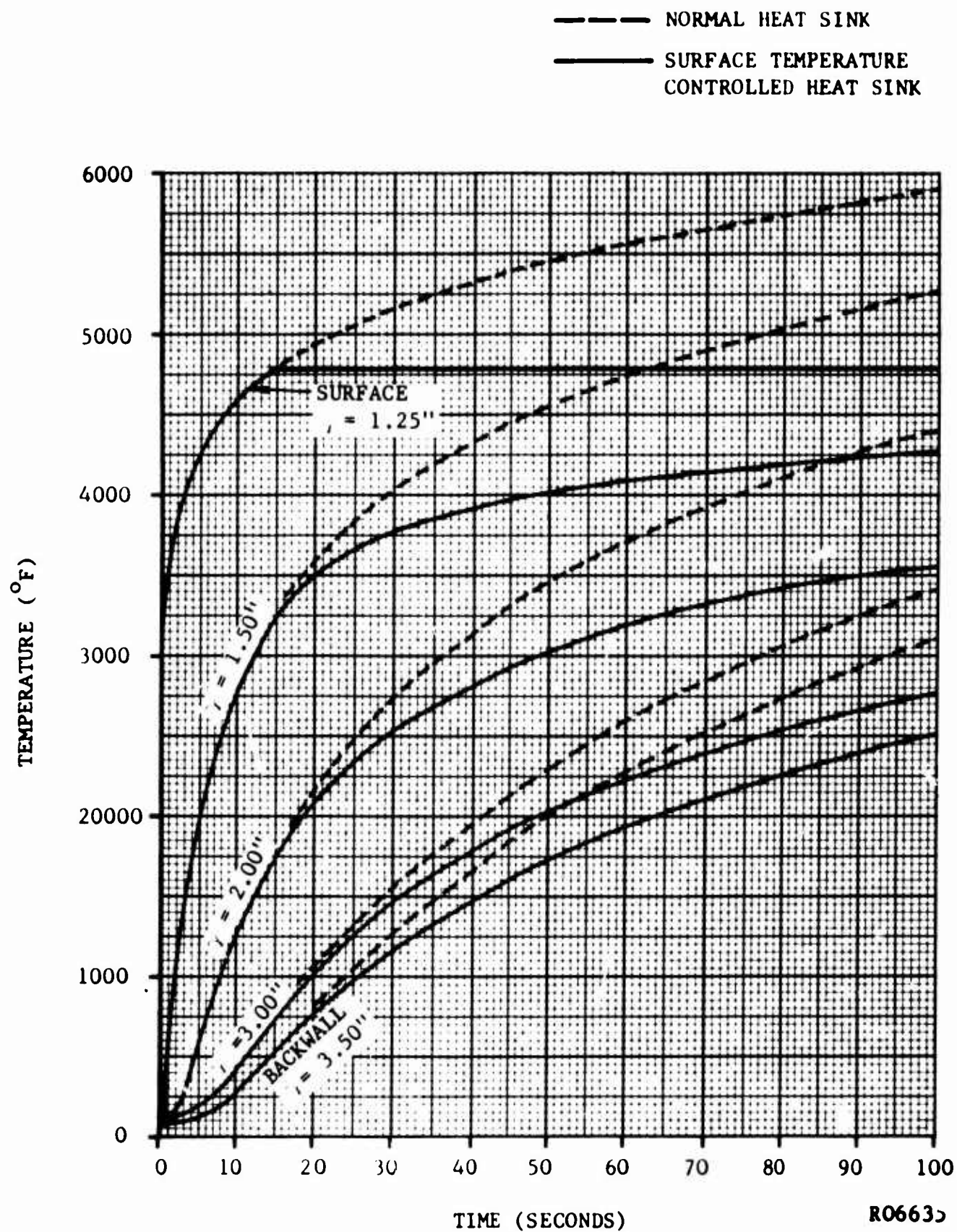
FIGURE 19. COMPARISON OF TEMPERATURE HISTORIES WITH AND WITHOUT
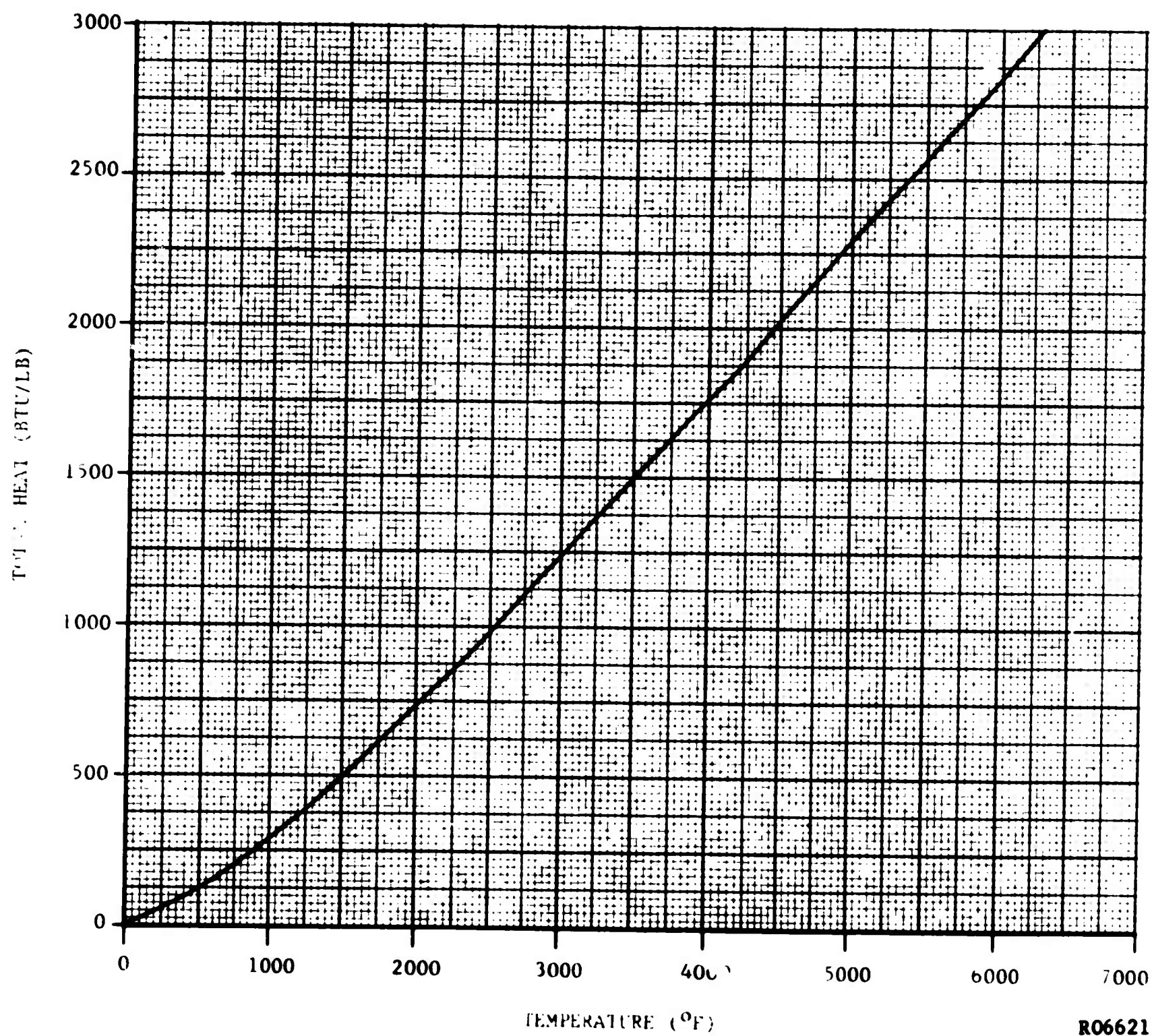SURFACE TEMPERATURE CONTROL

FIGURE 20.   TOTAL HEAT OF PYROLYTIC GRAPHITE VERSUS TEMPERATURE
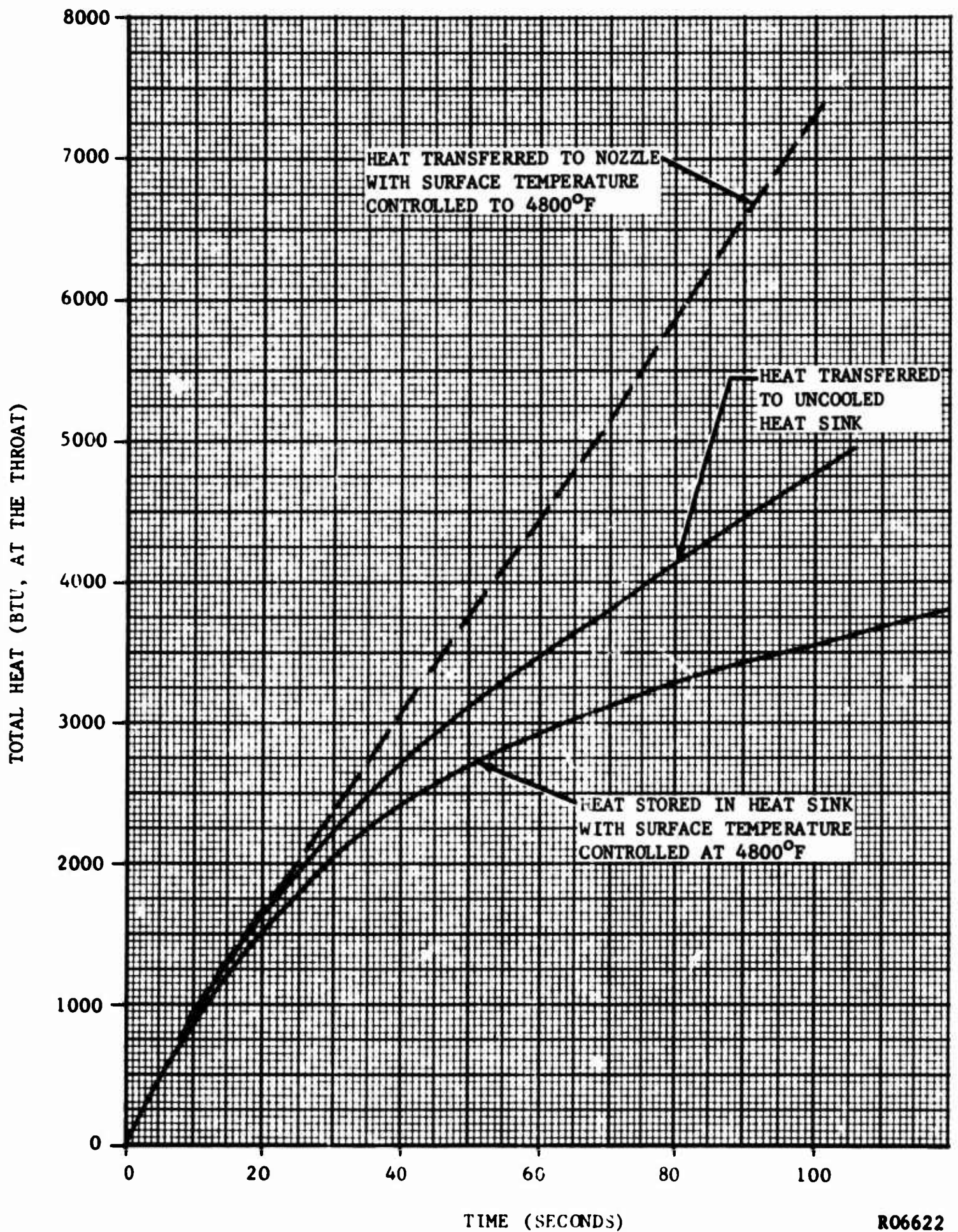
R06621

FIGURE 21. EFFECTS OF SURFACE TEMPERATURE CONTROL ON HEAT TRANSFERRED AND STORED
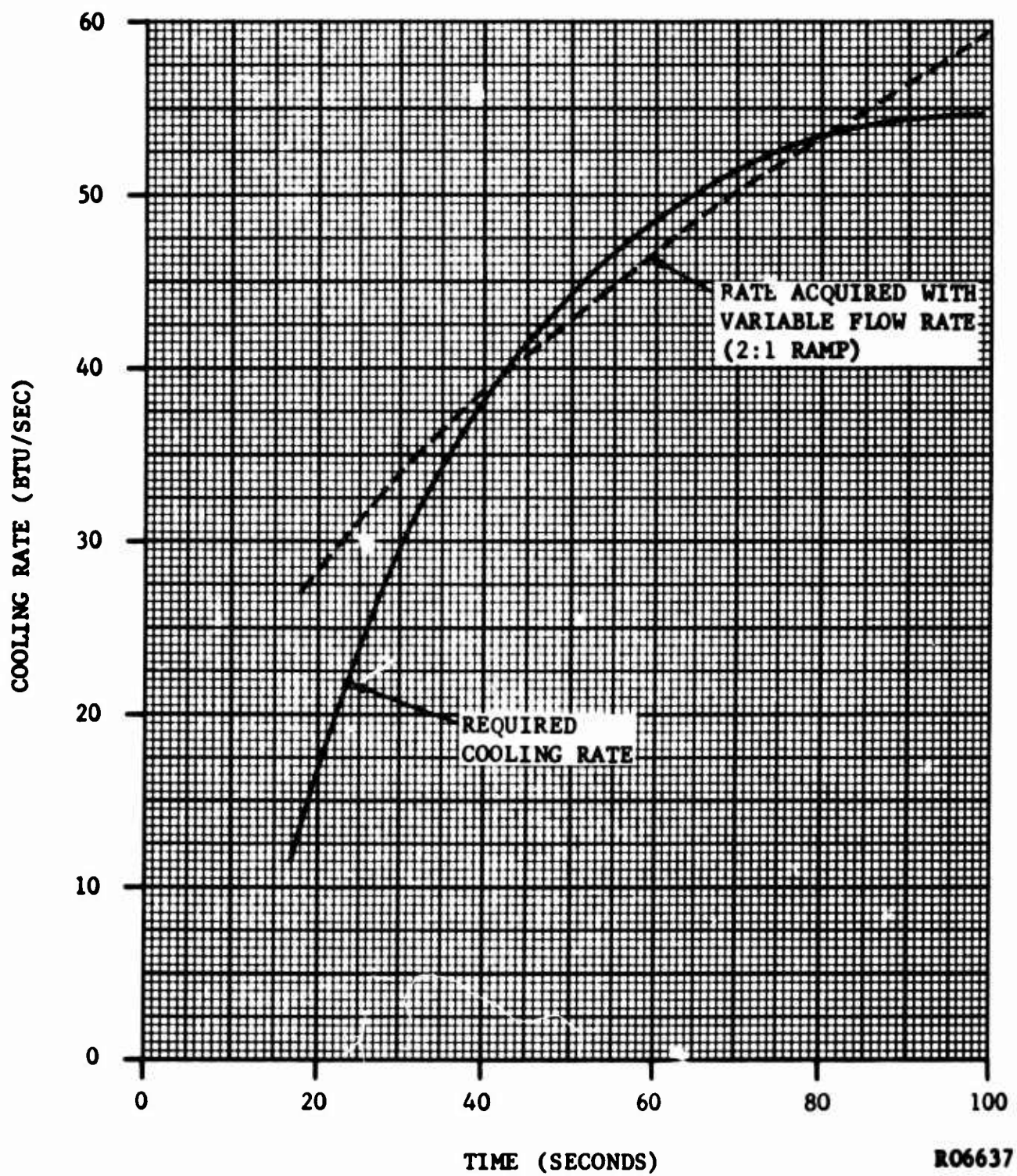
FIGURE 22. COOLING RATE TO MAINTAIN CONSTANT 4800°F WALL TEMPERATURE

are conservative. Once the calculations are finalized, a previous computer run will be repeated to determine the effect. Temperatures measured in the sub-scale tests will verify these effects.

Figure 23 shows typical results of a computer run. There is a steep, rather linear temperature gradient between the surface and the cooling passage. From the cooling passage to the backwall are the normal transient profiles. For comparison, a temperature profile of an uncooled heat sink of the same configuration and subjected to the same conditions is shown.

A search through the literature for thermal properties of pyrolytic graphite indicated that the only widely published thermal conductivity data at high temperature was obtained at Raytheon (Reference 10, 11, 12 & 13). Another source of data was the High Temperature Material Inc. catalogue which contained extropolated data. The latter was 20% lower at high temperature (4000°F and above). The Raytheon and HTM curves are shown in Figure 24 . Each of these curves were input into the computer program with otherwise indentical conditions. The following table shows the comparative surface temperatures at the throat.

TABLE II

Surface Temperatures for Two P. G. Conductivities

Time(sec.)	Surface	Temperature(^{o}F)
	HTM Data	Raytheon Data
10	4844	4833
20	5165	5094
30	5314	5221
40	5404	5305
50	5468	5368
60	5515	5418
70	5551	5469
80	5580	5493
90	5603	5522
100	5622	5547

As can be seen, the effect on wall temperature is relatively small. However, as the surface temperature is decreased by increasing the cooling rates, the difference will become more pronounced because of the higher heat flux. Since the rate of change of heat storage in the graphite between the surface and the passages is small (See Figure 23), a steady state calculation using the equation

$$q = h_g \ A \ (T_g - T_s) = \frac{k \ A_m}{x} \ (T_s - T_p)$$

CONDITIONS:

$T_G = 6720 °F$

$h_G = 0.0059$ BTU/SEC IN.^{2} $°F$

$\dot{W}$(METHANE) $= 0.0325$ LB/SEC

PASSAGE DIA $= 0.03$ INCH

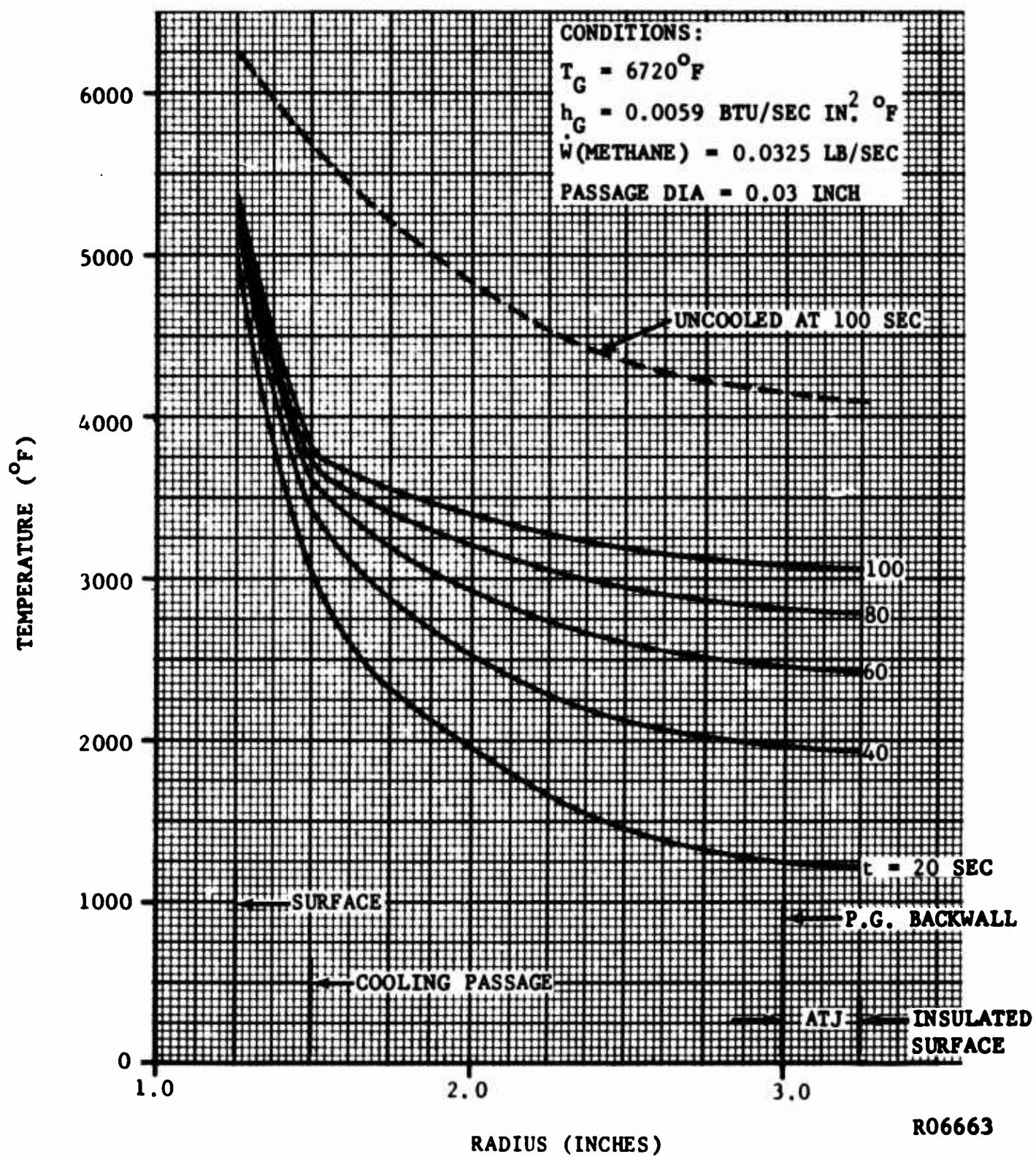FIGURE 23. TEMPERATURE PROFILES IN 5000 LB THRUST NOZZLE WITH CONVECTION COOLING
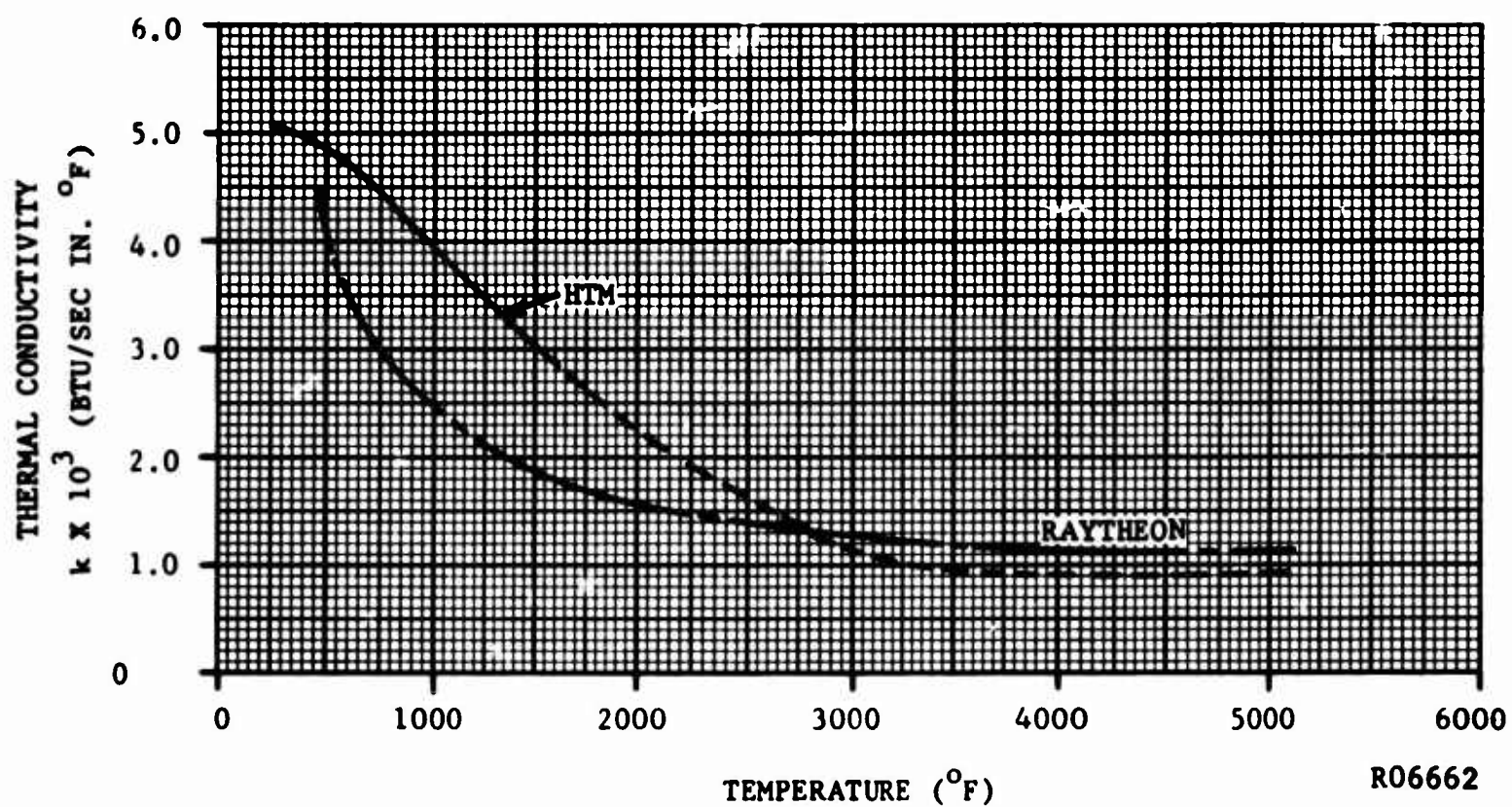
FIGURE 24. "A" DIRECTION THERMAL CONDUCTIVITY OF PYROLYTIC GRAPHITE

can be made to determine $(T_s - T_p)$ for any values of k/x and T_s. Because T_s cannot be determined without the transient solution, only the relative effect of k/x can be determined. It should be noted that the cooling effectiveness of convection is strongly dependent on T_p, hence the highest possible value of k/x is desireable. Physically, the value of x is limited to approximately 0.25 or greater for designs using washers. Because pyrolytic graphite has the highest thermal conductivity of any suitable materials at high temperatures, no other material is currently being considered.

A computer run was made using the properties of heat treated pyrolytic graphite obtained from Reference 13 . The conductivity is higher than "as deposited" pyrographite until the heat treat temperature is reached (approximately 5000°F). The wall temperature of the heat treated material lagged that of the "as deposited" material somewhat and at 100 second was only 9°F lower. Hence the results indicated that heat treatment in this application was not warranted.

Computer runs studying the effect of heat sink size have been made, however, optimization studies using these results have not as yet been made. The study will involve trade-offs of heat sink weight vs. coolant system weight.

A series of five computer runs were made to study the effects of coolant flow rate and cooling passage diameter. The following conditions were fixed:

$$T_g = 6720\ ^oF$$
$$h_{gt} = 0.00585\ BTU/sec\ in^2\ ^oF$$
$$D_t = 2.50\ in.$$
$$D\ (heat\ sink) = 6.00\ in.$$
$$X = 0.25\ in.$$
$$Number\ of\ passages = 50$$
$$Coolant - methane$$
$$k - Raytheon\ Data\ (Figure\ 24\ )$$

The variables were passage diameter of 0.03 in. and 0.04 in. and coolant flow rates of 0, 0.0325, and 0.0475 lb/sec. In one run the flow was varied linearly from 0.0216 to 0.0434 lb/sec with an average of 0.0325 lb/sec. The effects of surface temperature at the throat is shown in Figure 25 .

Another series of computer runs showed the effect of reducing the hot gas side heat transfer coefficient. Since the actual effects of film injection is as yet not know, the runs were made using 75% and 50% of the values used in other runs (See Section 2.3c). The results at the throat are shown in Figure 25 .
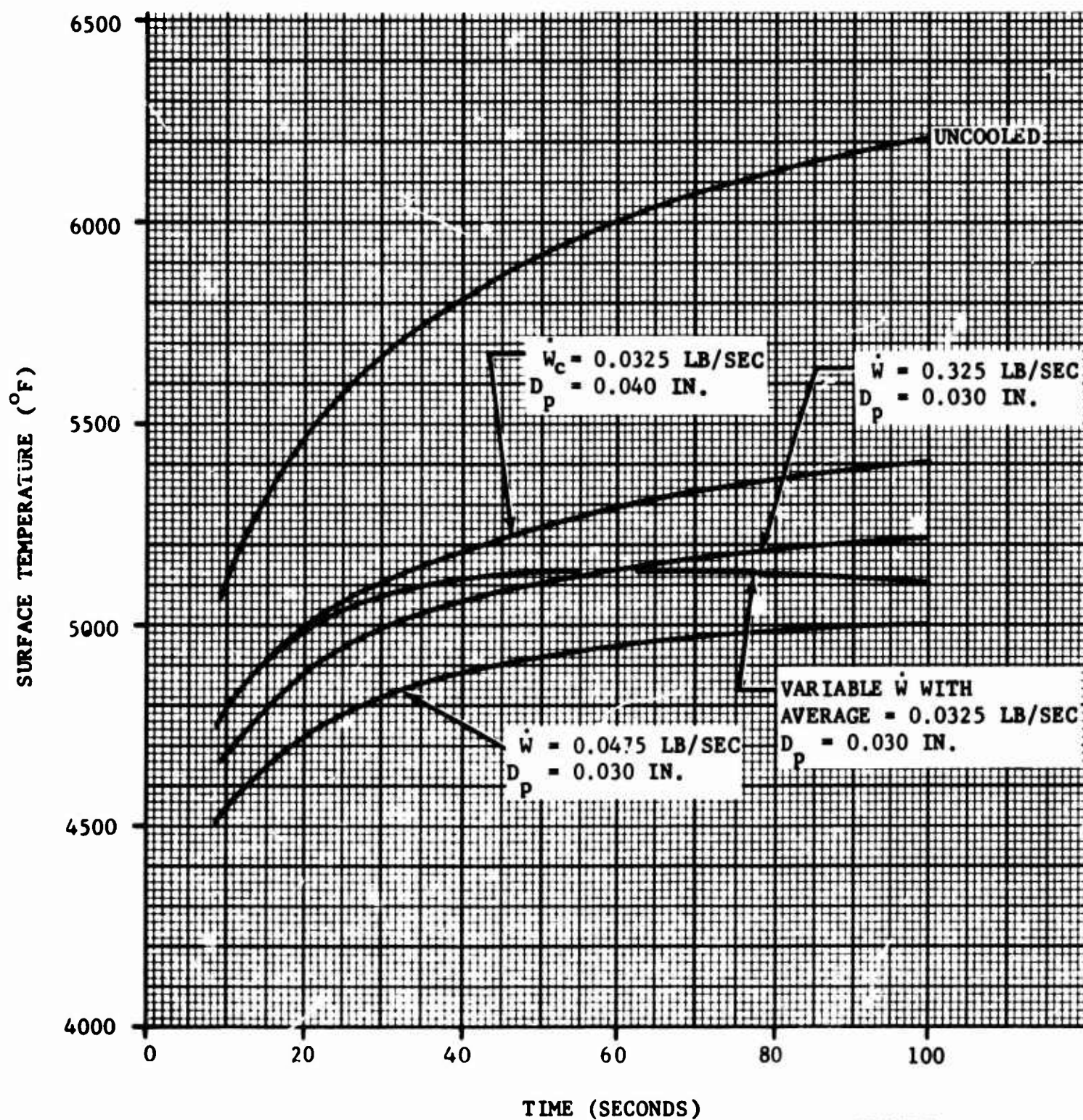
FIGURE 25. SURFACE TEMPERATURE AT THROAT WITH VARIOUS COOLING CONDITIONS

The chart contains the following labeled parameters:

D(HEAT SINK) = 6.00 IN.

$D_{.P}$ = 0.030 IN.

W_c = 0.0325 LB/SEC (METHANE)

Curves labeled: 1.0 h_g, 0.75 h_g, 0.50 h_g

X-axis: TIME (SECONDS), ranging 0 to 100

Y-axis: SURFACE TEMPERATURE ($^\circ$F), ranging 3000 to 5500

RJ6661

FIGURE 26. SURFACE TEMPERATURE AT THROAT WITH VARIATIONS OF HOT GAS SIDE CONVECTION COEFFICIENT

Using the results of the 5000 lb. thrust nozzle, a rough hand calculation was made to estimate the number of cooling passages and the methane flow rate for the sub-scale (1000 lb. thrust) nozzle to obtain a 5000°F surface temperature in 100 sec. The result indicated 28 holes and a flow rate of 0.028 lb/sec.

Runs were made at flow rates of 0.028 and 0.021 lb/sec. The surface temperatures at the throat at 100 second was 5280°F and 5410°F respectively. The temperature with $\dot{w}$ = 0.028 lb/sec at 50 seconds is 5023°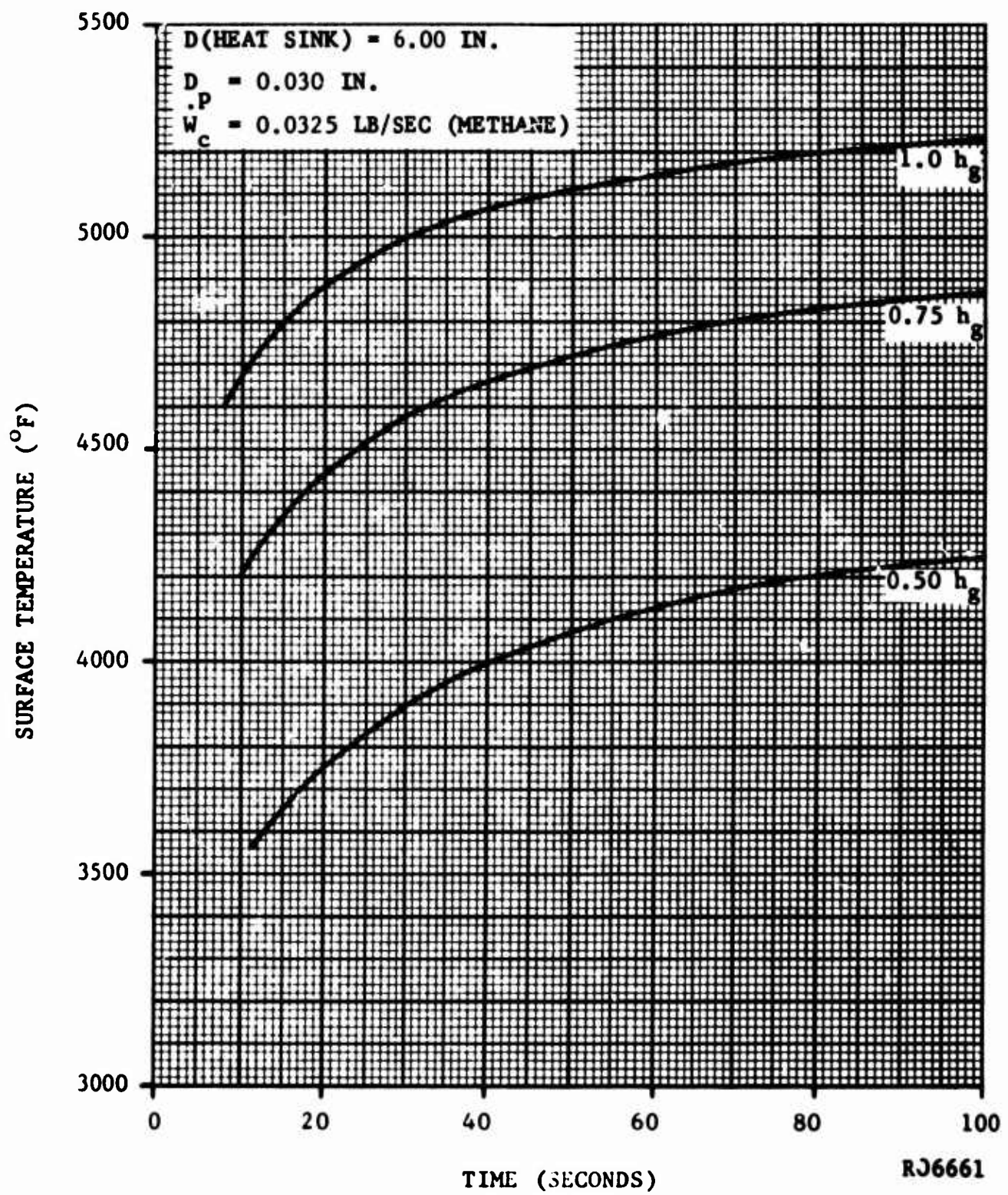F. Fifty seconds is the planned test duration. In actuality, this temperature will probably be lower since the conservative values of coolant heat transfer, coefficient were used. It is interesting to note that the 5000 lb. thrust nozzle requires 0.16% coolant flow rate compared to propellant flow rate to obtain 5300°F surface temperature, whereas the sub-scale requires 0.50% to obtain that temperature.

(4) Methane Convection Coefficient

As shown in previous analyses for 100 second firing periods, the coolant rather than the pyrolytic graphite mass behaves as the major heat sink. Therefore, considerable effort must be devoted to formulation of analytical techniques for prediction of both convective and radiative heat transfer to the coolant from adjacent wall surfaces. As previously shown, methane gas is an attractive coolant from materials compatibility and protective film considerations. This section will (1) review development of analytical techniques used to evaluate methane as a heat transfer medium and (2) present results of a typical application of methane cooling in the nozzle.

The laboratory experiments (Section 3.0   ) reveal that methane dissociates to carbon and hydrogen at simulated nozzle cooling passage wall temperatures. Carbon particles collected from these tests had a mean diameter of about 0.1 micron. From these observations it is apparent that a meaningful correlation for convective heat transfer to the methane must account for the following:

(1) Solid particle production and growth adjacent to the heating surface.

(2) Methane dissociation near the heating surface, i.e. effects of chemical reaction and composition change.

(3) Selection of proper reference states for evaluating pertinent properties and composition of the coolant.

Thermal radiation will occur between the wall surface and coolant. The following steps were taken to evaluate its maximum magnitude.

(1) Determination of gas total absorptivities for black body radiation emitted from the high temperature passage surfaces.

(2) Determination of total emissivities of the coolant.

(3) Calculation of maximum radiating heat flux and equivalent radiative heat transfer coefficient (h_r) for comparison with convective heat transfer coefficients.

-51-

A literature survey was conducted regarding heat transfer to fluids containing suspensions of small solid particles. It is consistently reported that presence of solid particles enhances the convective film coefficients. This result is generally interpreted as a thickness reduction or modification of the film layer adjacent to the heating surface caused by the turbulence induced from solid particle motion. Most information relating to heat transfer to gas-solid mixtures has been presented since 1957. At this time Farber and Morley[14] presented extensive test data for heat transfer to an alumina-silica catalyst suspended in a carbon tetrachloride fluid system. The particle size (diameter) distribution was from 10 to 210 microns. Farber and Morley correlated heat transfer data for the mixture flowing in a tube by (Note: Nomenclature is presented at end of section):

$$Nu = 0.14 \ Re^{0.6} \left(\frac{G_s}{G_g} \right)^{0.45} \qquad \qquad (1)$$

As a typical example of film coefficient increase with addition of solid particles, the following quantitative observation from Farber and Morley's data is presented. With a constant gas mass velocity of $1.50 \frac{lb}{hr \ ft^2}$ the convection film coefficients increased by factors of 1.32 to 2.87 as the solids loading ratios, represented by G_s/G_g, increased in value from 2.0 to 10.5.

The correlation, equation 1, was derived for specific fluids, solids and particle size distributions, and therefore is probably not suitable for the dissociating methane system. In fact, it appears that particle size is a governing parameter in the convective heat transfer process. Wen and Miller[15] very roughly correlated the convective heat transfer for suspensions of solids with an equation containing particle diameters as a variable. It was also very recently suggested[16] that particle size and composition would be of importance in a general type correlation. There is, however, no acceptable general correlation in existence at present.

Very fortunately there is heat transfer data available for solid suspensions with particle sizes and compositions similar to those anticipated in the dissociating methane. In 1959 and 1960 the Babcock and Wilcox Company presented results of an extensive heat transfer and pressure drop testing program conducted with graphite suspensions in nitrogen, helium, and Freon (CF_4) gas flows. The primary goal of the program was to develope means for increased heat transfer performance in gas cooled nuclear reactors. In general, the graphite particle diameters, as determined by electron microscope examination, varied between 0.1 and 6 microns. Mean particle diameters were approximately 1 micron. The correlation established from the Babcock and Wilcox heat transfer tests in smooth tubes is:

$$Nu = 0.0195 \; (RePr)_g^{0.80} \left(\frac{W_s C_s}{W_g C_g} + 1 \right)^{0.45} \tag{2}$$

As shown in Reference [19], this correlation is applicable for a wide range of graphite loadings of nitrogen, helium and CF_4 gases. The subscript g signifies that the parameter (RePr) is evaluated for the gaseous component of the flow only. It is assumed that pertinent properties are evaluated at bulk gas temperatures.

In the present case of cooling, the methane operates over a greater wall to bulk fluid temperature difference. It was therefore judged necessary to re-establish a correlation interms of parameters to be evaluated at specified reference temperatures. The correlation is developed from the basic Babcok and Wilcox heat transfer data. Presented in Reference 19 , this data is specifically for flow consisting of various solids loadings of graphite in nitrogen, helium, and CF_4. Solid to gas weight fractions ranged from 1.14 to 10.33 in the nitrogen, 8.65 to 81.4 in helium and 0.360 in CF_4. All tests were conducted in a 0.313 inch I.D. tube. Deissler and Presler [20] conducted analysis on the determination of reference temperatures for property evaluation for heat transfer to helium , argon, hydrogen, air, and carbon dioxide under conditions of wall temperature variation from 2000 to $6000^{\circ}F$. The recommended reference temperature is calculated from $T_x = T_b + x (T_w - T_b)$. The quantity x is a function of the fluid Reynold's Number and the wall temperature. Specific reference is made to Figure 27.

A correlation of the form

$$Nu_{gx} = C_1 Re_{gx}^{0.8} Pr_{gx}^{0.4} \left(\frac{W_s C_s}{W_g C_g} + 1 \right)_x^{0.45} \tag{3}$$

was established from the Babcock and Wilcox data by evaluating gas properties at appropriate reference temperatures. Figure 26 illustrates the correlation of various data points and establishes the constant $C_1 = 0.023$. As in the Babcock and Wilcox correlation, Equation 2, the Nusselt, Reynolds and Prandtl numbers are evaluated from the gas properties only.

In the case of dissociating methane allowance must be made for effects of chemical reaction on heat transfer rates. As explained by Butler and Brokaw [21], reacting gases in chemical equilibrium may have considerably higher effective conductivities than gases of frozen composition. The increase in the conductivity
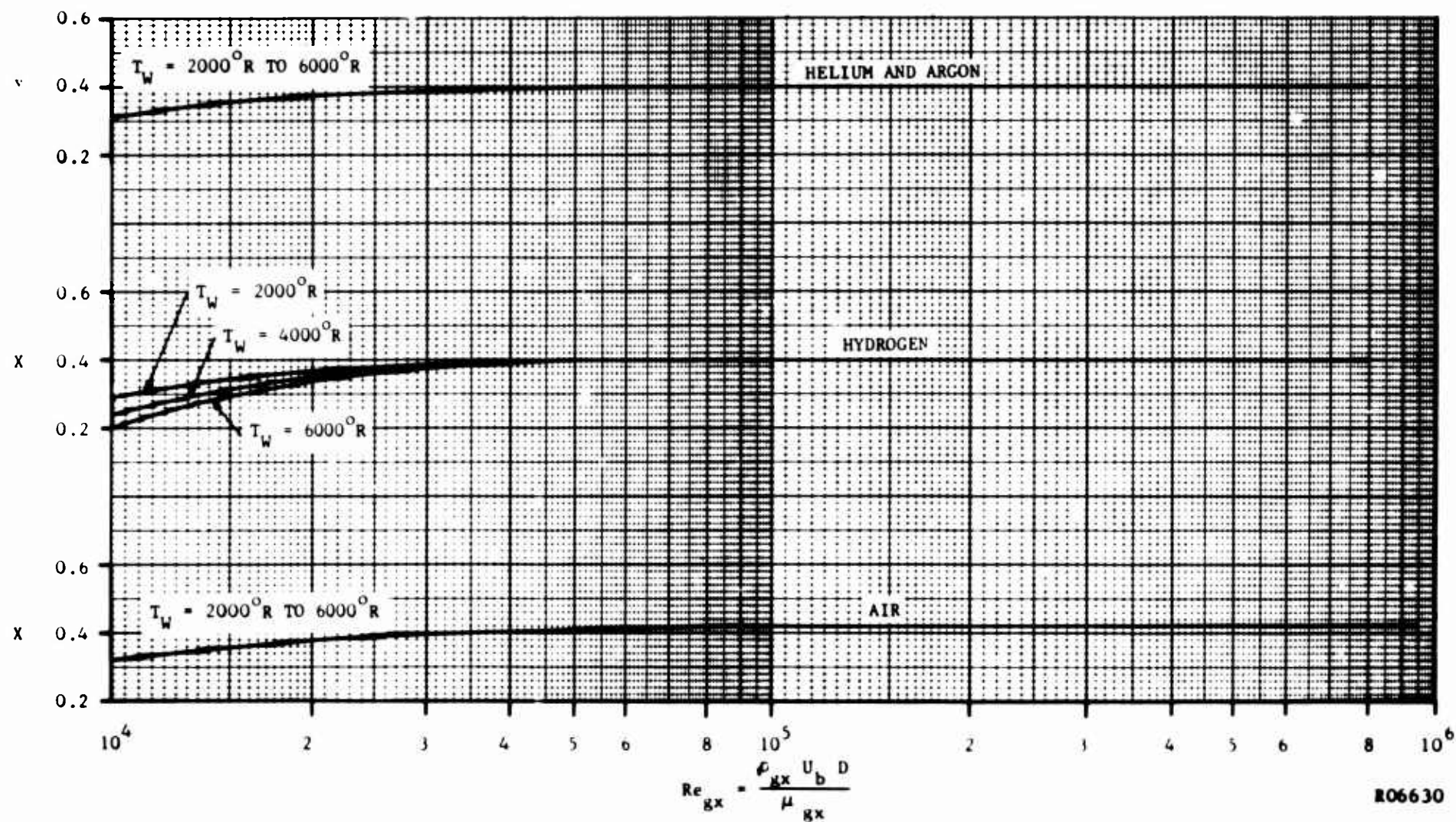
BLANK PAGE

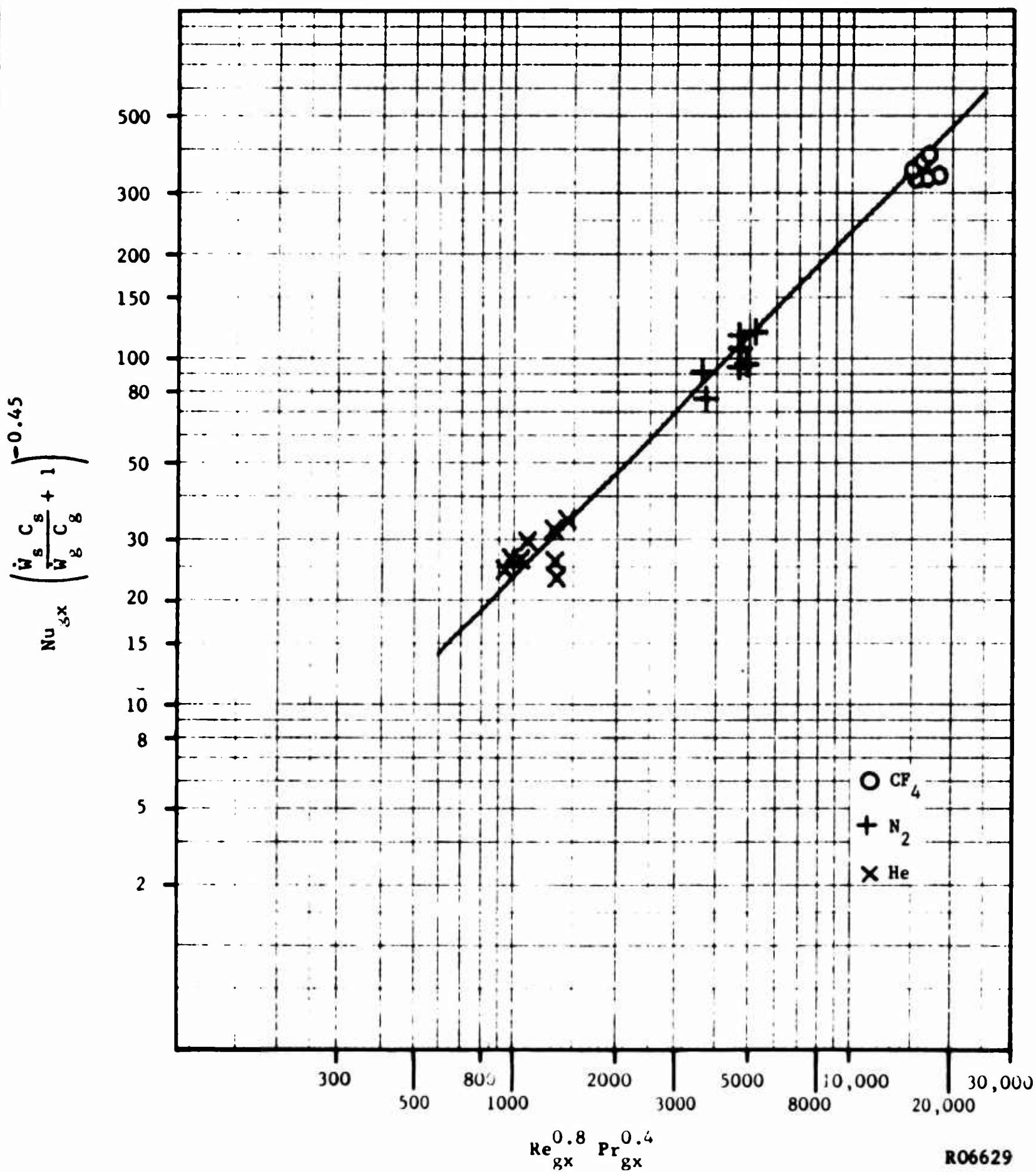FIGURE 27. VALUES OF X FOR CALCULATING REFERENCE TEMPERATURES FROM
DEISSLER AND PRESLER

R06630

-54-

FIGURE 28. TYPICAL CORRELATION OF BABCOCK AND WILCOX DATA USING
REFERENCE TEMPERATURE FOR PROPERTY EVALUATION

-55-

is interpreted as a result of transport of chemical enthalpy of molecules which diffuse according to concentration gradients established by chemical reaction. The concentration gradients and therefore the effective thermal conductivities are governed by the variation in the equilibrium gas composition with temperature.

Considerable information is available on suitable convective heat transfer correlations for flow with chemical reactions. Relatively low velocity turbulent pipe flow heat transfer with chemical reaction has been correlated by the following approach according to Bartz[24]:

$$\dot{q} = St(\rho U)(H_w - H_b)$$

The Stanton number is identical to that defined for non-reactive flow. As indicated, the enthalpy difference of the fluid at wall and bulk states is essentially the driving potential for heat transfer. Additional background for the general use of equation 4 for chemically reactive heat transfer is presented in References 25 and 26 by E. R. G. Eckert. The major restriction on its use is the requirement of unity Lewis Number. As stated in Ibele[27] and interpreted from Altman and Wise[28], the Lewis number very closely approaches unity for turbulent flow.

Turbulent Lewis number $= \dfrac{D + \epsilon}{\alpha + \epsilon} = 1$ because $\epsilon > D$, and magnitudes of D and α are not too different

where

$D =$ moleculardiffusivity
$\alpha =$ thermal diffusivity, $\dfrac{K}{\rho C_p}$
$\epsilon =$ turbulent eddy diffusivity

The methane flowing through the nozzle cooling passages will exhibit considerable turbulence. Based on gas phase properties and tube diameter the Reynold's Numbers are within the range 5,000 to 11,000. Furthermore, the formation and growth of carbon particles will induce turbulence near the wall-fluid interface.

The correlation, equation 3 for solid suspension flow is simply changed into the form of equation 4:

$$St_{gx} = \frac{Nu}{Pr_{gx} \, Re_{gx}}$$

from Equations 3 and 5:

$$St_{gx} = \frac{0.023}{Re_{gx}^{0.2} Pr_{gx}^{0.6}} \left(\frac{W_s C_s}{W_g C_g} + 1 \right)_x 0.45$$

(6)

from Equations 4 and 6:

$$\dot{q} = \frac{0.023}{Re_{gx}^{0.2} Pr_{gx}^{0.6}} \left(\frac{W_s C_s}{W_g C_g} + 1 \right)_x^{0.45} \rho_{gx} U_b'(H_w - H_b)$$

(7)

It is again pointed out the subscript g refers to parameter and/or property evaluation for the gaseous components only.

In application of Equation 7, the selection of a proper reference state for property ev luation poses some question. If the assumptions leading to the reference temperature technique presented in Reference 20 remain valid in the case of dissociating flow with solid particle production, then Equation 7 properties may be evaluated accordingly. An alternative method, which may prove applicable, has been presented by Eckert[25], in which properties are evaluated at a reference enthalpy. This approach, however, is especially adapted for heat transfer from high velocity flows.

As an example of the application of the derived correlation, Equation 7, heat flux and corresponding convective film coefficients were calculated for combinations of wall temperature and bulk coolant temperature expected to exist at four positions along the nozzle cooling passages. Results are presented on Figure 29 . For purposes of comparison, coefficients calculated for the case of non-dissociating methane gas are also included. Physical properties in both cases were evaluated at reference temperatures according to Reference 20 and shown in Figure 27 . For reference temperature selection, coolant composition adjacent to the heating surface was assumed to be primarily hydrogen. In the comparison case of non-dissociating methane gas, the Reynold's number was based on bulk fluid mass velocity. The pertinent properties and parameters required in these calculations are shown in Figures 30, 31, and 32. The specific heat, thermal conductivity, and viscosity data for methane and hydrogen were obtained from Svehla[29]. Properties of equilibrium hydrogen and methane mixtures were then determined from alignment charts presented in Brokaw[30]. Equilibrium composition of methane and its dissociating products were obtained from an Aeronutronic computer program in which JANAF Thermochemical Data [31] is utilized.
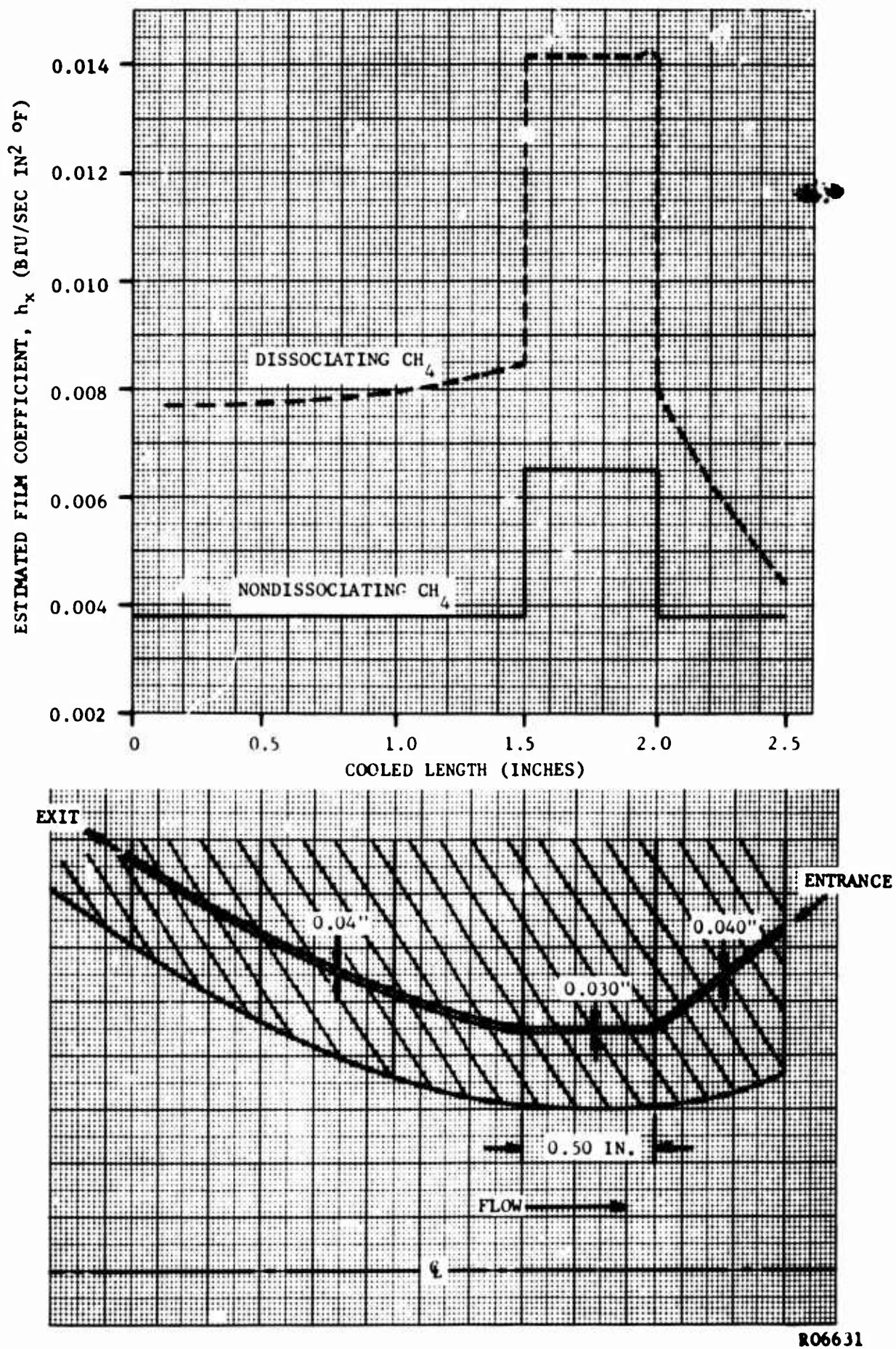
FIGURE 29. COMPARISON OF ESTIMATED CONVECTIVE FILM COEFFICIENTS
FOR DISSOCIATING AND NON-DISSOCIATING METHANE
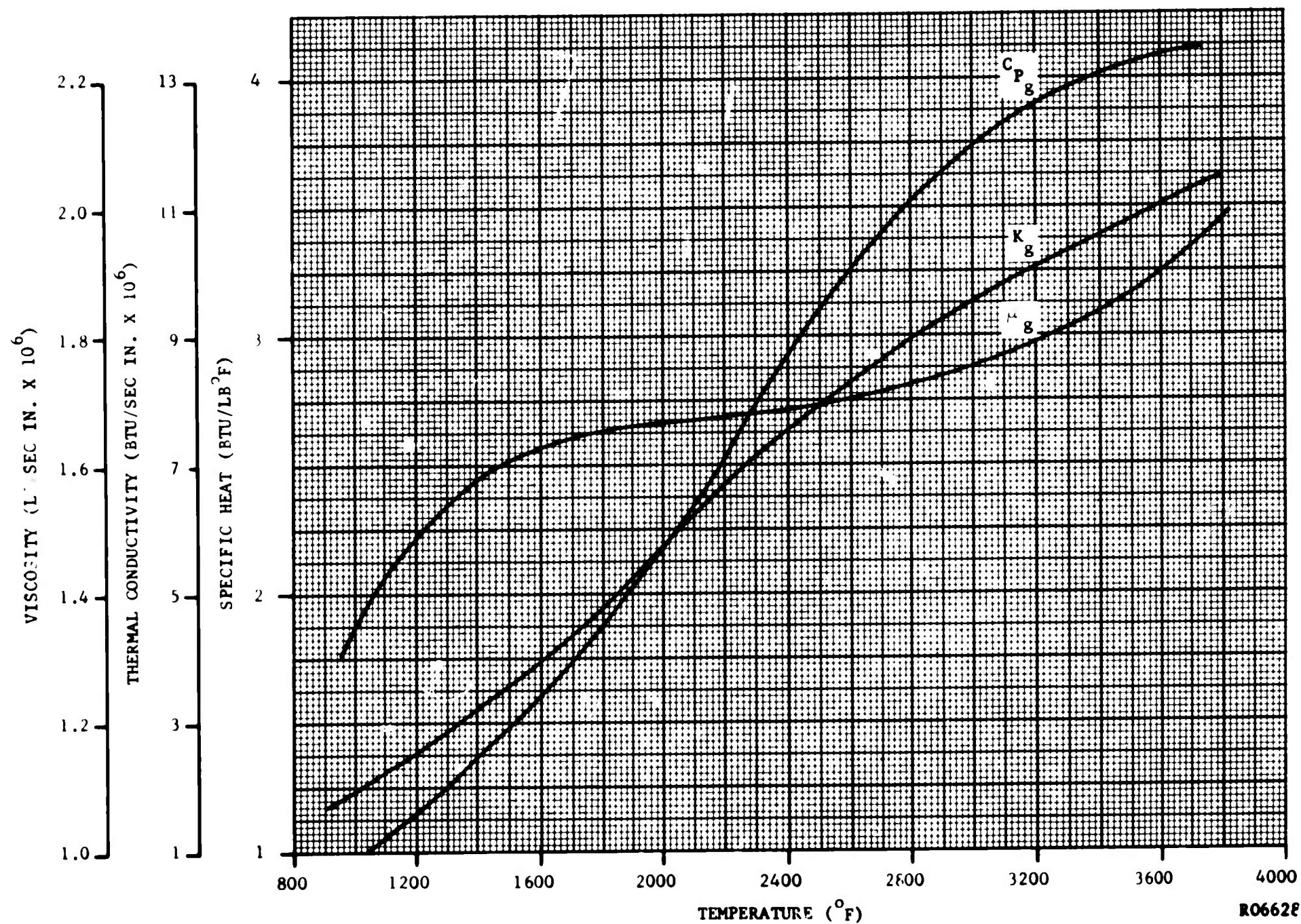
FIGURE 30. VISCOSITY, THERMAL CONDUCTIVITY, AND SPECIFIC HEAT
OF METHANE AND GASEOUS DISSOCIATION PRODUCTS

R06628
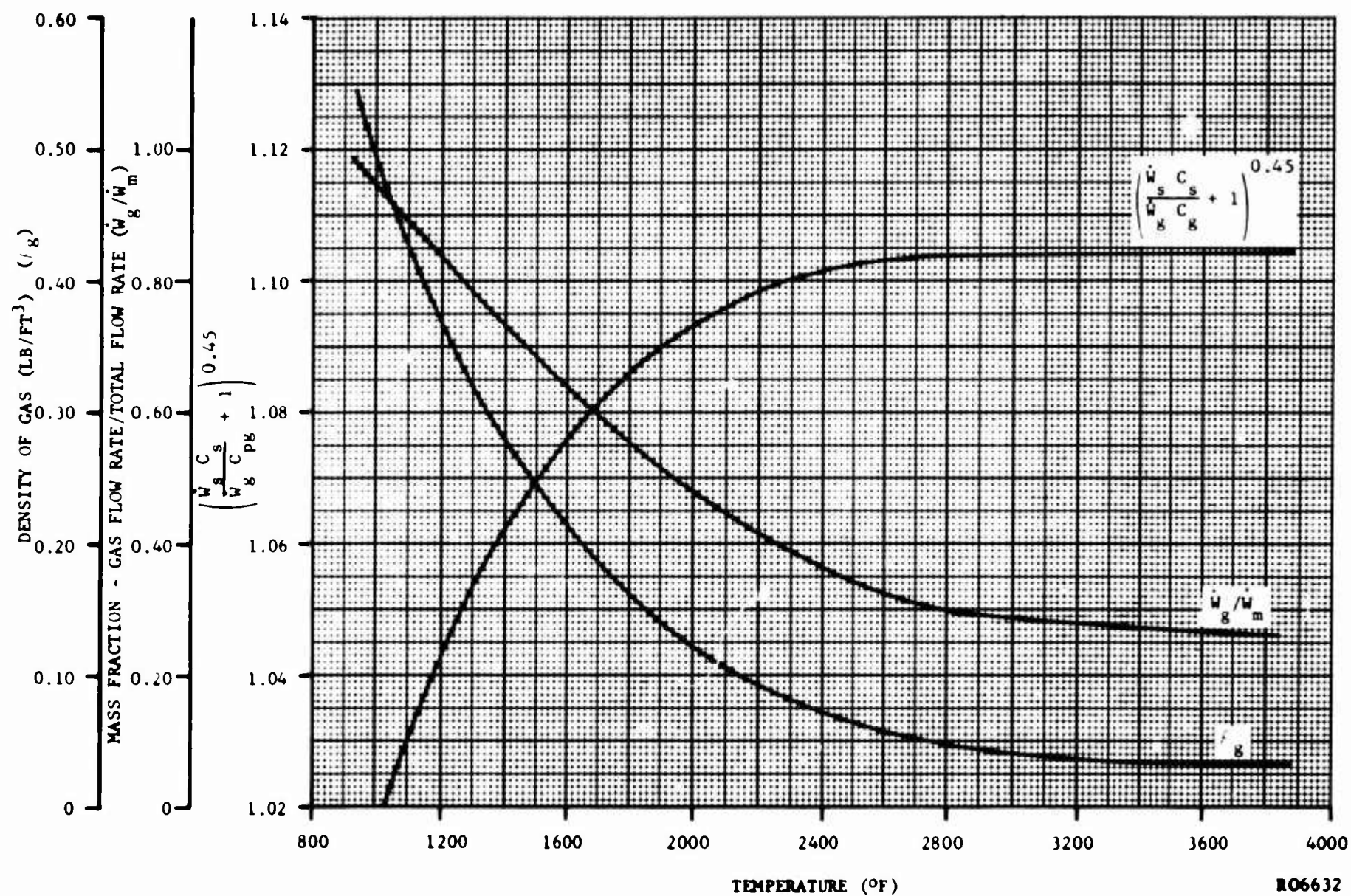
FIGURE 31. DENSITY, MASS FRACTION, AND FACTOR $\left(\dfrac{W_s C_s}{W_g C_g} + 1\right)^{0.45}$

OF METHANE AND GASEOUS DISSOCIATION PRODUCTS

R06632
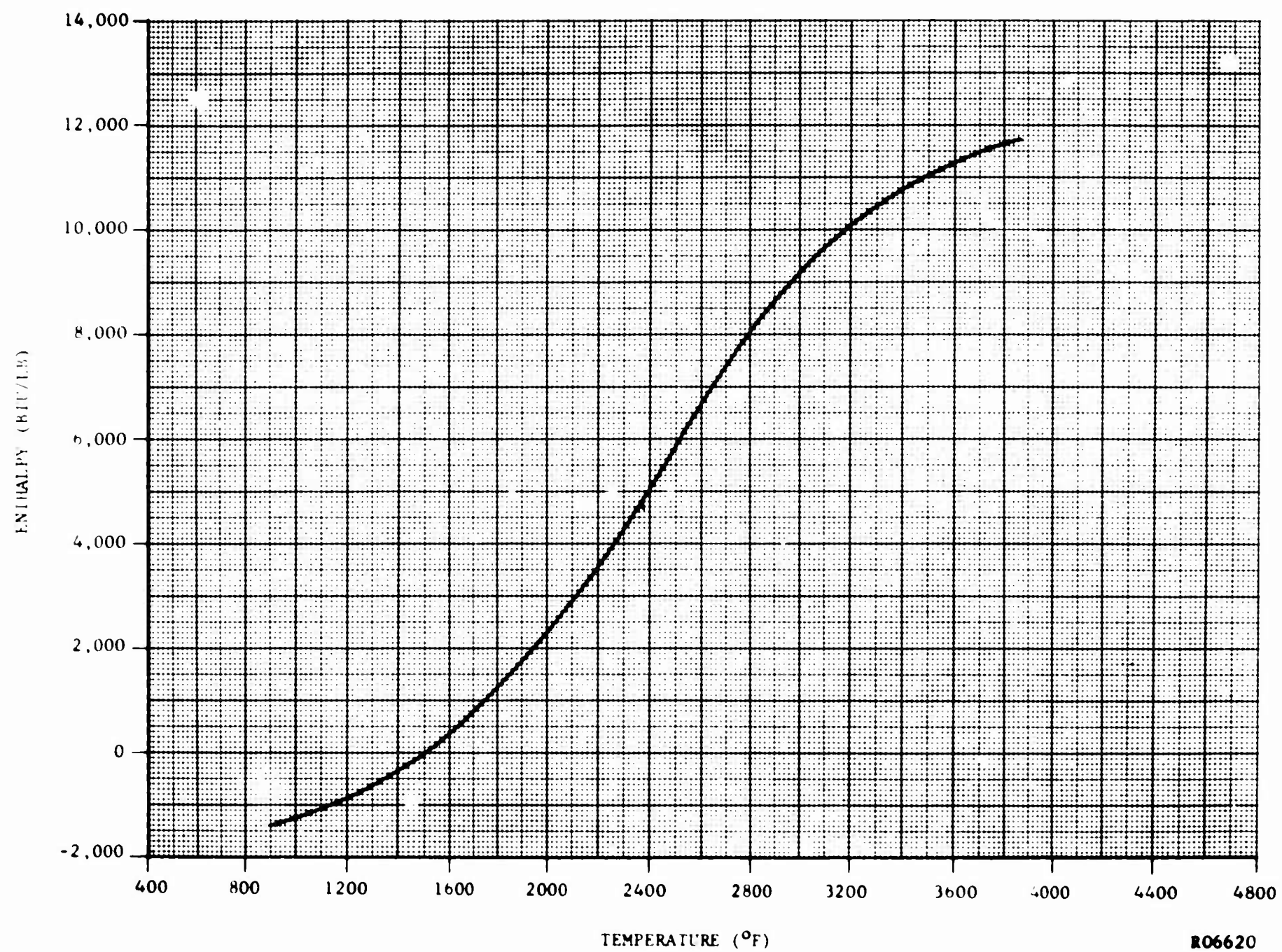
FIGURE 32.   ENTHALPY OF METHANE AND ITS GASEOUS DISSOCIATION
            PRODUCTS AT 700 PSIA

R06620

The enthalpy term of Equation 7 refers to enthalpies of gaseous components only by virtue of the definitions of demensionless parameters of equations 3 and 5. These enthalpies, shown on Figure 32 , are also obtained from the Aeronutronic computer program and JANAF Thermochemical Data.

The information presented on Figure 29   shows that the convective film coefficients with dissociation and solid carbon suspension is roughly twice that calculated for heat transfer to non-reacting methane for identical passage wall and bulk fluid temperatures levels.

In an effort to obtain the magnitude of thermal radiation an analysis has been made at the location of highest passage wall temperature. Radiation properties of the coolant were obtained from a paper by Stull and Plass [32] which presents monochromatic emissivity data for thermally decomposing hydrocarbon gases containing various sizes and distributions of carbon particles. According to this data, the decomposing methane in the highest temperature region of the nozzle cooling passages will behave as a black body over the entire range of applicable radiation wavelengths. With the assumption that the pyrolytic graphite cooling passage wall behaves as a black body, a net radiative heat flux may be determined by Equation 8:

$$\dot{q} = \sigma \left(T_w^4 - T_b^4 \right) \tag{8}$$

An equivalent radiative heat transfer coefficient may be found from Equation 9.

$$h_r = \sigma \frac{\left(T_w^4 - T_b^4 \right)}{T_w - T_b} \tag{9}$$

For the maximum wall surface temperature of $3470^{\circ}F$ and corresponding bulk coolant temperature of $1414^{\circ}F$ the radiative heat transfer coefficient is equal to 3.67×10^{-4} $\frac{BTU}{sec\ in^2\ ^{\circ}R}$. This is far less than the convective heat transfer coefficient which has a magnitude of 78.4×10^{-4} $\frac{BTU}{sec\ in^2\ ^{\circ}R}$ at the same location.

The following observations summarize the major results of a heat transfer analysis to the nozzle cooling passages:

1. Dissociating methane coolant yields higher convective film heat

transfer coefficients than non-dissociating methane. The increase is due primarily to the chemical reaction itself. The effect of small solid carbon particle formation in increasing convection is secondary according to correlations developed from data of References 17, 18 & 19.

2. Radiation heat transfer from the wall surface to the coolant is lower than convective heat transfer, though it was determined that both coolant and wall surface behave as black bodies.

Additional work will be required in the following areas in order to complete the analytical treatment of cooling passage heat transfer.

1. Thorough examination of applicability of various reference temperatures or enthalpies for property evaluation in the correlation for convective heat flux. The importance of reference point selection is illustrated in Figures 30 and 31 where properties vary considerably with temperature. The Deissler and Presler[20] reference temperature technique, which is used to predict results of Figure 29, is derived originally for non-reacting flows. Should an alternative approach be required, a modification of the Eckert reference enthalpy parameter may be utilized. Heat transfer data from the initial subscale tests will be useful in evaluating selection of reference points.

2. The objective of the nozzle coolant heat transfer analysis is to obtain input data for the thermal analyzer digital computer program which predicts temperature profiles through the pyrolytic graphite heat sink and coolant bulk temperatures. Because the convective heat transfer coefficients are functions of both wall and bulk coolant temperatures, it will be necessary to establish an iteration procedure in the computer program.

NOMENCLATURE

c_p . . . . Specific heat, $\dfrac{BTU}{lb\,^oF}$

d . . . . Tube diameter, in.

G . . . . Mass velocity, $\dfrac{lb}{sec\ in^2}$

h . . . . Convective film coefficient $\dfrac{BTU}{sec\ in^2\ ^oF}$

H . . . . Enthalpy, BTU/lb

k . . . . Thermal conductivity, $\dfrac{BTU}{sec\ in^2\ \frac{^oF}{in}}$

Nu . . . . Nusselt number, $\dfrac{hd}{k}$

Pr . . . . Prandtl Number, $\dfrac{\mu c_p}{k}$

$\dot{q}$ . . . . Heat flux, BTU/sec in^2

Re . . . . Reynold's Number, $\dfrac{\rho U d}{\mu}$

St . . . . Stanton Number $\dfrac{h}{\rho\ U\ Cp}$

T . . . . Temperature, ^oF, (^oR for radiation)

U . . . . Velocity, in/sec

$\dot{w}$ . . . . Flow rate, lb/sec

μ . . . . Viscosity, $\dfrac{lb}{sec\ in}$

ρ . . . . Density, $\dfrac{lb}{in^3}$

σ . . . . Stefan-Boltzmann Constant

Subscripts

b . . . . Bulk fluid states or properties
g . . . . Denotes gaseous components
m . . . . Denotes mixture
r . . . . Pertaining to thermal radiation
w . . . . Wall states or properties
x . . . . Reference point states or properties

c.   Flame Side Convection

The primary objective of the film injection is to modify the chemical composition of the boundary layer in the nozzle throat region in such a way that chemical attack is reduced or eliminated. Because the convection fluid cannot be injected at temperatures which approach the design surface temperature, a significant film cooling effect and consequently an increase in coolant thermal efficiency will result. The investigation of both the chemical and heat transfer effects requires a complete characterization of the convection boundary layer without injection. Such analysis also provides the basis for the design of the convectively cooled (no injection) heat sink nozzle. It should also be recognized that the nozzle convective heat transfer problem remains the subject of general interest within the industry. During the first quarter, efforts were devoted to (1) surveying the recent literature pertaining to boundary layer analysis, (2) evaluating the J.P.L nozzle heat transfer program, (3) performing preliminary heat transfer calculations for the sub-scale nozzle designs, and (4) the selection of an improved radiation heat transfer analysis.

Recently reported results of nozzle heat transfer studies have provided some additional enlightenment but no major progress has been recorded. The existence of laminar and transitional boundary layer flows in nozzles has been demonstrated in Reference 33 . From these results it is evident that turbulent boundary layers will persist throughout the inlet and throat sections of nozzles to be tested in this program. This, of course, is not an unexpected result for gas flows and the presence of a condensed phase is expected to increase turbulence. Reference 33 has also made contributions to the understanding of the effects of boundary layer acceleration and nozzle entrance conditions. It has also become apparent, from the literature discussed in Section 2.2 that the effects of transpirational injection of resin pyrolysis products in the chamber and upper inlet section may have a significant influence on boundary layer development. However, it seems likely that such effects could easily be obscured by acceleration, radiation, and condensed phase effects. It can also be deduced from Reference 33 that the anticipated variations of chamber and nozzle surface temperatures will have a significant influence on boundary layer development in addition to the usual effects on radiation and gas properties.

Considering all the aspects of the boundary layer development and heat transfer problem, the most logical approach to predicting heat transfer is to use existing methods in such a way that the results can confidently be expected to be conservative. Then, an overcooled nozzle design, when properly instrumented, can be expected to provide reasonable empirical corrections to the original predictions. Data obtained from undercooled nozzle tests is usually compromised by partial or total failure of the inlet or throat surfaces. The convection cooled nozzle designs (no injection) are expected to provide the means to make empirical estimates or corrections to the predicted heat transfer. It should be noted that the term overcooled really implies that superior structural and erosion performance is the observed result of actual testing. This is simply because the maximum or optimum design operating conditions cannot as yet be predicted analytically.

At the start of this program it was decided to use the modified Bartz method for calculating boundary layers. The method and associated computer program are well described in Reference 34 and will not be presented here. This

analysis has been reviewed to determine its applicability for boundary layer calculations, both with and without injection. It was found that a number of minor improvements could be made to both the theory and programming. These have not been carried out, primarily because the program may also ultimately be revised for use with the film analysis. For the no injection case, the major difficulty in applying the analysis arises from the spatial and temporal variations in surface temperature (or enthalpy of the gas at the wall). Fortunately, the convection cooled nozzle design operates with relatively constant, in time, surface temperatures and the important axial variations in surface temperature can be predicted without extensive iteration. However, it is important to realize that the heat transfer during the major surface temperature transient (the first 20 to 30 seconds of operation) cannot be easily predicted. Such calculations would be possible if the behavior of the alumina were known.

For the film injection case, the computer program could be used, to estimate film heat transfer and chemical mixing. This method was not described in Section 2.2 and is referred to as a far-field solution. It would be assumed that the momentum mixing region is negligible. Thus, a new 1/7th power profile could be constructed at the point of injection via the conservation equations. The initial wall temperature would be taken to be equal to the fluid temperature at the point of injection. A simplified diffusion analysis could then be formulated to determine the chemical mixing and the consequent density variations. Preliminary considerations suggest that this technique may have merit if more accurate solutions appear to be impractical.

Several computer calculations were performed to provide a preliminary estimate of the nozzle heat trasnfer. The predictions were slightly higher than the values deduced during contract AF 04(611)-8387 for the same propellant. To facilitate the calculations, on arbitrary geometry was chosen and surface temperatures were held constant at 4500°F. The results of these calculations are not presented in detail because neither the geometry nor temperature conditions have been preserved in the final designs. Improved geometry, property data, enthalpy and surface temperature data will be utilized in subsequent computer calculations.

During the next quarter of the contract period, a radiation analysis of the convergent section will be performed. The stimulus for this analysis was that recent data obtained at Philco Research Laboratories on the emissivity of a two phase mixture indicates that the radiation heat flux may be somewhat higher than previously suspected. Presented below are the general expressions that will be used for analysis of the gaseous-particle radiation heat flux. Using the network method, the following equations can be written:

$$q_1/A_1 \; = \; \frac{\epsilon_1}{\epsilon_1 - 1} \; (E_1 - J_1)$$

$$A_1 J_1 \; = \; \epsilon_1 E_1 A_1 + (1 - \epsilon_1) A_1 G$$

where:

q_1 = heat flux to A_1

ϵ_1 = emissivity of area A_1 under consideration

E_1 = emissive power of A_1

J_1 = radiosity of A_1

G = irradiation to A_1

Assuming that the particles may be treated as a gas (including scattering), the irradiation from the two phase mixture and an area A_2 to an area A_1 is References 35 and 36:

$$A_1 G = \int_{A_1} \int_{A_2} J_2 \, \tau_g \, \frac{\cos \beta_1 \cos \beta_2}{\pi r^2} \, dA_2 \, dA_1$$

$$+ \int_{A_1} \int_{\phi} \int_{\beta_g} \frac{E_g}{\pi} \, \epsilon_g \sin \beta_3 \cos \beta_g \, d\beta_g \, d\phi \, dA_1$$

where:

E_g = emissive power of two phase mixture

τ_g, ϵ_g = transmissivity and emissivity of two phase mixture

β_1 = angle between normal of A_1 and line connecting centers of A_1 and A_2

β_2 = angle between normal of A_2 and line connecting centers of A_1 and A_2

ϕ = azimth angle

β_g = polar angle

It may be noted that, for two phase gaseous radiation, one employs spherical coordinates, as the transport of energy is a volume phenomenon. With

particles, the transmissivity and emissivity of a gas are defined as

$$\epsilon = 1 - \tau = 1 - e^{-as}$$

where:

        s = path length

        a = absorption coefficient including scattering induced
               by the particles.

At Philco Research Laboratories, experiments are being performed [under contract NOnr 3907(00)] on emissivity measurements of an Al_2O_3 - H_2O rocket engine. The particle concentration, size and temperature are equivalent to those that exist in the film protected nozzle. The results from these experiments will be utilized in the radiation analysis.

SECTION 3

LABORATORY EXPERIMENTS

3.1 CHEMICAL REACTIONS

A series of laboratory experiments have been initiated to define the extent of interaction of the various promising injection gases with the graphite capillaries. An attempt has been made to simulate the nozzle design conditions of flow velocity, temperature gradient and pressure. Three grades of graphite were tested, Great Lakes HLM-85, Basic Carbon Graph-i-tite GX and pyrolytic graphite.
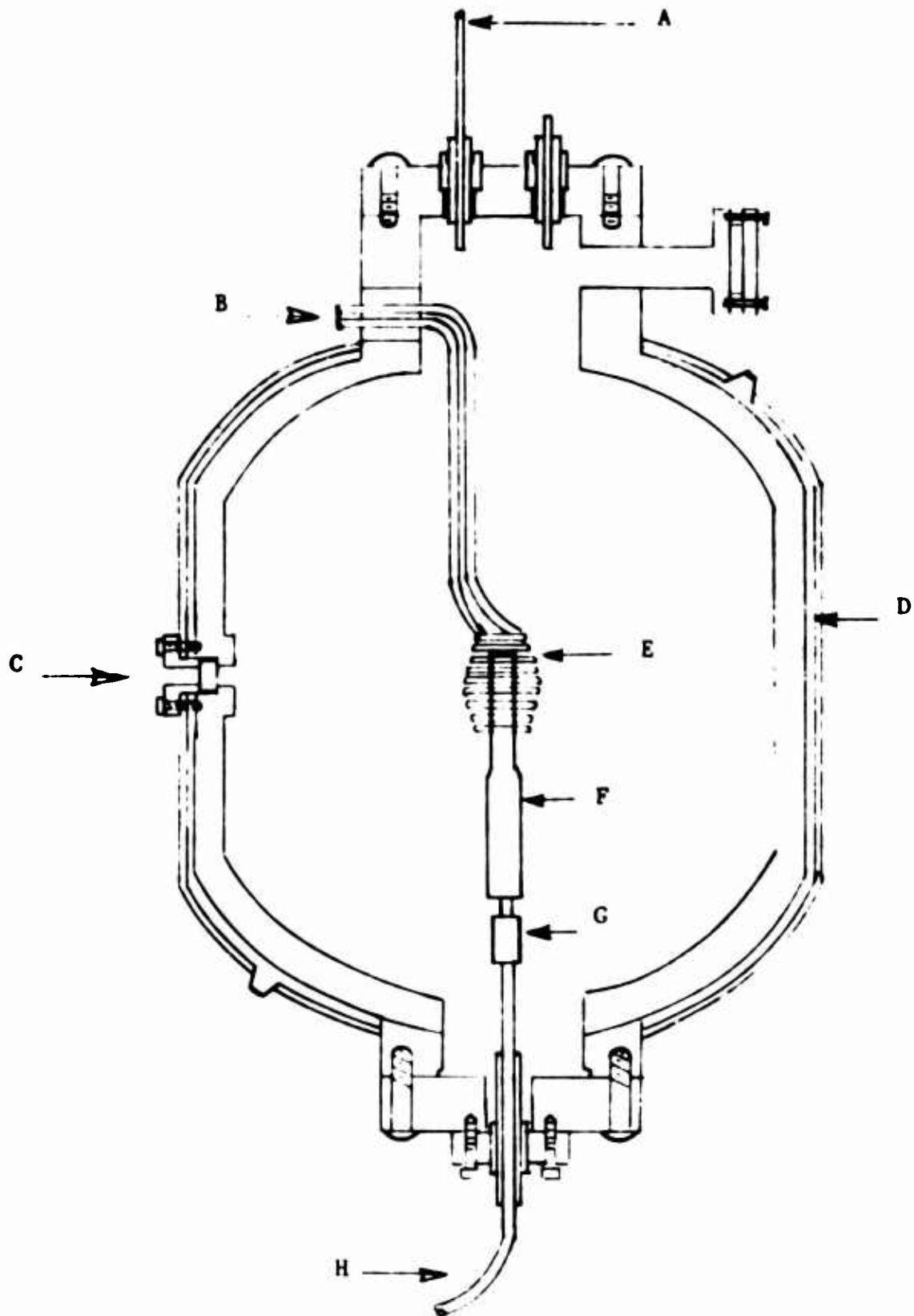
a. Experimental

The experimental apparatus is shown schematically in Figure 33 Essentially, it consists of all stainless steel high pressure chamber that can be evacuated and then back-filled. The system has been designed to accommodate gas pressures to 600 psig. All tests were performed under forced gas flow conditions with provision for metering of gas, and ballast valves for maintaining constant pressure.

Test specimens consist of graphite rods, 7/8-inch diameter by 8-1/2 inches long, with the top 2-1/2 inches containing the capillaries to be tested. The specimens are inductively heated by means of a Lepel vacuum tube radio frequency generator having an operating frequency of 450 kilocycles and an output rating of 20KW. The furnace consists of a multi-turn, barrel-shaped coil wound in a helix around the test specimen.

Operational procedure involves first pressurizing the chamber to 250 psia with argon and then introducing the injection gas through the capillary at a predetermined flow rate (STP) and a constant delivery pressure of 350 psia (differential pressure of 100 psia). After passing through the capillary, the injection gas mixes freely with the argon in the chamber. Constant chamber

A	EXIT BALLAST VALVE	E	BARREL-SHAPED R-F COIL
B	INDUCTION POWER LEADS	F	TEST SPECIMEN
C	WINDOW FOR TEMPERATURE MEASUREMENT	G	BORON NITRIDE INSULATOR
D	SS 304 PRESSURE VESSEL	H	GAS INLET

R06532

FIGURE 33. SCHEMATIC DRAWING OF HIGH PRESSURE FURNACE ASSEMBLY

pressure is maintained by the use of micrometer ballast valves at the chamber and at the gas supply cylinder.

Sample temperatures are measured with a Pyrometer Instrument Company disappearing filament-type, optical pyrometer by sighting on the exterior surface of the specimen through a ground quartz window. Thus, all recorded temperatures are brightness temperatures of the exterior surfaces. It is recognized that the capillary wall temperatures may be one hundred to two hundred degrees cooler. All tests were performed at an exterior surface tempe.ature of $2100^{\circ}C$.

The power is turned on immediately after injection gas flow is started. Approximately 15 seconds are required to bring the graphite sample to the test temperature of $2100^{\circ}C$. Where possible, tests ran for three minutes. Shorter duration tests were necessary in some of the methane pyrolysis experiments due to accumulation of carbon on the furnace coil with resultant electrical arcing.

b.   esults

(1) HLM-85

Six gases; methane, carbon dioxide, ammonia, boron trifluoride, carbon monoxide, and hydrogen, were tested for their compatibility with HLM-85 graphite at or near $2100^{\circ}C$ by passing the injected gas through a 0.040-inch diameter by 2.5 inches long capillary. With the exception of ammonia, gas flow rates varied from 60 to 120 cubic feet per hour. Ammonia is available commercially only as a liquified gas under its own vapor pressure of 130 psia at $70^{\circ}F$. In order to maintain a differential pressure of 100 psia, the chamber was pressurized only to 30 psia with argon. Under these conditions, the maximum flow rate which could be achieved with ammonia was 8 cubic feet per hour.

The results are shown in Figures 34 through 37 . All tests were of three minutes duration. Figure 34 represents a side view of the test specimens after test and Figure 35 a top view. Major chemical attack of the graphite capillary was noted for ammonia and CO_2 with probable formation of gaseous CN and CO, respectively, as products of reaction. Minor corrosion (10% hole enlargement) was noted for BF_3 and H_2. In the case of methane, large quantities of amorphous carb n were found, not only on the exterior surface of the test speciment as seen in Figure 34 , but also over the entire chamber assembly. The 0.040-inch capillary was found to be completely open, with no evidence of carbon deposition along the walls. Figures 36 and 37 are cross-sections of the specimens after test. These were prepared by carefully machine milling through the specimens until the capillary walls were exposed. The material around the CH_4 test specimen is an organic "potting" resin, used to insure that the amorphous carbon on the exterior of the specimen did not flake off.

Figure 38 is an electron photomicrograph (10000 X) of the carbon products collected from the top area near the orifice of the CH_4 test specimen. The carbon particles were spherical and ranged in size from 0.1 to 0.05 microns. As can be seen, the particles were highly agglomerated.

CH$_4$ CO$_2$ NH$_3$ BF$_3$ CO H$_2$ UNREACTED

R06521
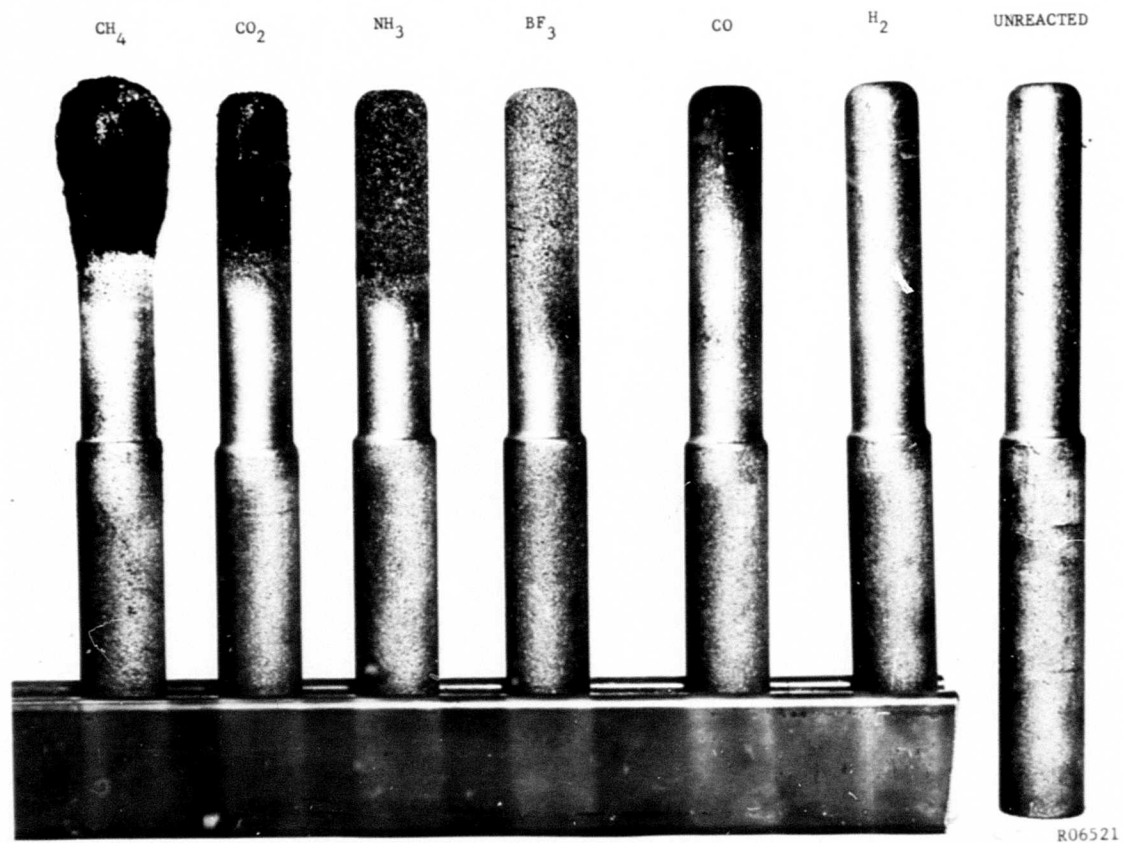
FIGURE 34. HLM-85 GRAPHITE - APPROXIMATELY 2/3X
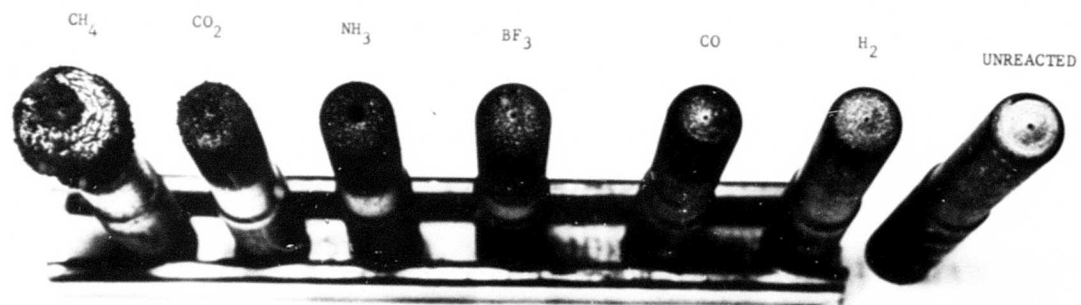
FIGURE 35.   HLM-85 GRAPHITE - TOP VIEW - APPROXIMATELY 2/3X
ORIGINAL HOLE SIZE - 0.040 INCH

R06522

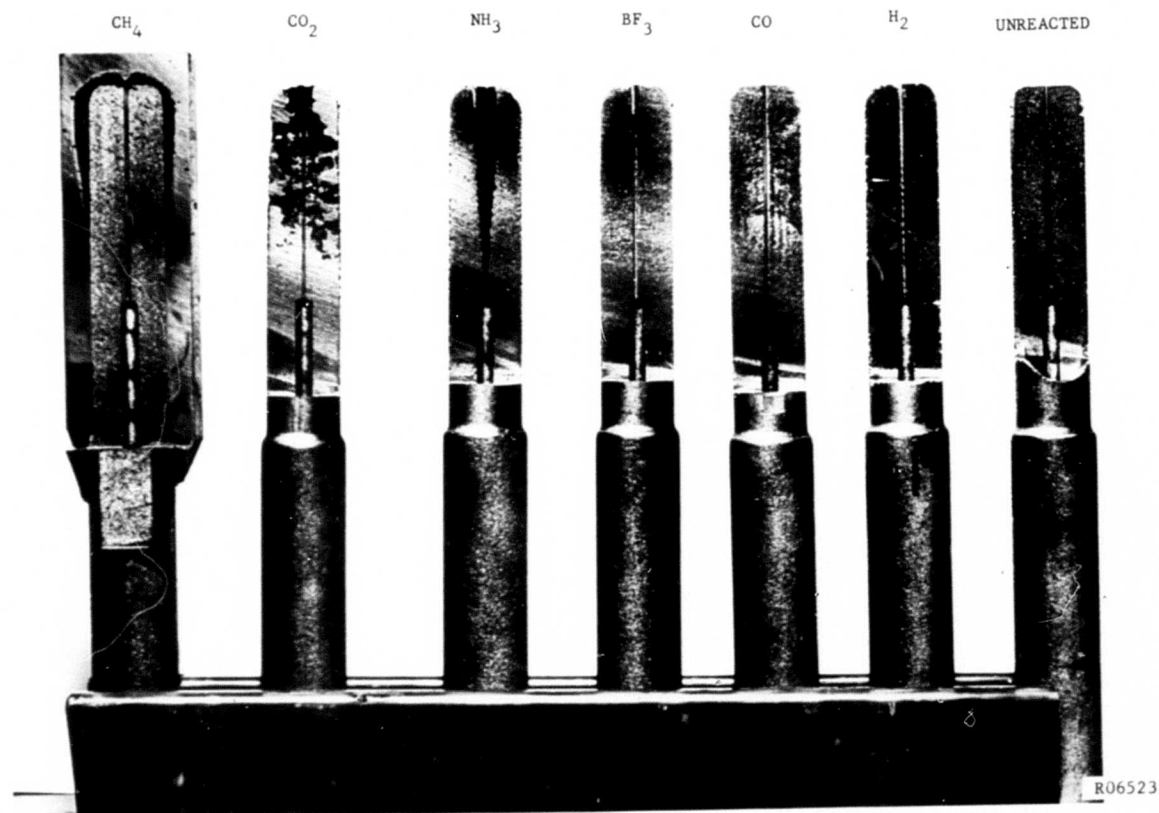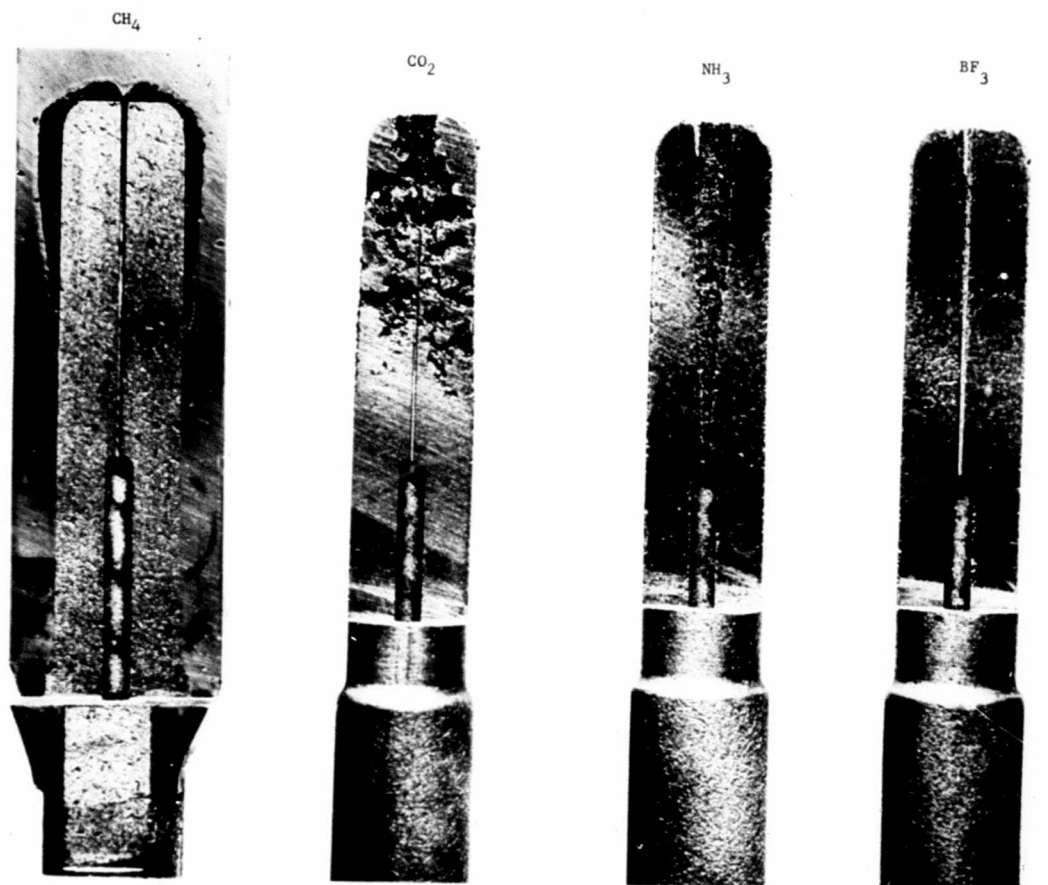CH$_4$ CO$_2$ NH$_3$ BF$_3$ CO H$_2$ UNREACTED

R06523

FIGURE 36. HLM-85 GRAPHITE - SECTION VIEW AFTER TEST 2/3X

CH₄ CO₂ NH₃ BF₃

R06520

FIGURE 37. HLM-85 GRAPHITE - SECTION VIEW AFTER TEST -
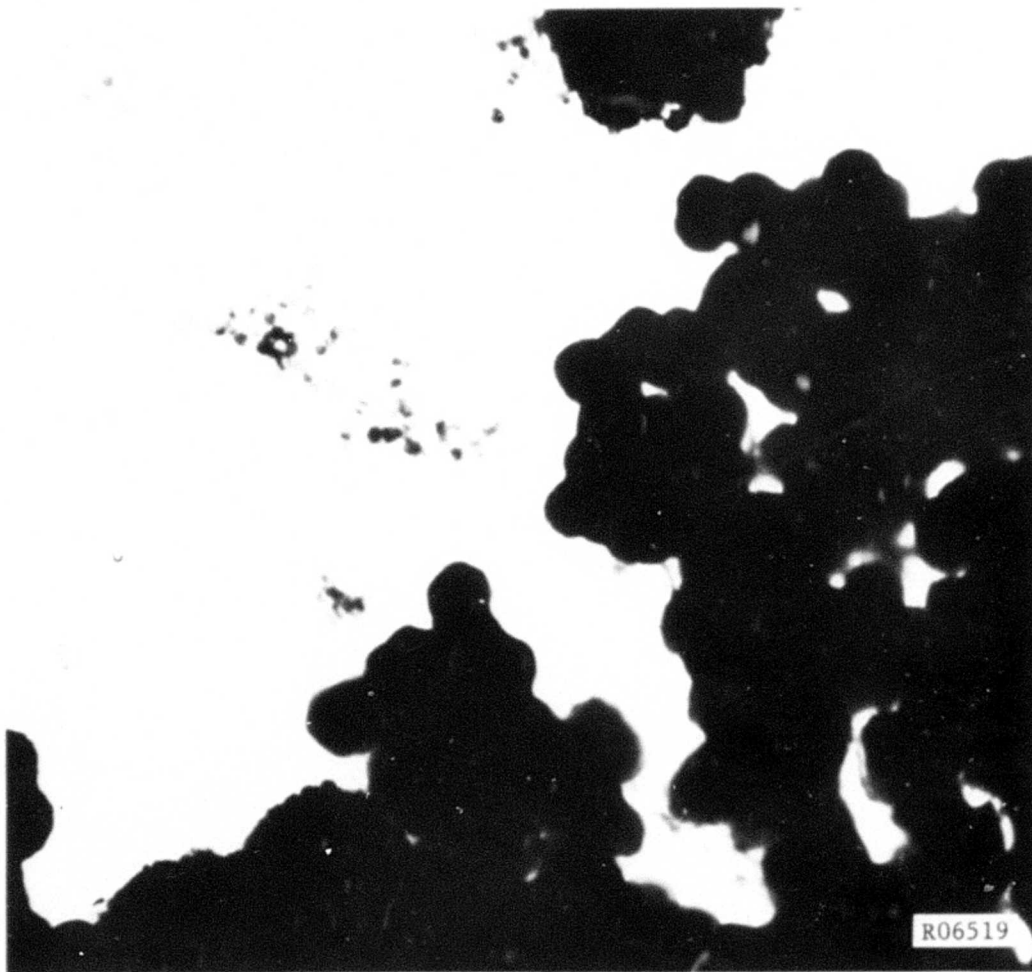APPROXIMATELY 1.2X

FIGURE 38. ELECTRON PHOTOMICROGRAPH OF CARBON PARTICLES 10000X
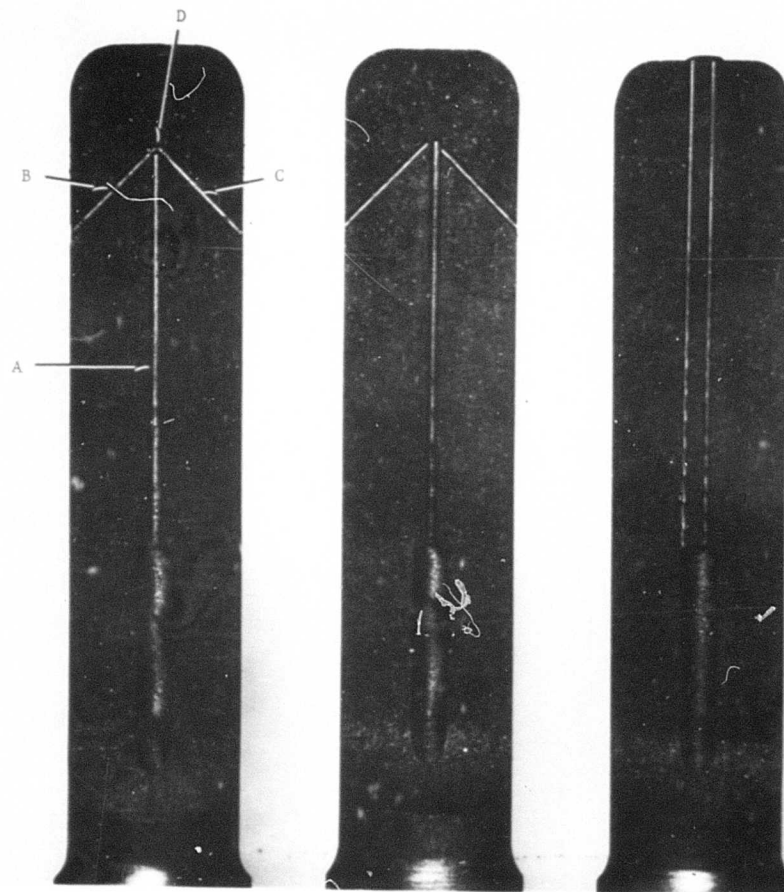
(2) Graph-i-tite

Since no evidence of carbon deposition along the capillary walls was found when methane was injected over HLM-85, the test was repeated with Basic Carbon Graph-i-tite GX, a higher density, finer grained graphite. The results for a three minute test at a methane flow rate of 60 cubic feet per hour were essentially the same as for HLM-85. No evidence of carbon deposition along the capillary walls was found. Considerably less carbon was found, however, along the exterior walls of the test specimen, probably reflecting the decrease in porosity of Graph-i-tite over HLM-85. Carbon particles collected from the top area near the orifice were spherical and ranged in size from 0.1 to 0.05 microns. Again, a high degree of agglomeration was noted.

Since the carbon particles presumably originate in the capillaries from the pyrolysis of methane, the question arose as to whether or not sharp angles in the Graph-i-tite capillary walls would cause deposition, i.e., will the carbon particles follow the main gas stream in making sharp bends or will they accumulate at the bend. In order to study this, the capillary was modified to include two 135 degree turns, as shown in cross-section Figure 39 . The entrance capillary, A, was 0.100-inch diameter by 2 inches long; and the two exit capillaries, B and C were 0.040-inch diameter by 9/16 inch long. The junction, D, thus represents a plenum where carbon particle accumulation would be expected. Two tests were run, one with a total methane flow rate of approximately 120 cubic feet per hour (60 cubic feet per hour per exit capillary) and the second with a total methane flow rate of approximately 60 cubic feet per hour (30 cubic feet per hour per exit capillary). The first speciment (120 cubic feet per hour methane flow) was run at temperature for 75 seconds and the second for 60 seconds. In both cases, the experiments were terminated due to accumulation of carbon on the furnace coil with resultant electric arcing. As can be seen in Figure 39 , no accumulation of carbon was found in either test. Figures 40 and 41 are side views of the first specimen (120 cubic feet per hour methane flow) showing the two open capillaries. It is of interest to note that the grey pyrolytic graphite areas appear to reflect the exit methane flow patterns. From electron microscope studies, carbon particles near the exit holes were again found to be spherical and ranged in size from 0.1 to 0.05 microns.

An additional experiment was made with Graph-i-tite in which two "straight-through" capillaries, each 0.040-inch diameter by 2-1/2 inches long, were provided. The total methane flow rate was approximately 120 cubic feet per hour (60 cubic feet per hour per exit capillary). Again, no accumulation of carbon was found in either capillary as evidenced in Figure 38.

(3) Pyrolytic Graphite

Pyrolytic graphite washers were stacked in an arrangement shown schematically in Figure 42 . The ATJ graphite shell served as a suscept-heater. Two tests were run, both with a methane flow of approximately 60 cubic feet per hour. In the first test, lasting 70 seconds, the top washer shifted slightly during the run, effectively closing the exit capillary. As a result, the carbon particles from the pyrolysis of the methane backed up and clogged the capillaries of the remaining pyrolytic graphite washers. For the second test, the top washer

FIGURE 39. GX GRAPH-I-TITE - AFTER TEST APPROXIMATELY 1.3X

R06518

EXIT HOLE
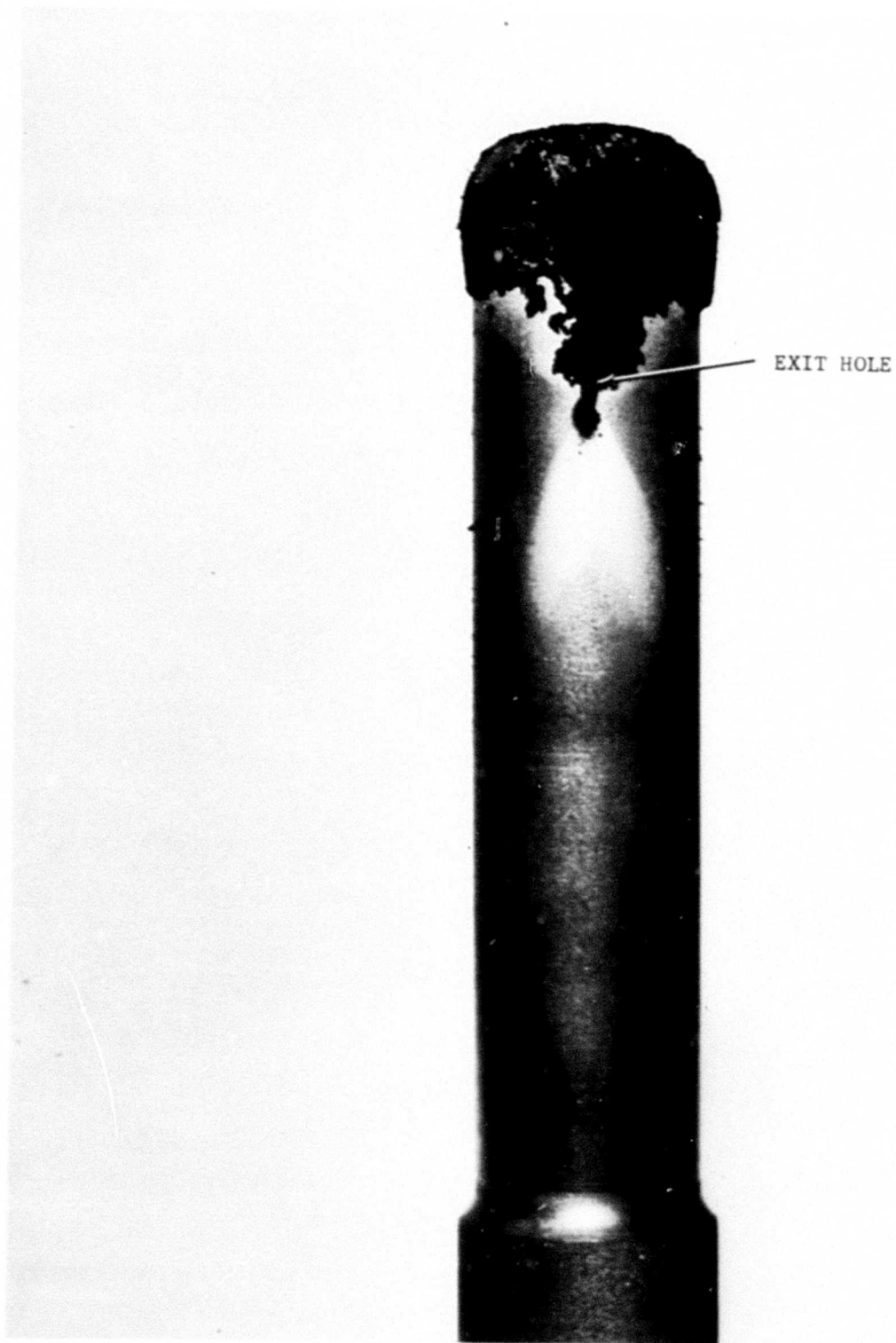
R06517

FIGURE 40. GX GRAPH-I-TITE - AFTER TEST APPROXIMATELY 1.5X

EXIT HOLE

R06516

FIGURE 41. GX GRAPH-I-TITE - AFTER TEST APPROXIMATELY 1.5X

-80-
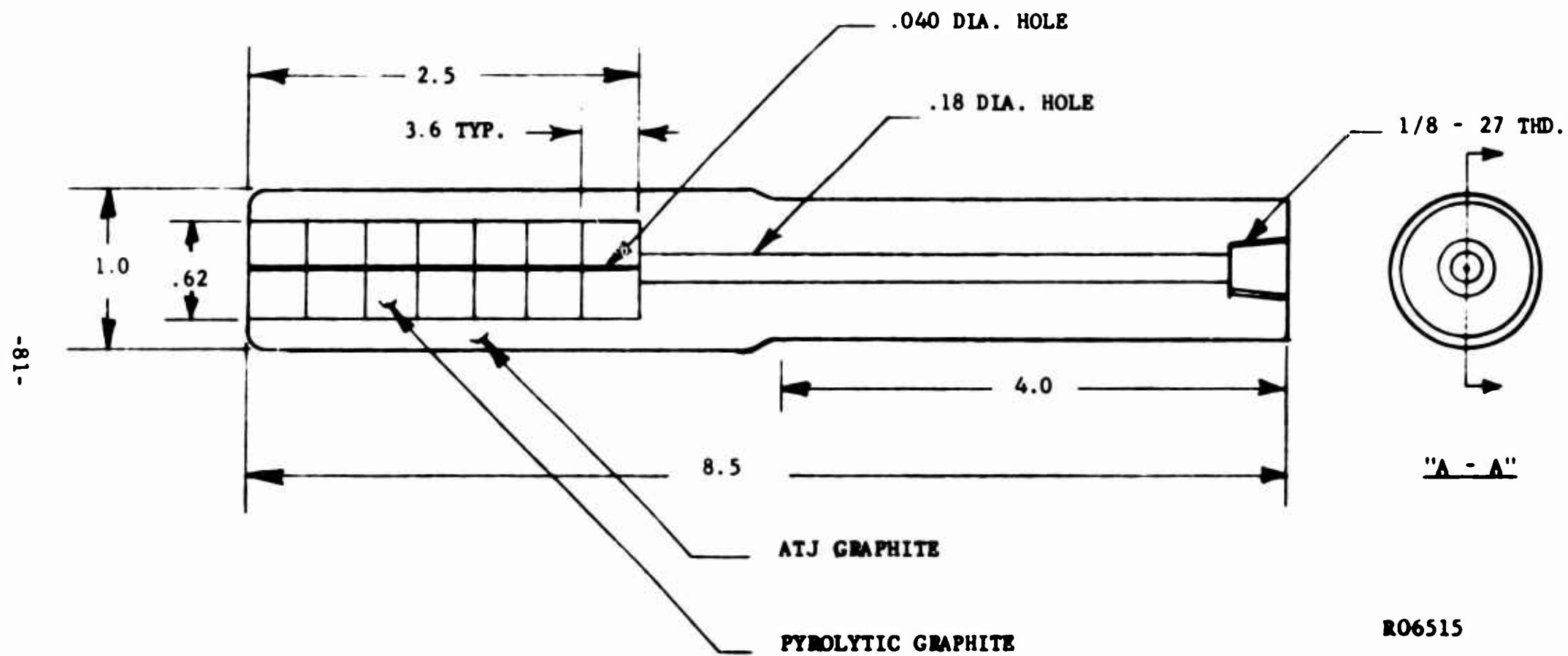
FIGURE 42.   PYROLYTIC GRAPHITE WASHER SPECIMEN - SCHEMATIC

was securely anchored to the ATJ graphite sleeve by three dowel pins. This resulted in a satisfactory test lasting for 60 seconds. After test, the capillary was found to be completely open with no evidence of carbon deposition along the capillary walls.
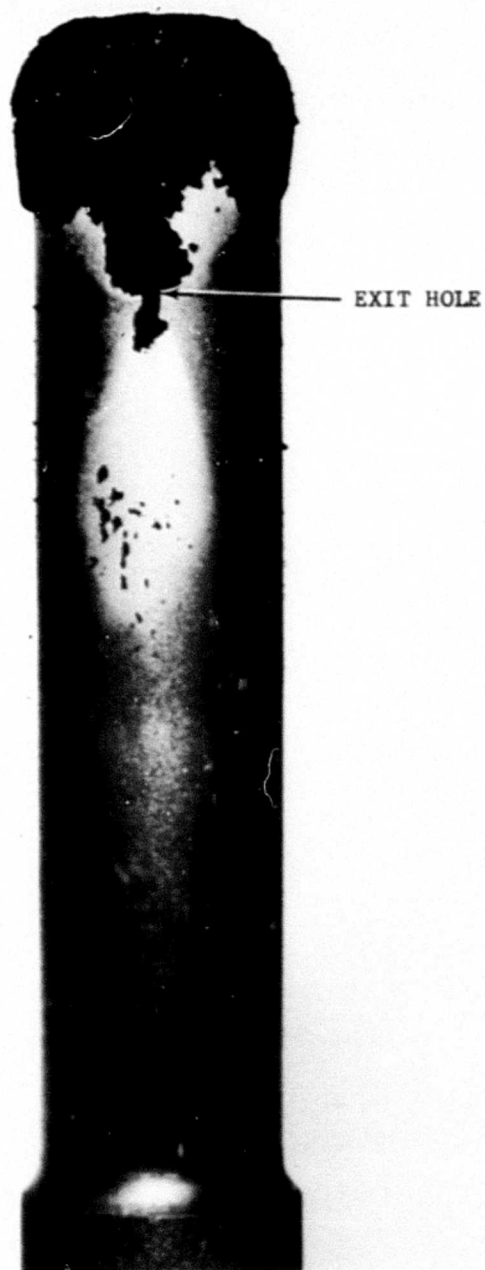
c.   Conclusions

(1) Ammonia and carbon dioxide severely attack graphite at the temperatures of interest. Minor corrosion ($< 10\%$ hole enlargement) was noted for BF_3 and H_2.

(2) Under the experimental conditions discussed, methane pyrolyzes to form large quantities of amorphous carbon. The carbon particles were found to be spherical and ranged in size from 0.1 to 0.05 microns. No major problems were encountered with respect to clogging of 0.040 inch capillaries.

(3) Where the use of segmented sections such as pyrolytic graphite washers is contemplated, the alignment of the capillary holes is critical.

3.2 COLD FLOW TESTS

a. Introduction.

There are a number of parameters that effect the efficiency of mass injection in thermal and chemical protection of nozzle walls. The interrelation between these parameters and the complicated behavior of the fluid mechanics of a 3-dimensional wall jet make a mathematical treatment impractical(References 4 and 37). In order to investigate the dependence of important parameters on the fluid dynamic properties of a wall jet, a cold flow experiment was designed. The results obtained from these cold flow tests will aid in the design of an injection hole geometry to obtain an efficient wall jet.

From a fluid dynamic approach, an efficient wall jet design is one that will cover a large amount of nozzle wall area with a protective film. With this in mind, the important parameters effecting wall coverage of a 3-dimensional jet (i.e. jet spreading and downstream protection) are: (1) hole spacing, (2) hole size, (3) , (axial location in nozzle of injection holes, (4) ρU, ρU^2, and U ratios of jet to free stream, and (5) hole angle. It may be noted, that the first four of the above parameters are all interdependent and difficulty may arise in their separation.

b. Apparatus

The 3-dimensional conditions in the nozzle are simulated by the use of a 1-1/2" diameter clear plastic tube, in which fully developed turbulent flow at the point of injection is insured by a six foot entrance section.

The ρU^2 profiles are obtained with a hypodermic needle mounted on a copper tube. The needle was ground to a 0.011" I.D. and 0.014" O.D. and excepted only after inspection under a microscope. The needle and copper tube (Pitot probe) is held in position by two metal collars, which in turn are supported by four radial positioning studs. The positioning studs are then bolted to an end section for rigidity. The metal collars allow the Pitot probe axial and circumferential degrees of freedom. The needle's location with respect to the wall and injection hole is determined from (1) radial pointer allowing axial and circumferential measurements and (2) a dial indicator attached to one positioning stud for radial distance from the wall.

The Pitot tube and a static pressure tap are connected to a water manometer resulting in a ρU^2 measurement of the flow. The water manometer is inclined 17° from the horizontal to give an accuracy of $\pm$ 5 lb/ft-sec^2 in ρU^2 measurement.

Injection gases with different densities are used in the experiment (1) study the effect of density gradient on the fluid mechanics of a jet, and (2) provide a method of varying injectant mass and momentum rates when the velocity is held constant. To provide a wide range of injection densities the following injection gases are used in a nitrogen main stream: (1) helium, (2) ammonia, (3) nitrogen and (4) freon-22. It may be noted here, that ρU^2 is chosen as the fluid dynamic parameter in comparing different experiments. This choice is

based on two reasons: (1) the fact that no concentration measurements are taken
in the cold flow tests, and (2) the magnification in velocity profile. That is,
the variation of the velocity through the boundary layer is magnified due to the
squared velocity term in ρU^2 .

Jet wall coverage can be determined in one of two ways. The first
method utilizes the ρU^2 profiles near the wall; but due to the small magnitudes in
ρU^2 and the error in probe location, the relative jet spreading at the wall
cannot be determined accurately. A much simpler and more accurate scheme is to line
the wall surface, downstream of injection, with Ozalid paper and NH_3 as the injection
gas. This results in a photographic method of determining wall coverage.

c.   Results

In the first quarter of the contract period, a comprehensive study
of a single 3-dimensional wall jet was achieved with the cold flow apparatus.
The study consisted of (1) the investigation of jet detachment (jet separation
from wall), (2) development of the jet's ρU^2 profile with axial and circumferential
positions, and (3) dependence of hole geometry on wall coverage. A discussion of
the conclusions obtained in the above areas is presented below.

In the area of jet detachment, it was required to substantiate the fact
that the radial momentum of the wall jet in the actual nozzle did not induce separa-
tion. This was accomplished by experimentally obtaining maximum radial momentum
rates that insured jet attachment for given free stream velocities. For a constant
main stream flow and injection hole diameter of 0.0625" (inclined 45° from the tube
axis), the jet's momentum rate was varied and jet separation was determined from a
ρU^2 traverse. It may be noted that the momentum rate of the jet was varied in
one of two ways: (1) utilizing gases of different densities, and (2) changing the
injection mass flow.

Typical ρU^2 profiles for the attached and detached jet are given
in Figures 43 and 44 , respectively, with measurements taken at the circum-
ferential center of the jet. From the figure one may conclude that near injection,
the ρU^2 profile for the detached jet, can be divided into, essentially, three
regions. The first region is near the wall in which the velocity is practically
zero. The development of this stagnation region may be compared to the stagnation
region at the back side of a cylinder in cross flow; that is, when detachment occurs
the jet (near the injection point) behaves as a cylinder in cross flow. The second
region consists of the injected gas, which may be called a free jet. This free
jet region is bounded on both sides by the main stream gas and is the "cylinder"
referenced previously. The third flow region is that of the main stream. Between
these three regions are areas of large momentum transfer (large shearing stress)
and, therefore, the ρU^2 profile changes rapidly in the axial direction. It may
be of interest to notice the redevelopment of the profile in the region downstream
from where the stagnation region persisted. This region is strongly deficient in
momentum and due to the 3-dimentional shape of the jet, the flow pattern of the main
stream around the jet tends to develop a profile of its own.

The attached wall jet profile is separated from that of the main stream
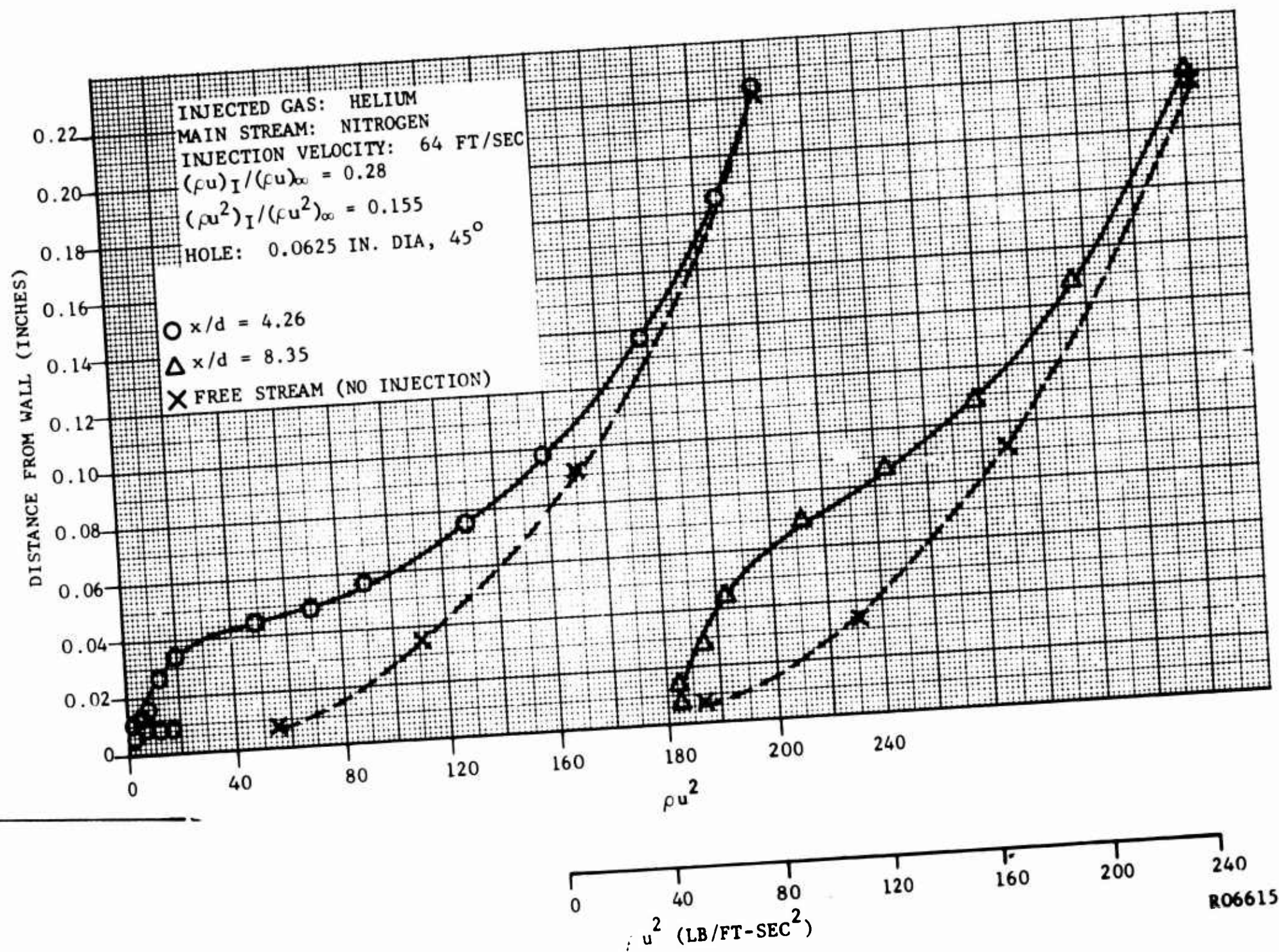
-84-

BLANK PAGE

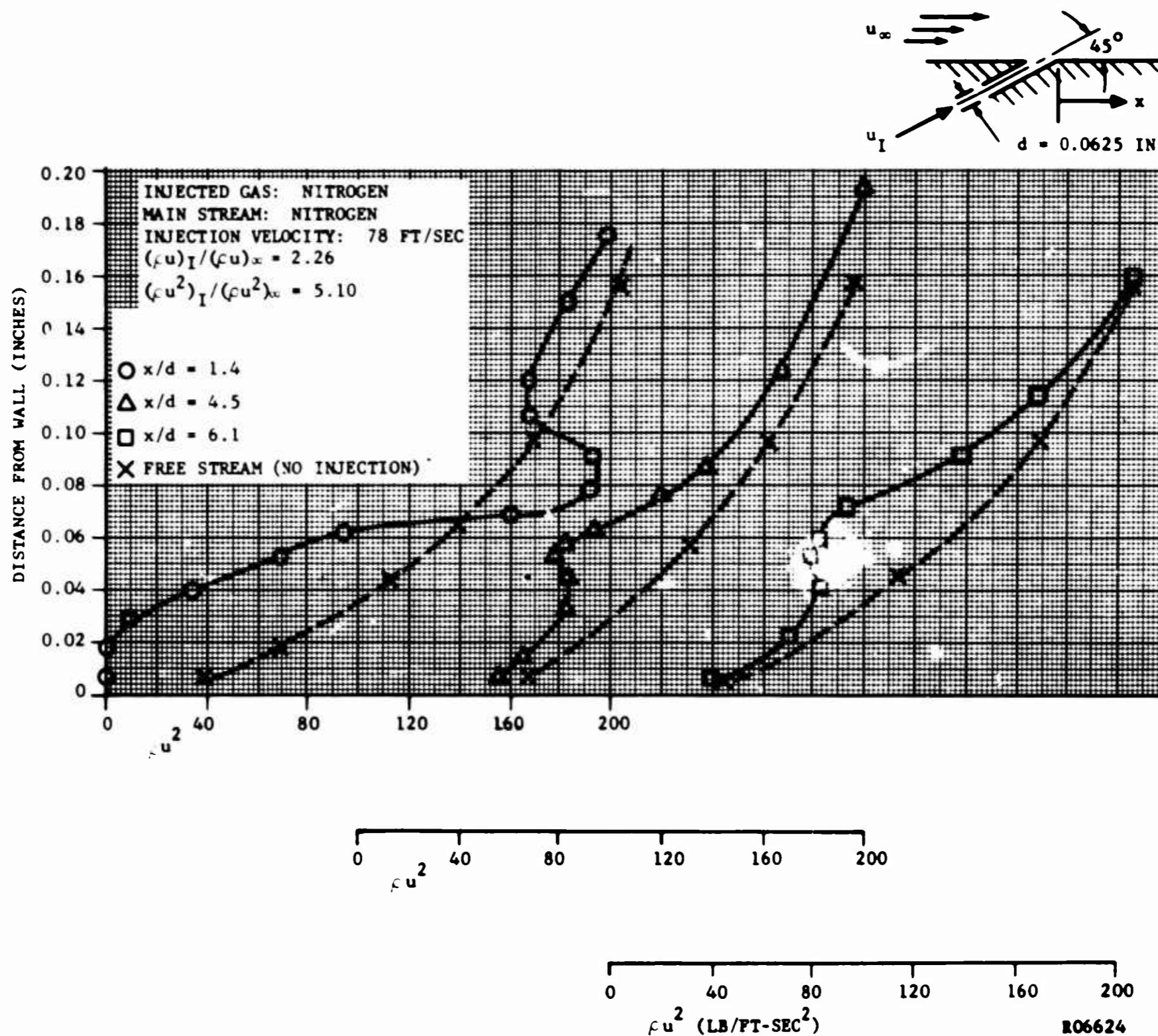FIGURE 43. 'ρu^2' PROFILE FOR JET ATTACHMENT

FIGURE 44. 'ρu^2' PROFILE FOR JET DETACHMENT

by a free shear layer (Figure 43). The shearing stress acting upon both the main stream and jet tends to re-establish the flow into that of a fully developed turbulent profile. This down-stream re-establishment region is usually called "the mixing region" of a wall jet.

In Table III is presented the results of jet detachment, in which the radial momentum rate of the jet is defined as (QU_r), where U_r is the velocity in the radial direction and Q is the injection mass flow per unit area. Since the velocity boundary layer completely fills the tube in developed pipe flow, the momentum rate (ρU^2) of the free stream was taken at a height from the wall equal to the radius of the injection hole (the average free stream axial momentum rate acting upon the wall jet). From the table a maximum radial momentum ratio of approximately 0.40 is obtained for jet attachment. The resulting radial momentum rate is applied to the nozzle only as an order of magnitude in predicting jet separation, as some questions may arise as to the validity of its direct application to the actual nozzle. For example, from References 4 and 38, the fluid mechanics of a wall jet is dependent on (1) temperature gradient, (2) pressure gradient (3) compressibility effects, all of which, were not included in the cold flow tests.

TABLE III

CORRELATION OF JET DETACHMENT WITH MOMENTUM RATE

GAS	$QU_r/(\rho U^2)_\infty$ Experimental	$Q_r/(\rho U)_\infty$	Position of Jet with Respect to wall	$(QU_r/\rho U^2)_\infty$ Theoretical
N_2	3.60	2.26	Detached	0.60
He	3.18	0.80	Detached	0.60
N_2	3.14	2.10	Detached	0.60
Freon-22	1.94	2.90	Detached	0.60
He	0.95	0.44	Detached	0.60
He	0.38	0.28	Attached	0.60
Freon-22	0.38	1.28	Attached	0.60
N_2	0.24	0.53	Attached	0.60

There have been devised several mathematical solutions to the problem of jet detachment in the field of thrust vector control. An analysis which is applicable to our case is that of Zukowski and Spaid, Reference 39 . In their solution, one assumes the shape of the 3-dimensional wall jet near injection (i.e., quarter sphere followed by an axisymmetric half body) and then calculates the pressure forces along the assumed body shape. Applying the conservation of momentum to the radial direction, the radial pressure force equals the radial momentum rate of the jet. With this expression, either one of two parameters may be found. The first parameter is that of jet detachment. By assuming a body shape with accompanying dimensions, jet detachment may be determined from the fact that the radial pressure force is not great enough to eliminate the radial momentum rate of the jet. The second parameter is that of body size. If the body shape is assumed, the body dimensions may be found by equating the radial pressure force and momentum rate. This method will be used in determining the jet height in the actual nozzle.

To obtain a simple analysis of jet separation, similar to the method of Zukoski and Spaid, a cylinder in cross flow was assumed. Since the pressure distribution or drag on a cylinder is very easily found Reference 40 , the radial component of the drag was equated to the radial momentum of the injection gas. Jet detachment occurs if the radial momentum rate exceeded the radial drag. This analysis is very approximate in that cylinder height had to be assumed, which was found from experiment, in determining the drag force. The numerical results are presented in Table III by the tabulation of the maximum momentum rate ratio, $(QU_r / \rho U^2)_{theory}$ (see page 3-7 for definition) that can exist for jet attachment.

In the study of jet detachment that was carried out in the first quarter, the phenomenon of downstream jet reattachment was not included. That is, due to jet expansion a detached jet may reattach to the wall downstream of injection. This phenomenon will be studied in a very simple manner in the next quarter.

The development of the ρU^2 profile with both axial and circumferential position was obtained in the cold flow tests in order to acquire knowledge of the complicated jet mixing region and, indirectly, aid in a boundary layer analysis. A mathematical treatment of the mixing region results in a set of non-linear differential equations, Reference 37, with a very costly and time consuming solution. Therefore, by performing a simple cold flow experiment the radial, axial and circumference ρU^2 distribution of a 3-dimension jet was obtained in the mixing region.

Radial and axial ρU^2 profiles are presented in Figure 45 , while the circumferential traverses are shown in Figure 46 . The injected gas was Freon-22 with a hole size of 0.070 and injected 20° from the tube axis. It may be noted that a similar experiment was performed using N_2 as the injected gas (identical ρU^2, hole size and angle) with the ρU^2 profiles of N_2 falling precisely on those of Freon-22. It cannot be concluded that the ρU^2 profile is independent of gas type until further study has been carried out. Although it is suspected that, in the mixing region, the flow field of a wall jet is relatively independent of gas type, since (1) diffusion velocities are small, compared to axial velocities, (2) difference in the eddy viscosity $\epsilon = $ constant $(dU/dy)^3 / (d^2U/dy^2)^2$ is negligible between different gases; and (3) equivalent turbulent mixing at injection occurs (i.e. approximately equal injection Reynold's Number)
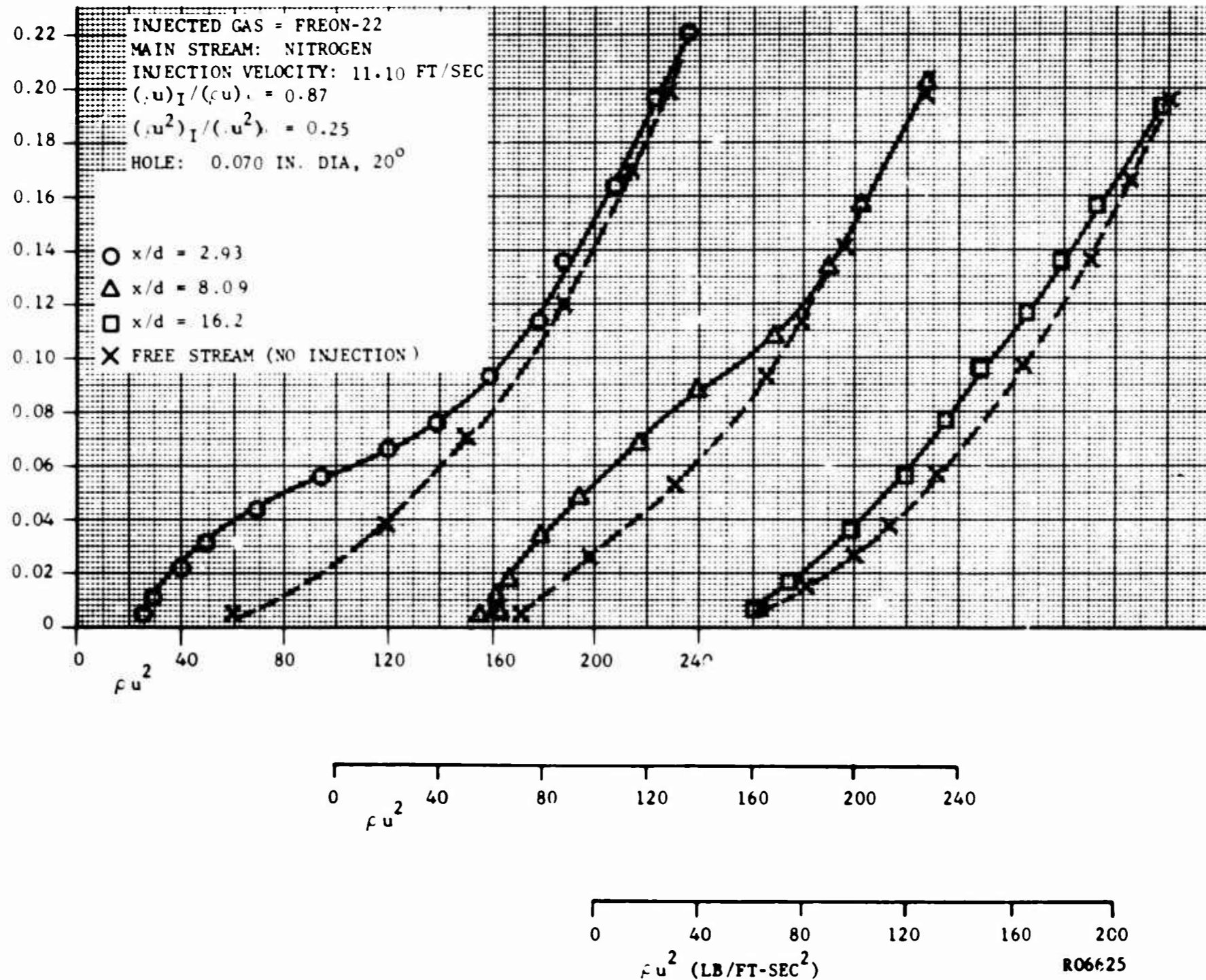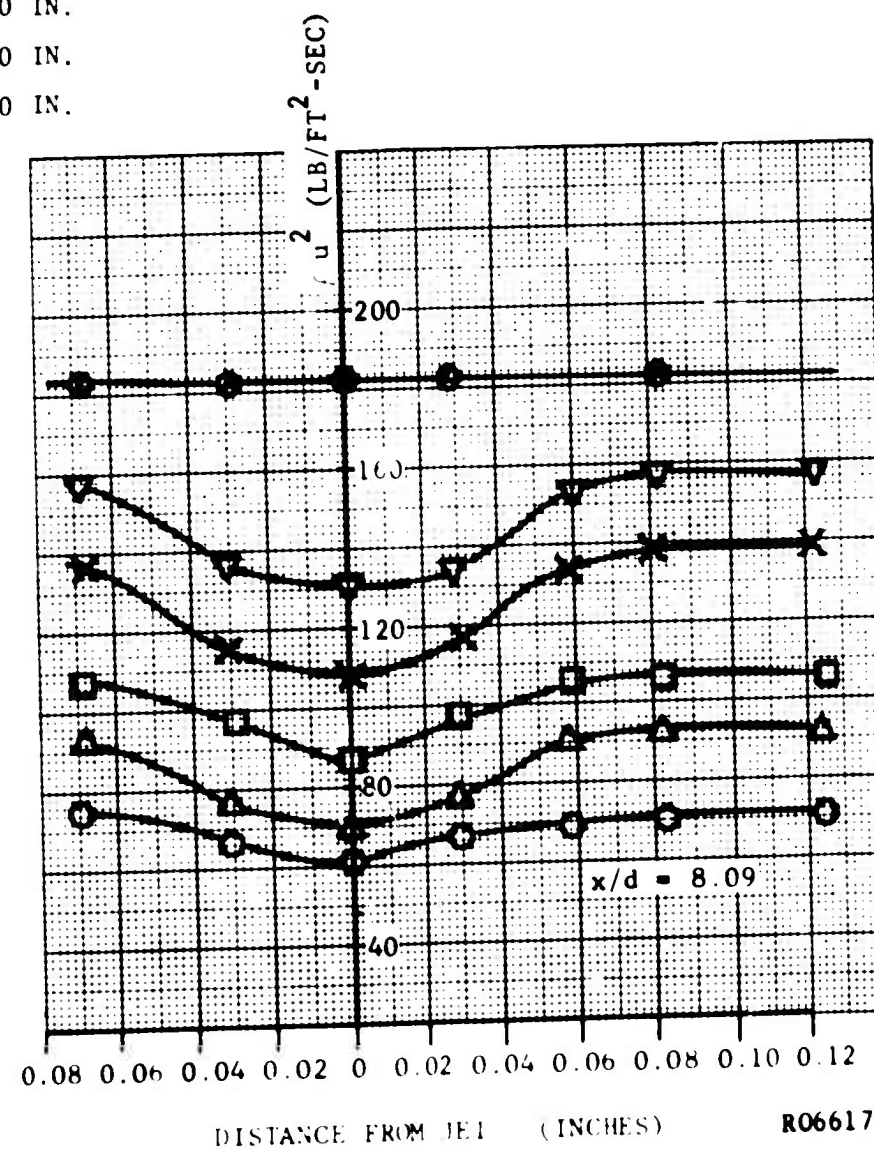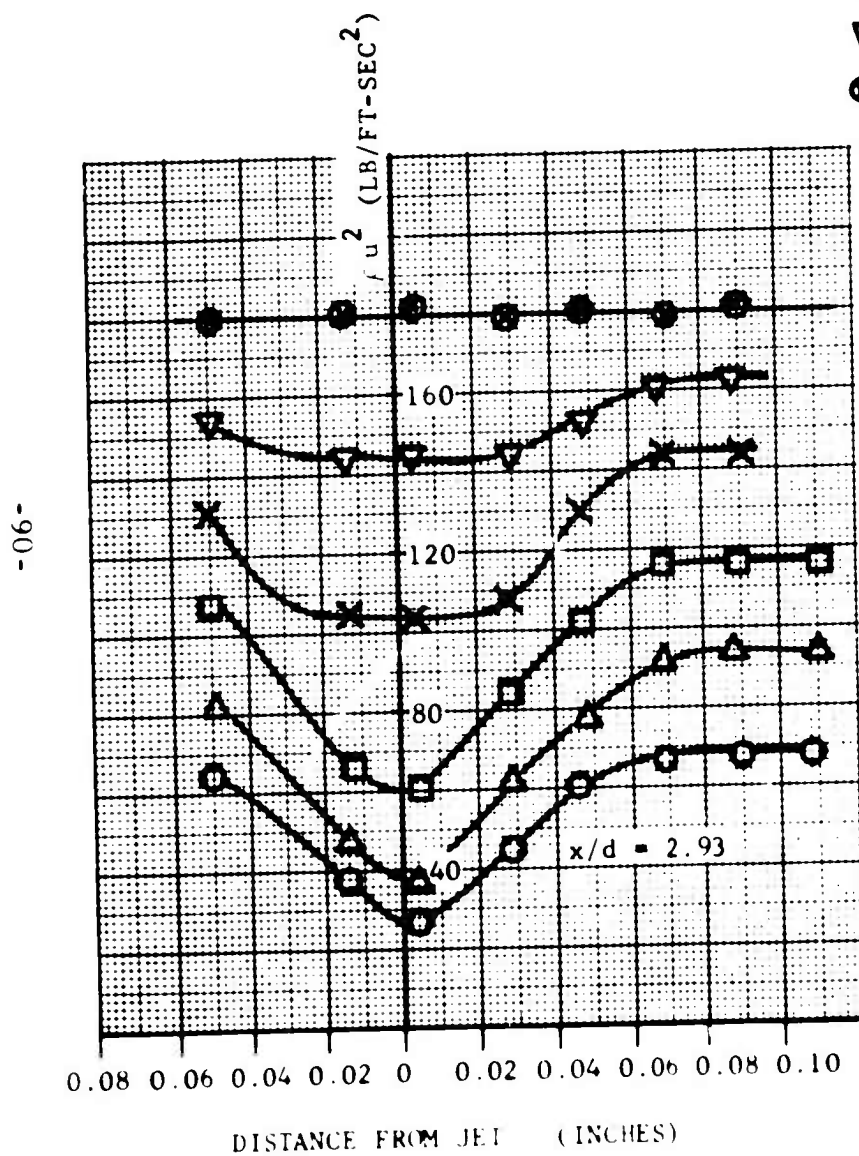
-88-

FIGURE 45. 'ρu^2' PROFILE DEVELOPMENT FOR A 3-DIMENSIONAL
WALL JET WITH AXIAL POSITION

FIGURE 46. CIRCUMFERENTIAL ' ρu^2 ' PROFILES

With the effect of ρU^2 on velocity magnification, discussed earlier, in mind; the mixing region may be considered to terminate at an x/d between 8 and 16 (elimination of the inflection point in the velocity profiles). Seban and Korst Reference 4 obtained, analytically and experimentally, the downstream location at which the wall shear and free jet boundary merge; which in essence is only another definition of the mixing region. When the flow properties of Figure 45 are applied to the results of Seban and Korst, one obtains an x/d of approximately 13 for the termination of the mixing region.

Probably the most important investigation performed by the cold tests is the interrelation of hole geometry on wall coverage. To obtain efficient chemical and thermal protection of a nozzle wall, the film must cover the maximum amount of nozzle surface. In order to achieve this, the amount of jet spreading must be established and then the hole size, shape, spacing and axial location designed accordingly. An analysis of jet spreading is no simple matter, as the majority of spreading occurs in the complicated jet mixing region. Therefore, by lining the tube wall with Ozalid paper and using NH_3 as the injection gas, an idea of wall coverage is obtained in isothermal flow. This scheme is currently in progress with investigation being centered in areas of jet interaction, hole spacing, radial angle of injection (i.e. angle producing a velocity in the circumferential direction of a nozzle) and free stream boundary layer thickness.

As noted before, direct application of the cold flow results to the actual nozzle is not possible. This is due to the fact that jet expansion is very dependent on injection and free stream ρU, ρU^2 and U ratios; Reynold's numbers; density and thermal gradient between film and free stream; momentum and displacement thickness of main stream at injection, and free stream gradients. Therefore, it is proposed that in the next quarter of the contract period a study be made to determine the effect of the above parameters on thermal and chemical protection of the actual nozzle.

SECTION 4

ROCKET MOTOR TESTS

4.1 CHEMICAL DIFFUSION TESTS

A technique has been devised to study the relative performance of injection fluids. Basically, it consists of a source of high-temperature corrosive gas, a gas-injection system, and a cylindrical test section. The hot-gas source is a small hydrogen-oxygen gas generator. The gas-injection system consists of the gas supply, a means of internal distribution, and two injection slots. The injection fluid source will be a high-pressure gas bottle for fluids which are gases at the storage pressures and temperatures. The cylindrical test specimen is simply a metallic tube, the inner surface of which has been polished. The polished surface will act as a chemical reaction indicator by changes in its surface reflectivity and by color changes caused by the formation of the various metal oxides. During a test, two quadrants of the tube will be exposed directly to the hot combustion products to provide a check on the injector, to observe the circumferential expansion of the injected film, and to provide a direct visual comparison of the effectiveness of the gas injections. The appearance of the other two quadrants of the test section should, for stable film injection, vary from its original appearance to something close to that of the unprotected sections at sufficient distances from the point of injection. The chemical insulation distance can be determined visually and checked by microscopic examination. The instrumentation will include measurement of the generator chamber pressure and two sets of temperature measurements on the outer surface of the protected and unprotected quadrants of the metal tube inserts.

Most of the tests will be run under standard operating conditions which are estimated to be the following:

(1)	Combustion temperature	$1800^{\circ}F$
(2)	Combustion pressure	600 psig
(3)	Operating time	30-60 sec
(4)	Injection slot width	5-10 mils
(5)	Tube length	6 inches

Adjustments in any or all of the above may be required to achieve reasonable chemical insulation lengths, general economy, and good oxidation comparisons. Deviations from the standard conditions will be made to evaluate changes in both injection and combustion parameters.

As mentioned earlier, it is planned that the polished inner surface of the metallic tube will act as a chemical reaction indicator by color changes caused by the formation of metal oxide. Nickel oxide, NiO, is black and the copper oxides are reddish-brown Cu_2O, and black CuO. In order to study the effectiveness and sensitivity of nickel and copper as indicators, several small scale experiments were made in which nickel and copper were subjected at 200 psia to small partial pressures of oxygen. The temperature range studied was $600^{\circ}F$ to $900^{\circ}F$. The exposure times at temperature ranged from 0.5 min. to 3 min. and the oxygen concentration ranged from 0.5 to 10 volume percent. Oxygen was chosen rather than gaseous H_2O on the basis of thermochemical calculations, which showed H_2O to be more stable than either NiO, Cu_2O or CuO at the temperatures of interest. Thus, the hot gas stream would have to contain an excess of oxygen in order for the metal to act as an indicator.

Under the experimental conditions of temperature, oxygen concentration and short exposure times, NiO did not form. On the other hand, above $900^{\circ}F$ copper oxidized readily, even at low oxygen concentrations, 0.5 volume percent, and short exposure times, 0.5 min. On this basis, copper has been chosen as the chemical reaction indicator for the initial gas-injection studies. The test hardware has been completed and the initial firing has been scheduled for the first week of the second quarter.

4.2 SIMULATOR TESTS (SUB-SCALE)

a. Solid Propellant Simulator

The Simulator is a rocket motor which utilizes gaseous, liquid and slurried propellants to simulate the exhaust products and temperatures of a given solid pro-pellant. In this program, the requirement was to simulate a high energy solid con-taining 16% aluminum and having a combustion temperature between $6600^{\circ}F$ and $6800^{\circ}F$. A chamber pressure of 700 psia was required.

The simulation used produces a theoretical combustion temperature of $6720^{\circ}F$ with an equilibrium C* of 5320 fps. Assuming 97% combustion efficiency a total flow rate of 5.35 lb/sec will produce 700 psia chamber pressure with a 1.25 in. diameter throat.

The propellant consists of gaseous oxygen and nitrogen and a slurried fuel containing powdered aluminum. Exhaust products are given in Table I , Section 2.1.

b. Description of First Sub-scale Nozzle

The first sub-scale nozzle (See Figure 47) will be a pyrolytic graph-ite heat sink convectively cooled with methane. There will be no film injection
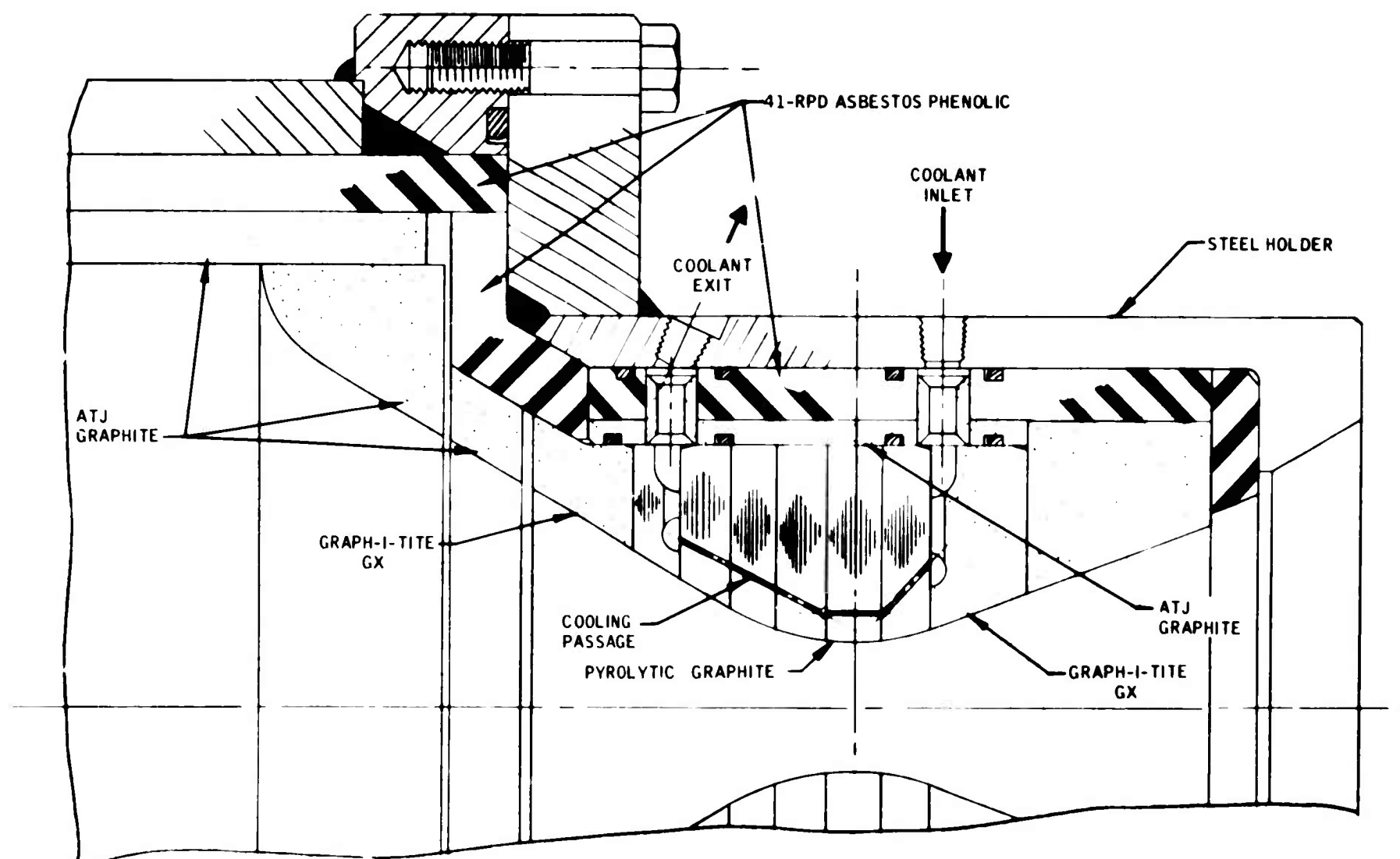
FIGURE 47. NOZZLE FOR FIRST SUB-SCALE TEST

in this test. The cooling passages will be nominally 0.25 inches from the surface and follow the contour as nearly as possible. The throat washer contains 28-0.030 in. diameter holes. The upstream and downstream washers contain 28-0.040 in. diameter holes. The coolant will be introduced downstream and flow toward the nozzle inlet.

The nozzle throat diameter is 1.25 inches and the heat sink outside diameter is 5.00 inches.

The methane coolant flow rate of 0.001 lb/sec/hole giving a total of 0.028 lb/sec. According to the computer results the surface temperature at the throat should not exceed $5020^\circ F$ in 50 seconds (the planned duration).

Instrumentation will include chamber pressure, propellant flow rates, thrust, methane pressures to determine flow rate and pressure drops, methane outlet temperature, and heat sink temperatures at five selected locations.

REFERENCES

1. Librizzi, J. and Cresci, R. J., "Transpiration Cooling of a Turbulent Boundary Layer in an Axisymmetric Nozzle," AIAA Journal, Vol. 2, No. 4, April 1964.

2. Deissler, R. G., "Analysis of Turbulent Heat Transfer, Mass Transfer and Friction in Smooth Tubes at High Prandtl and Schmidt Numbers," NACA TN 3145, May 1954.

3. Denison, M. R. and Baum, E., "Compressible Free Shear Layer with Finite Initial Thickness," AIAA Journal, Vol. 1, No. 2, February 1963.

4. Seban, R. A. and Back, L. H., "Effectiveness and Heat Transfer for a Turbulent Boundary Layer with Tangential Injection and Variable Free-Stream Velocity," Journal of Heat Transfer, p.235, August 1962.

5. Seban, R. A., "Heat Transfer and Effectiveness for a Turbulent Boundary Layer with Tangential Fluid Injection," Journal of Heat Transfer, p. 303, November 1960.

6. Hartnett, J. P., Birkebak, R. C., and Eckert, E. R. G., "Velocity Distributions, Temperature Distributions, Effectiveness and Heat Transfer for Air Injected Through a Tangential Slot into a Turbulent Boundary Layer," Journal of Heat Transfer, p. 293, August 1961

7. Papell, S. S., "Effect on Gaseous Film Cooling of Coolant Injection Through Angled Slots and Normal Holes," NASA TN D-299, September 1960.

8. Armour, W. H., et al, "Applied Research for Advanced Cooled Nozzles," Final Report, Philco Research Laboratories RTD-TDR-63-1122, December 1963 (Confidential).

9. "Pyrolytic Graphite Data Book," Lockheed Missile and Space Division, April 14, 1961.

10. "Final Report, Pyrographite Research and Development," Raytheon Co. Document 5-347, 1 April 1960 - 1 August 1961.

11. Mehan, R. L., Literature Review, Materials - 1" (U) General Electric Document No. 635D712, August 20, 1963.

12. Johnson, W. and Watt, W., "The Thermal Conductivity of Pyrolytic Graphite at Elevated Temperatures," Royal Aircraft Establishment, Tech. Note CPM. 14, April 1963.

13. Pappis, J. and Blum, S. L., "Properties of Pyrolytic Graphite," J. Amer. Ceramic Soc. 44, 592, 1962.

14. Farber, L. and Morley, M. J., "Heat Transfer to Flowing Gas-Solids Mixtures in a Circular Tube," Ind. and Eng. Chemistry 49, pp. 1143-1150, July 1957.

15. Wen, C-Y. and Miller, E. N., "Heat Transfer in Solids - Gas Transport Lines," Ind. and Eng. Chemistry 53, pp. 51-53, January 1961.

REFERENCES, continued

16. Danziger, W. J., "Heat Transfer to Fluidized Gas-Solids Mixtures in Vertical Transport," *Ind. Eng. Chemistry, Design and Development* 2, pp. 269-276 October 1963.

17. Babcock and Wilcox Co., "Gas-Suspension Coolant Project Final Report," BAW-1159, 1959.

18. Babcock and Wilcox Co., "Gas-Suspension Task II Final Report," BAW-1181, 1959.

19. Babcock and Wilcox Co., "Gas-Suspension Task III Final Report" and "Supplement," BAW-1201 and BAW-1207, respectively, 1960.

20. Deissler, R. and Presler, A., "Computed Reference Temperature for Turbulent Variable-Property Heat Transfer in a Tube for Several Common Gases," *International Developments in Heat Transfer* (ASME), pp. 579-584, 1961.

21. Butler, J. and Brokaw, R., "Thermal Conductivity of Gas Mixtures in Chemical Equilibrium," *Journal of Chemical Physics*, pp. 1636-1642, 26 June 1957.

22. Beal, J. and Lyerly, R., "The Influence of Gas Dissociation on Heat Transfer," WADC Tech. Report 56-494, 1956.

23. Krieve, W., "Heat Transfer in Reacting Systems: Heat Transfer to N_2O_4 Gas Under Turbulent Pipe Flow Conditions," JPL Progress Report 20-366, 1958.

24. Bartz, D. R., "Rocket Heat Transfer Literature, Predictions of Thermal Properties," Journal of Heat Transfer, p. 165, August 1960.

25. Eckert, E., "Survey on Heat Transfer at High Speeds," WADD Technical Report 54-70, 1954.

26. Eckert, E., "Survey on Boundary Layer Heat Transfer at High Velocities and High Temperatures," WADC Technical Report 59-624, 1960.

27. Ibele, W., *Modern Developments in Heat Transfer*, Academic Press, pp. 19-59, 1963.

28. Altman, D.& Wise, H., "Effect of Chemical Reactions in the Boundary Layer on Convective Heat Transfer," Jet Propulsion, pp. 256-259, April 1956.

29. Svehla, R., "Estimated Viscosities and Thermal Conductivities of Gases at High Temperatures," NASA TR R-132, 1962.

30. Brokaw, R.,"Alignment Charts for Transport Properties Viscosity, Thermal Conductivity and Diffusion Coefficients for Nonpolar Gases and Gas Mixtures at Low Density," NASA TR R-81, 1961.

31. JANAF Thermochemical Tables, Quarterly Supplement No. 12, Dow Chemical Company, December 31, 1963.

REFERENCES, continued

32. Stull, V. and Plass, G., "Emissivity of Dispersed Carbon Particles," _Journal of the Optical Society of America_ 50, February 1960.

33. Back, L. H., Massier, P. F. and Gier, H. L., "Convective Heat Transfer in a Convergent-Divergent Nozzle," Technical Report No. 32-415, Jet Propulsion Laboratory, California Institute of Technology, November 15, 1963.

34. Elliott, D. G., Bartz, D. R. and Silver, S., "Calculation of Turbulent Boundary-Layer Growth and Heat Transfer in Axi-symmetric Nozzles," Technical Report No. 32-387, Jet Propulsion Laboratory, California Institute of Technology, February 15, 1963.

35. Tien, C. L. and Abu-Romia, M. M., "Radiative Energy Transfer to Outer Base Regions of Cylindrical and Conical Gas Bodies," Report No. AS-63-4, I.E.R., University of California, Berkeley, California (1963).

36. Eckert, E.R.G., and Drake, R. M., _Heat and Mass Transfer_, McGraw-Hill (1959).

37. Vulis, V. A., Leontiyeva, T. P., Palatnik I. B., Sakipov, Z. B. and Ustimenko, B. P., "Transfer Processes in a Free (Jet) Turbulent Boundary Layer," AID Report T-63-73.

38. Pai, S. I., _Fluid Dynamics of Jets_, D. Von Nostrand Co., New York, 1954.

39. Zukoski, E. E., and Spaid, F. W., "Secondary Injection of Gases into a Supersonic Flow," Cal. Inst. of Tech., Daniel and Florence Guggenhiem Jet Propulsion Center, October 1963.

40. Schlichting, H., _Boundary Layer Theory_, McGraw-Hill Book Company, New York, Fourth Edition, 1962.